DEVELOPMENT AND CHARACTERIZATION OF EXPANDED GRAPHITE FOR OIL SORPTION APPLICATION

By

ELBIDI MOAMMAR IBRAHIM MOAMMAR

Thesis Submitted to the School of Graduate Studies, Universiti Putra Malaysia in Fulfilment of the Requirements for the Degree of Doctor of Philosophy

March 2024

FK 2024 21

DEDICATION

This thesis is dedicated to:

My mother and my father for their endless love and wishes for their son to achieve this higher dream,

My siblings who have been a source of inspiration and support to me throughout my study, and,

My wife and children who endured hardships all my study years.

Abstract of thesis presented to the Senate of Universiti Putra Malaysia in fulfilment of the requirement for the degree of Doctor of Philosophy

DEVELOPMENT AND CHARACTERIZATION EXPANDED GRAPHITE FOR OIL SORPTION APPLICATION

By

ELBIDI MOAMMAR IBRAHIM MOAMMAR

March 2024

Chairman : Associate Professor Mohamad Amran bin Mohd Salleh, PhD
Faculty : Engineering

Expanded graphite (EG) is a versatile material with various unique properties, making it useful in various industrial and commercial applications. As a carbon-based sorbent with high porosity, EG has recently been prepared using different methods, most of which focus on environmental and economic perspectives. In this thesis, EG is prepared using two methods: a one-step method, which focuses on economic aspects by minimizing energy use, and a two-step method, which avoids using strong acids and is considered more environmentally friendly. Due to its strong oleophilic properties towards various oils and its hydrophobic nature, EG is widely used as a sorbent to address oil spills in oceans resulting from fossil fuel transportation.

EG was prepared by a sulfur-free EG preparation process that is believed to be eco-friendly because it limits the use of sulfur, which is considered a key component in EG preparation in traditional methods. Eco-friendly EG was prepared using natural flake graphite as a precursor in a two-step chemical oxidation method. In the first step "oxidation," the chemical intercalation process was carried out at room temperature

for 30 min with an optimum weight ratio of 1 g: 5.1 g: 0.2 g of natural flake graphite (NFG), hexadecanoic acid, and potassium permanganate. Then, in the second step "intercalation," nitric acid, acetic acid, and potassium permanganate were employed as the intercalating agents to further increase the expanded volume of EG. Under the optimal conditions, a maximum expanded volume of 470 mL/g was obtained.

An efficient and energy-conserving preparation process to obtain EG, in which flake graphite is intercalated and expanded at room temperature. The flake graphite was expanded using a simple and effective method in which graphite intercalation and expansion are accomplished using a binary system of concentrated sulfuric acid (H_2SO_4) and inorganic salts, specifically sodium peroxydisulfate ($Na_2S_2O_8$). The optimal conditions were at room temperature, with mass ratios of graphite to $Na_2S_2O_8$ of 1:7 and graphite to concentrated H_2SO_4 of 1:20. This gave a maximum expanded volume of 140 mL/g.

XRD, SEM, and FT-IR were utilized to characterize the microstructures, morphologies, and functional groups of the expanded graphite. Following expansion, the flake graphite transformed into a worm-like structure, with minimal damage to the graphite sheets. Additionally, the findings revealed that the interlayers of natural flake graphite were fully opened and transformed into a structure resembling a fluffy, rope-like form, similar to a worm, upon expansion.

Furthermore, the two types of fabricated expanded graphites were applied to oil sorption. Both types show promise as engineering materials for water purification sorbents and demonstrate significant oil sorption capacities. ATEG and EG-SF

exhibited maximum oil sorption capacities of 27 g/g and 89 g/g, respectively. When compared to their expanded volumes, ATEG absorbed more oil than EG-SF. These results suggest that the preparation methods for EG have a significant impact on its oil adsorption capacity.

Keyword: Expansion, Graphite, Oil Spill, Sorption, Sulfuric Acid

SDG: GOAL 6: Clean Water and Sanitation, GOAL 9: Industry, Innovation and Infrastructure, GOAL 12: Responsible Consumption and Production

Abstrak tesis yang dikemukakan kepada Senat Universiti Putra Malaysia sebagai memenuhi keperlan untuk ijazah Doktor Falsafah.

PEMBANGUNAN DAN PENCIRIAN GRAFIT YANG DIPERKEMBANGKAN UNTUK APLIKASI PENYERAPAN MINYAK

Oleh

ELBIDI MOAMMAR IBRAHIM MOAMMAR

Mac 2024

Pengerusi : Profesor Madya Mohamad Amran bin Mohd Salleh, PhD
Fakulti : Kejuruteraan

Expanded graphite (EG) ialah bahan serba guna dengan pelbagai sifat unik, menjadikannya berguna dalam pelbagai aplikasi industri dan komersial. Sebagai sorben berasaskan karbon dengan porositi tinggi, EG baru-baru ini telah disediakan menggunakan pelbagai kaedah, kebanyakannya memberi tumpuan kepada perspektif alam sekitar dan ekonomi. Dalam tesis ini, EG disediakan menggunakan dua kaedah: kaedah satu langkah, yang menumpukan kepada aspek ekonomi dengan mengurangkan penggunaan tenaga, dan kaedah dua langkah, yang mengelakkan penggunaan asid kuat dan dianggap lebih mesra alam. Disebabkan sifat oleofilik yang kuat terhadap pelbagai jenis minyak dan sifat hidrofobiknya, EG digunakan secara meluas sebagai sorben untuk menangani tumpahan minyak di lautan yang berpunca daripada pengangkutan bahan api fosil.

EG telah disediakan melalui proses penyediaan EG bebas sulfur yang dipercayai mesra alam kerana ia mengehadkan penggunaan sulfur, yang dianggap sebagai komponen utama dalam penyediaan EG melalui kaedah tradisional. EG mesra alam ini disediakan

menggunakan grafit kepingan semula jadi sebagai bahan asas dalam kaedah pengoksidaan kimia dua langkah. Pada langkah pertama, "pengoksidaan", proses interkalasi kimia dilakukan pada suhu bilik selama 30 minit dengan nisbah berat optimum 1 g: 5.1 g: 0.2 g bagi grafit kepingan semula jadi (NFG), asid heksadekanoik, dan kalium permanganat. Kemudian, pada langkah kedua, "interkalasi", asid nitrik, asid asetik, dan kalium permanganat digunakan sebagai agen interkalasi untuk meningkatkan lagi jumlah pengembangan EG. Di bawah keadaan optimum, jumlah pengembangan maksimum sebanyak 470 mL/g telah diperoleh.

Satu proses penyediaan yang cekap dan menjimatkan tenaga untuk mendapatkan EG, di mana grafit kepingan diinterkalasi dan dikembangkan pada suhu bilik. Grafit kepingan dikembangkan menggunakan kaedah yang mudah dan berkesan di mana interkalasi dan pengembangan grafit dicapai menggunakan sistem binari asid sulfurik pekat (H_2SO_4) dan garam tak organik, khususnya natrium peroksidisulfat ($Na_2S_2O_8$). Keadaan optimum adalah pada suhu bilik, dengan nisbah jisim grafit kepada $Na_2S_2O_8$ sebanyak 1:7 dan grafit kepada H_2SO_4 pekat sebanyak 1:20. Ini menghasilkan jumlah pengembangan maksimum sebanyak 140 mL/g.

XRD, SEM, dan FT-IR digunakan untuk mencirikan struktur mikro, morfologi, dan kumpulan berfungsi bagi grafit yang dikembangkan. Selepas pengembangan, grafit kepingan bertukar menjadi struktur seperti cacing, dengan kerosakan minimum pada helaian grafit. Selain itu, dapatan kajian menunjukkan bahawa lapisan antara grafit kepingan semula jadi dibuka sepenuhnya dan ditransformasikan menjadi struktur yang menyerupai bentuk seperti tali gebu, mirip kepada cacing, selepas pengembangan.

Tambahan pula, kedua-dua jenis grafit yang dikembangkan ini digunakan untuk penyerap minyak. Kedua-duanya menunjukkan potensi sebagai bahan kejuruteraan untuk sorben penulenan air dan menunjukkan kapasiti penyerapan minyak yang ketara. ATEG dan EG-SF masing-masing menunjukkan kapasiti penyerapan minyak maksimum sebanyak 27 g/g dan 89 g/g. Apabila dibandingkan dengan jumlah pengembangan mereka, ATEG menyerap lebih banyak minyak berbanding EG-SF. Keputusan ini mencadangkan bahawa kaedah penyediaan EG mempunyai kesan yang ketara ke atas kapasiti penyerapan minyaknya.

Kata kunci: Pengembangan, Grafit, Tumpahan Minyak, Penyerapan, Asid Sulfurik

SDG: MATLAMAT 6: Kebersihan air dan Sanitasi, MATLAMAT 9: Industri, Inovasi dan Infrastruktur, MATLAMAT 12: Penggunaan dan Penghasilan yang Bertanggungjawab

ACKNOWLEDGEMENTS

Completion of this work would not have been possible without the help I received from many supporters. It has been a long exhaustive journey, but a most enlightening one too. I would like to express my respect and gratitude to my supervisor Assoc. Prof. Dr. **Mohamad Amran bin Mohd Salleh**, Department of Chemical and Environmental Engineering, Faculty of Engineering, University of Putra Malaysia, Malaysia for his keen interest, guidance, patience and assistance throughout this research work. I consider myself fortunate to have him as my guide. I am equally grateful to my committee members, Prof. Dr. Suraya binti Abdul Rashid and Dr. Mohamad Faiz Mukhtar bin Gunam Resul, without whose extraordinary help I would not have been able to accomplish the task. I also thank all the staff of the Department of Chemical and Environmental Engineering for their hospitability and cooperation whenever required during my work.

Finally, I would like to express my deep gratitude towards my mother, father, siblings, wife, kids and who have continuously provided their moral support and their love, affection and encouragement during my graduate studies. I am highly thankful to all of my friends and surrounding people who assist and encourage me to complete this research.

This thesis was submitted to the Senate of Universiti Putra Malaysia and has been accepted as fulfilment of the requirement for the degree of Doctor of Philosophy. The members of the Supervisory Committee were as follows:

Mohamad Amran bin Mohd Salleh, PhD
Associate Professor
Faculty of Engineering
Universiti Putra Malaysia
(Chairman)

Suraya binti Abdul Rashid, PhD
Professor
Faculty of Engineering
Universiti Putra Malaysia
(Member)

Mohamad Faiz Mukhtar bin Gunam Resul, PhD
Senior Lecturer
Faculty of Engineering
Universiti Putra Malaysia
(Member)

ZALILAH MOHD SHARIFF, PhD
Professor and Dean
School of Graduate Studies
Universiti Putra Malaysia

Date: 12 December 2024

TABLE OF CONTENTS

LIST OF TABLES

LIST OF FIGURES

LIST OF APPENDICES

LIST OF ABBREVIATIONS

AG	Acidized graphite
ATEG	Ambient Temperature Expanded Graphite
Avogadro's number	$6.023*10^{23}$ dimensionless quantity
c	Crystallographic c-direction
℃	Degree Celsius
d	Interlayer spacing
EG	Expanded Graphite
EV	Expanded volume
FTIR	Fourier Transform Infrared Spectroscopy
FWHM	Full Width at Half Maximum
GICs	Graphite intercalation compounds
HTEG	High Temperature Expanded Graphite
I_a	Mean graphite crystal dimensions in the a-direction
I_c	Mean graphite crystal dimensions in the c-direction
ITOPF	International Tanker Owners Pollution Federation
La	Lattice parameter refers to the distance between adjacent carbon atoms in the crystal lattice of graphite
Lc	Crystallite size
MEG	Magnetic expanded graphite
MW	Microwave
NGF	Natural graphite flakes
NOAA	National Oceanic and Atmospheric Administration
OAC	Oil adsorption capacity
PA	Palmitic acid
S°	Standard entropy at 25℃

SEM	Scanning Electron Microscopy
TEG	Thermally expanded graphite
XRD	X-ray Diffraction
ΔH	Enthalpy
ΔHco	Heat of combustion at 25℃
ΔS	Entropy
π	Covalent bond type π
σ	Covalent bond type σ

CHAPTER 1

INTRODUCTION

1.1 Study Background

Expanded graphite has gained significant global attention due to its numerous potential applications, leveraging its inherent properties such as low density, high porosity, and electrical conductivity. These properties make it a promising material for various applications including fuel cells, electromagnetic interference shielding, catalysts, vibration damping, supercapacitors, biomedical materials, and as an adsorbent for spilled oil (Lan et al., 2019; Qiu et al., 2019; K. H. Wu et al., 2021). The high effectiveness of EG in sorbing oil from water or pure oil was initially described by Inagaki and Toyoda two decades ago (Nirwan et al., 2021; Tarango-Rivero et al., 2022).

Expanded graphite, one of the most interesting ends uses of graphite. Expanded graphite, was discovered first time in United State of America by Carburet in 1968 (Tarango-Rivero et al., 2022), EG is a carbon porous material with a worm-like structure (B. Hou et al., 2020). Expanded graphite is a special form of flake graphite produced by intercalation of strong acidic anions. Upon immediate exposure to high temperatures, the anions within the graphite structure undergo evaporation, causing the crystals to break apart into extremely thin sheets, typically with a thickness of 100 nm or less. As a result, the graphite undergoes significant expansion, with the volume increasing by a factor of 300 or more (Murugan et al., 2021). When the graphite has a

degree of separation of a large portion of the carbon layers this called expanded graphite (Goudarzi & Hashemi Motlagh, 2019). Therefore, expansion is a process that results in this separation that can include chemical, mechanical, and thermal methods. The separation takes place between neighboring carbon layers, although not all carbon layers are usually separated (Murugan et al., 2021). Because of its unique porous structure and long-distance between carbon layers, expanded graphite is obtained by inserting atoms or molecules between the graphite layers by rapidly heating graphite intercalation compounds (GICs) (Lan et al., 2019; Murugan et al., 2021). GICs are organic or inorganic compounds that are inserted into the graphite layers. The GICs penetrate between graphite layers causing rapid vaporization or decomposition of the GICs, a significant expansion of the graphite c-axis will occur (Goudarzi & Hashemi Motlagh, 2019).

The conventional methods used for the preparation of expanded graphite have several drawbacks. Firstly, these methods involve complex and time-consuming steps, including the use of multiple chemical compounds for intercalation, water-washing, drying, and thermal or microwave expansion. This results in the consumption of large quantities of chemicals, time, water, and energy. Secondly, the excessive use of chemicals and washing steps not only depletes water resources but also poses environmental risks. Furthermore, the low expansion volume and the formation of residue in the produced EG limit its application performance, particularly in wastewater purification. These limitations restrict the wide-ranging potential applications of EG. Therefore, there is a pressing need to develop a simpler, scalable, and environmentally friendly approach for the production of EG that can cater to a diverse range of applications (Çalın et al., 2020; Sykam et al., 2018).

Over the past 150 years, fossil fuels, such as coal, oil, and natural gas, have been the primary source of energy for the world's economies, supplying approximately 80% of the world's energy. Due to rising demand, accidents involving oil spills from onshore facilities and oil tanker spills during transportation have become increasingly common (Pham et al., 2019; Singh et al., 2020). Frequent oil spills, ranging from small-scale incidents of a few gallons to large-scale disasters involving millions of barrels, occur worldwide. The U.S. National Oceanic and Atmospheric Administration (NOAA) is responsible for responding to approximately 150 oil spills each year. The total volume of oil released into the environment from tankers in 2020 was roughly 1000 tones (ITOPF, 2022). The oil spill has caused significant environmental damage to surrounding water bodies, mostly seas. A massive amount of leaked oil has not only a serious impact on the ecosystem but the lives of humans and living species and puts them at high risk (ITOPF, 2022). Polluted water harms humans, animals, and aquatic ecosystems. Marine oil pollution is one of the most significant environmental concerns in the petroleum industry, as it causes severe harm to marine ecosystems and a substantial loss of valuable resources (Rozi et al., 2017). Therefore, it is crucial to dispose of the oil pollutants as quickly as possible and efficiently after the accident has occurred to alleviate the pollution using a high effective technique (Lan et al., 2019).

Several techniques are used for cleaning up oil spills in water environments. These techniques aim to contain, recover, and remove oil from the water surface, minimizing its impact on the ecosystem (Ren et al., 2019). Each of these techniques has its own set of drawbacks, which encompass substantial capital and maintenance expenses, considerable energy demands, and the necessity for additional time-consuming treatment procedures. The adsorption process is a viable and practical alternative for water treatment. It operates by the accumulation of solute molecules on the surface of

a solid material in contact. Adsorption is highly regarded as a promising technique due to its simplicity, ease of operation, high capacity for pollutant removal, and rapid pollutant removal rates (Hadela et al., 2020; Soliman et al., 2020).

Sorbent materials where various sorbent materials, such as absorbent pads, booms, or specially designed sorbent-filled pillows, are deployed to selectively absorb and recover the oil from the water surface. These sorbents can be made from natural or synthetic materials and are effective at removing oil while minimizing water uptake. Various materials have been proposed as sorbents for oil spills, including foam, highly porous synthetic organophilic sorbents, silica aerogels, zeolites (Nassar et al., 2017), exfoliated graphite (Goudarzi & Hashemi Motlagh, 2019; Sykam et al., 2018), magnetic nanoparticles (Hadela et al., 2020), raw flax fiber (Mahmoud, 2020), magnetic wood sawdust as a nano-composite (Soliman et al., 2020). These materials have been utilized for the treatment of oil-contaminated water.

Porous carbon materials are extensively employed in wastewater treatment due to their microporous structure and exceptional adsorption capacity (S. Hou et al., 2017). Among carbon-based materials, activated carbon is commonly recommended as an effective agent for removing contaminants from water. However, its production and regeneration processes can be costly (Tarango-Rivero et al., 2022). Similarly, special carbon-based materials like carbon nanotubes and graphene have demonstrated remarkable performance, but their current high cost limits their practical use in oil clean-up applications (Xu et al., 2018).

1.2 Problem Statements

Expanded graphite can be produced by conventional methods using concentrated sulfuric acid as the intercalating agent and nitric acid as the oxidizing agent, achieving expansion volumes of up to several hundred times (Z. Liu et al., 2018; Saikam et al., 2022; Tarango-Rivero et al., 2022). However, these conventional processes come with several well-known drawbacks, including the emission of harmful gases, complex processing steps, long reaction times, and high energy consumption (B. Hou et al., 2020; Sykam et al., 2018; Ting & Xuesha, 2017).

Conventional techniques for expanded graphite preparation are not the optimal choices from an economic and environmental perspective. In terms of economic considerations, expanding graphite at room temperature is a rapidly developing technique. This energy-efficient approach can significantly reduce energy consumption.

This study focuses on modifying a simple and effective method for preparing expanded graphite with low energy consumption. The process is entirely energy-free, and the expanded graphite is obtained at room temperature.

From an environmental standpoint, the use of a sulfur-free method for producing expanded graphite through thermal expansion aligns with the principles of green chemistry. Green chemistry emphasizes the design of chemical products and processes that minimize or eliminate hazardous substances throughout their entire life cycle.

Oily water treatment methods can be limited by either high capital and maintenance costs or significant energy consumption. A practical alternative is the adsorption process, which is considered one of the most efficient methods due to its ease of operation, cost-effectiveness, minimal residue formation, and the ability to recycle adsorbent materials. (Singh et al., 2020; Tarango-Rivero et al., 2022). Expanded graphite has gained significant global attention as a potential adsorbent for spilled oil. This is due to its numerous intrinsic properties, including low density, high porosity, recyclability, affordability, ease of use, high oil removal capacity, accelerated pollutant removal, and remarkable effectiveness in sorbing oil from water or pure oil (Dong et al., 2021).

1.3 Researches Questions

1. How can expanded graphite be synthesized at room temperature to achieve optimal structural and functional characteristics for industrial applications?"
2. How can porous materials based on carbon materials, specifically graphite, be developed in a sulfur-free environment?
3. How do room-temperature expanded graphite and sulfur-free expanded graphite compare in terms of their effectiveness and capacity for oil sorption in environmental applications?

1.4 Research Objectives

The main aim of this study was to develop two types of expanded graphite: the first type involved a rapid expansion process at room temperature, while the second type focused on an eco-friendly sulfur-free method. The following objectives have been considered in the present study:

1. To synthesize expanded graphite at room temperature that exhibits desirable characteristics.

2. To evaluate the effects of the expansion process of palmitic acid as the intercalating agent to synthesize expanded graphite.

3. To investigate the potential of room-temperature expanded graphite and sulfur-free expanded graphite in oil sorption applications.

1.5 Scopes of the Study

The scopes of this research were defined to accomplish the objective of current research as following:

1. Expanded graphite was prepared by two different approaches including two main methods: namely, room temperature and sulfur free methods. The first method that used in this study to prepare EG at **room temperature** and this method will focus on the expansion volume of expanded graphite due to mixing ratio of sulfuric acid as intercalating agent and sodium peroxydisulfate as oxidant agent. Sodium peroxydisulfate was used as both an oxidant and an expansion agent, allowing for effective intercalation and expansion. The second method focus on the **sulfur-free approach** for producing expanded graphite through the thermal expansion technique. In which a two-step chemical oxidation process was proposed where PA used as the main intercalating agent with the aid of phosphoric acid and potassium permanganate were employed as oxidizing agent agents with the aid of nitric and acetic acids.

2. The characterization of both type of expanded graphite in which Scanning Electron Microscopy (SEM) produced microscopic images of samples to distinguish between the graphite and EG produced. The Fourier Transform Infra-Red (FT-IR) tests detected the change of functional groups during the modifications that generate the gas that was required to break down the Van der Waals force that caused the expansion. The structures of natural graphite flakes and expanded graphite samples were examined by X-ray diffraction (XRD).

3. The scope of the study involved measuring the amount of oil adsorbed and assessing the sorbent's ability to retain the oil. This was achieved by calculating the weight difference of the sorbent before and after exposure to the oil spill to determine the amount of oil adsorbed. Additionally, the oil retention capacity of the sorbent was determined by calculating the quantity of oil held by the sorbent. These measurements and calculations were used to evaluate the effectiveness of the sorbent in capturing and retaining oil during the experiment.

1.6 Significant of the Study

Exploring methods to create porous structures in graphite at room temperature can lead to the development of more energy-efficient and environmentally friendly processes for expanding graphite and creating porous carbon materials. This research opens up possibilities for investigating innovative approaches and techniques that can enhance the synthesis of porous materials and their potential applications in various fields such as energy storage, catalysis, and environmental remediation.

Development of porous materials using carbon materials, specifically graphite, without the use of sulfur-based compounds. Investigating methods for sulfur-free synthesis of porous carbon materials is important for addressing environmental concerns associated with the use of sulfuric acid and other sulfur-containing chemicals. It opens up avenues for exploring alternative intercalation and oxidation agents that are environmentally friendly and can achieve efficient expansion of graphite. By addressing the challenges of sulfur-free expansion, this research can contribute to the development of sustainable and eco-friendly processes for creating porous carbon materials with potential applications in various fields such as energy storage, filtration, and catalysis.

CHAPTER 2

LITERATURE REVIEW

2.1 Expanded Graphite

Expanded graphite is a material derived from natural graphite that has been treated to increase its volume and porosity to enhance its properties. This process, known as intercalation, involves inserting atoms or molecules between the layers of the graphite structure, causing them to expand. Expanded graphite is a non-toxic, layered material with a vermicular (worm-like) structure. It offers excellent flexibility, high chemical resistance, and exceptional thermal shock resistance (B. Hou et al., 2020; Murugan et al., 2021; Sykam et al., 2018; Yin et al., 2021).

For successful graphite expansion, overcoming the van der Waals attractions that exist between adjacent layers is required (Dai et al., 2019; Murugan et al., 2021). Expansion is often accomplished by applying additional external forces to overcome the attractive van der Waals interactions between layers. The commonly used techniques are ultrasonication and thermal treatment. During ultrasonication, shear forces and cavitation (the growth and collapse of micrometer-sized bubbles) act on the bulk material and induce expansion (Z. X. Liu et al., 2020; Fengzhen Zhang et al., 2018). In the thermal expansion of graphite, the pressure due to the decomposition of the functional groups and intercalates between layers overcomes the van der Waals attractions and results in expansion (Z. X. Liu et al., 2020; Trivedi et al., 2018).

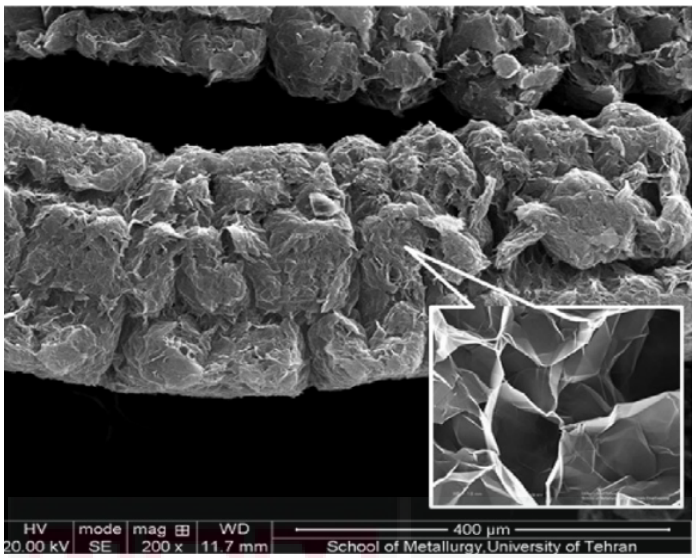

Figure 2.1: SEM photographs of expanded graphite
(Goudarzi & Hashemi Motlagh, 2019)

Expansion process results in a highly porous material with a unique set of properties that make it useful in a variety of industrial applications (Ardestani et al., 2022; Xu et al., 2018). EG is a very porous, worm-like, and light material with typical apparent densities of 0.002–0.01 g/cm^3 (Murugan et al., 2021; Q. Wei et al., 2023). This material "EG" with several existing and potential applications in energy storage (Chang et al., 2020; Murugan et al., 2021), hydrogen storage (Murugan et al., 2021), fuel cell (Li et al., 2020), sensor (Han et al., 2014), catalyst (Lan et al., 2019), biomedical materials (F. Chen et al., 2018), filler (Goudarzi & Hashemi Motlagh, 2019), and adsorbent (Pham et al., 2019). One of the most significant properties of expanded graphite is its ability to act as a flame retardant. The expanded structure of the graphite creates a barrier that can help prevent the spread of flames and limit the damage caused by fires. This makes it an ideal material for use in applications such as fireproofing insulation, gaskets, and seals (Huang et al., 2017). EG is also an excellent thermal conductor, which makes it useful in heat management applications. It can be used as a heat sink to dissipate heat away from electronic components and other heat-generating devices

(Trivedi et al., 2018). Another important property of expanded graphite is its chemical stability. It is resistant to most chemicals and can withstand high temperatures without degrading. This makes it useful in a range of harsh environments, including those found in the chemical processing and oil and gas industries (Zhuang et al., 2020). Finally, expanded graphite is a versatile material that offers a unique combination of properties, including flame retardancy, thermal conductivity, and chemical stability. These properties make it useful in a range of industrial applications where high-performance materials are required.

2.1.1 Graphite intercalation compounds "GICs"

Graphite can react with a variety of chemical substances to form different types of compounds. These compounds can be classified into three groups: surface compounds, substitutional compounds, and intercalation compounds (Chung, 2016). Graphite intercalation compounds "GICs", as exposed in Figure 2.2, are created by inserting foreign species like atoms, ions, or molecules between the layers of the graphite lattice (Goudarzi & Hashemi Motlagh, 2019; Murugan et al., 2021). These reactions are called intercalation. Intercalation compounds are produced by introducing a foreign substance into the host lattice. However, the structure of these compounds is different as the bond is a charge-transfer interaction (Çalın et al., 2020; Dai et al., 2019). This electronic interaction results in a significant increase in electrical conductivity in the ab directions (B. Hou et al., 2020; Nirwan et al., 2021). In this structure, the intercalated species occupy the interplanar interstitial sites between the layers, while the layered structure of the graphite lattice remains mostly unchanged (Chung, 2016).

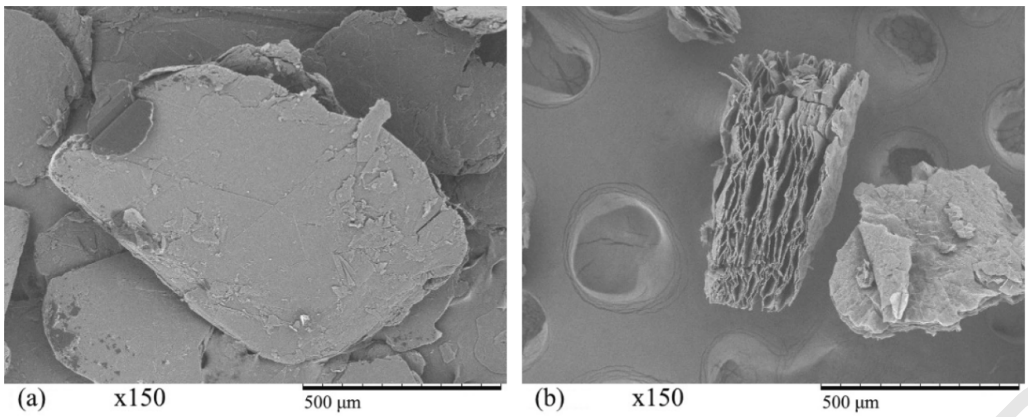

Figure 2.2: SEM photograph of GICs
(Y. L. Chen et al., 2023)

Direct synthesis is typically employed to produce the simplest binary and ternary compounds, whereas a variety of intercalation techniques are used to prepare the more complex materials. Because of their extreme reactivity, most graphite intercalation compounds are manufactured and stored in ampoules pressurized with an inert gas, a vacuum, or intercalate vapor. The stability of samples is considerably improved by cooling them (for instance, to liquid nitrogen temperatures) (Marrani et al., 2019; Q. Wei et al., 2023).

2.1.2 Staging

The staging phenomenon is the most significant and distinctive property of graphite intercalation compounds, which involves the periodic arrangement of intercalate layers between the graphite layers. The distance between adjacent intercalate layers is called the stage height, and the number of graphite layers between two adjacent intercalate layers is called the stage number (Murugan et al., 2021; Yin et al., 2021). Unlike other lamellar substances, where intercalating species enter the interlayer galleries sporadically, graphite can form intercalation compounds of varying and well-

defined structures; this phenomenon is called staging. Intercalation compounds have a large spread of composition as the percentage of intercalated material changes by regular steps as shown in Figure 2.3. In the first stage, intercalation reaches a maximum and the material is considered stoichiometric and is known as a first-stage compound (Çalın et al., 2020; Goudarzi & Hashemi Motlagh, 2019).

Intercalation compounds exhibit a wide range of compositions as the proportion of intercalated material varies in regular increments. At the first stage, intercalation reaches its maximum, and the material is deemed stoichiometric, also known as a first-stage compound. The stage decreases as the concentration of the intercalate increases (Chung, 2016).

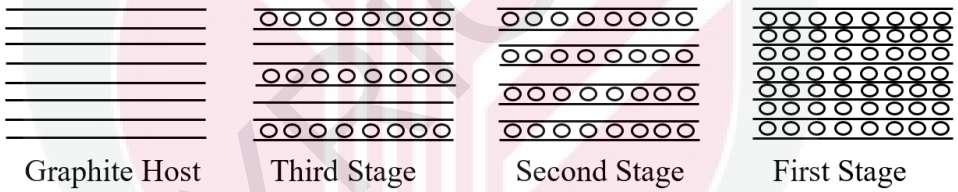

Figure 2.3: Schematic illustration of staging in intercalate compounds. The solid line represents the host layer, the dots a gust layer.
(Jacobson & Nazar, 2011)

In many cases, reactions occur near ambient temperature, but in general the reaction temperature should be high enough to ensure mobility of the guest species but not so high that the strong bonds are broken and the structure of the host lattice is rearranged. Many intercalation compounds are metastable because of the inherent anisotropy in the chemical bonding (Bannov et al., 2021; Jacobson & Nazar, 2011).

2.1.3 Thermal behavior of GICs expansion

The initial notable decrease in weight occurs within the temperature range of 150 to 300 °C, which is typically attributed to the evaporation of water (steam) and the release of gases from the more readily detachable functional groups (Marcano et al., 2010; Tarango-Rivero et al., 2022).

Botas et al. proposed that this phenomenon is caused by a series of events that correspond to the decomposition of oxygen functional groups slightly attached to the carbon structure, beginning with the release of a small amount of water at the initial heating stage and culminating in a dramatic loss at 150-300 °C (Botas et al., 2013).

At higher temperatures, specifically in the range of 400 to 950 °C, a gradual and slower decrease in mass occurs. This phenomenon is typically ascribed to the elimination of more stable oxygen functional groups, primarily resulting in the generation of gases such as H_2 and CO (Tarango-Rivero et al., 2022). Generally, a characteristic where the material has the ability to withstand high temperatures without thermal degradation is thermal stability (Tarango-Rivero et al., 2022).

2.2 Graphite Expansion

Graphite intercalation compounds (GICs), whether they are covalent or ionic type, are generally expandable upon heating. This is because the intercalated species occupy the interlayer spacing, and upon heating, they can expand the distance between the layers of the host graphite lattice. The degree of expansion depends on the type of intercalated

species, the amount of intercalation, and the temperature of expansion (Chung, 2015; Mukhopadhyay & Gupta, 2012).

Among the different graphite compounds obtained through acid intercalation, graphite bisulfate (graphite-H_2SO_4) is widely used to expand and produce EG. This compound is formed by the chemical reaction between graphite, concentrated sulfuric acid, and an oxidizing agent (Bannov et al., 2021; Cai et al., 2012). The reaction between graphite and concentrated sulfuric acid can be represented by the following equation 2.1 (Salvatore et al., 2017):

$$m\,(graphite) + mH_2SO_2 + \frac{m}{2}(O) \rightarrow n(graphite\,.\,HSO_4) + \frac{m}{2}H_2O \qquad (2.1)$$

Where (O) is the oxidizing agent and the (graphite. HSO_4) is the GICs which consist of graphite layers intercalated by bisulfate molecules.

The acid molecules penetrate the layers of graphite, and then applying the intercalated graphite to a thermal shock in an electric furnace (Çalın et al., 2020; Nirwan et al., 2021; Yin et al., 2021), microwave (Saikam et al., 2022; Tarango-Rivero et al., 2022), plasma (Vocciante et al., 2022), programmable heating (Bannov et al., 2021), leads to the rapid vaporization of the intercalated species. The expulsion of these gaseous products generates a force that expands the graphite layers, resulting in a substantial increase in volume. As a result, expanded graphite (EG) with a notably low density is obtained (Goudarzi & Hashemi Motlagh, 2019).

Microwave heating is often chosen as a method for expanding graphite intercalation compounds (GICs) because it provides rapid and uniform heating. The unique heating mechanism of microwaves allows for efficient and selective energy transfer to the GICs, leading to their rapid expansion. This uniform heating feature of microwave irradiation contributes to the consistent and controlled expansion of GICs (Tarango-Rivero et al., 2022).

When exposed to a significant thermal shock up to 1000 ℃ or excessive heating, such as in a domestic microwave oven, graphite bisulfate undergoes irreversible expansion along the c-axis. This expansion can reach hundreds of times the original size. The expansion ratio, which is calculated as the reciprocal of the apparent density, can be remarkably high, reaching values as high as 300 (Goudarzi & Hashemi Motlagh, 2019; Murugan et al., 2021). The expanded graphite (EG) obtained after the expansion of graphite bisulfate is characterized by its non-compact nature as shown in Figure 2.4.

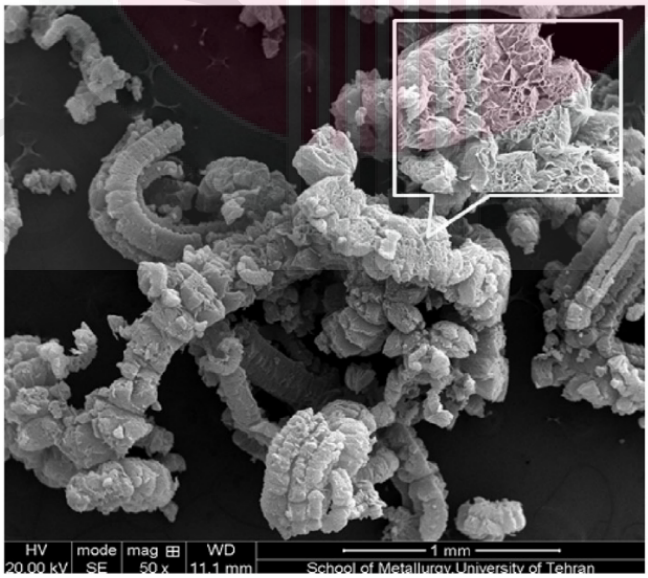

Figure 2.4: SEM images of expanded graphite
(Goudarzi & Hashemi Motlagh, 2019)

2.2.1 Expansion process

Graphite expansion reactions can be divided into three stages (oxidation, intercalation, and expansion). In the first stage of the graphite expansion process, the oxidant reacts with the edges of the graphite layers, leading to the loss of electrons and the creation of positive charges. These positive charges are then transferred to all the layers of graphite due to the carbon atoms' conjugate structure. The original binding between the layers, which is primarily governed by van der Waals forces, is affected by this transfer of positive charges. As a result, electrostatic repulsion occurs, leading to an increase in the spacing between the layers. In the second stage of the graphite expansion process, the intercalation agent penetrates the interlayer space of the graphite. As it does so, some anions from the intercalation agent are attracted to and adsorbed onto the graphite layers through electrostatic forces. This process contributes to the intercalation of foreign species between the layers of the graphite lattice. At high temperatures, the intercalation agent undergoes decomposition, generating gases as a byproduct. These gases exert a force, known as thrust, that acts to compress the layers along the axial direction of the graphite sheet. This compression leads to the expansion of the graphite, resulting in an increase in its volume (Dai et al., 2019; Murugan et al., 2021).

2.2.2 Mechanism of graphite expansion

Intercalation is a complex process where the intercalation process in graphite is chemical as well as physical in nature (Chung, 2016; T. Liu et al., 2018). When the chemicals ions form a chemical bond with atoms of the graphite. As the graphite

surface is not electrically neutral, and the atoms are built to bond in three dimensions. In principle, we are considering what happens at a solid-liquid interface. Actually, this 'surface' is much more complicated; it allows various types of bonds between ions and molecules on both sides of the solid-fluid interface. At the microscopic level, assuming that equilibrium exists at every point on the fluid-solid interface. Equilibrium here means between the graphite and the concentration of the species in that film. Primarily, this means equality of the chemical potentials on both sides of the liquid-solid interface. Next step is either oxidation and charge transfer, or diffusion of ions and molecules into the lattice or a combination of both processes. Some ion exchange theories proposed the presence of a thin liquid boundary layer (= film) that covers the solid. The time characterizing ion exchange depends on the relative times of (1) transport of the ions from the bulk solution to the boundary layer and (2) diffusion through the layer. In the case of a porous solid matrix, ions diffuse into the porous solid to adhere on the internal surface of the porous solid. Ion exchange involves also the transport of the released ions back to the bulk solution. The limiting rate is often dictated by the various diffusive steps, rather than by the actual exchange process. Firstly, the oxidant oxidizes the edges of the graphite layers, which causes its electron loss to be positively charged. Due to the conjugate structure of the carbon atoms, these positive charges transfer onto all the layers. The layers are originally bound by van der Waals forces. After the positive charges are transferred, the layer spacing increases because of electrostatic repulsion. Then, the intercalation agent penetrates the interlayer space, and some anions are adsorbed onto the layers through electrostatic attraction as schematically exhibited in Figure 2.5 (Dai et al., 2019; Murugan et al., 2021; Peng et al., 2018; Sykam et al., 2018).

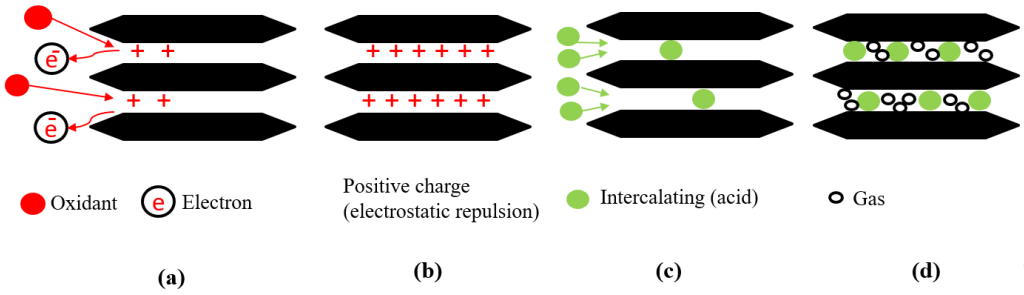

Figure 2.5: Mechanism diagrams of the complete reaction process. (a) and (b) Oxidation; (c) Intercalation; (d) gas release

2.2.2.1 Mechanism of expansion process of ATEG

The original structure of natural graphite flakes was altered to develop a worm-like morphology. Sodium peroxydisulfate decomposition involves the release of gases into graphite interlayer spaces. It is feasible that increasing pressure from gases will be sufficient to overcome the van der Waals forces within the interlayers, resulting in a certain thrust and the effective expansion of graphite in the direction of the C-axis (B. Hou et al., 2020). Therefore, it is concluded that when a binary-component solution containing sodium peroxydisulfate and concentrated sulfuric acid is employed for EG synthesis, portions of sodium peroxydisulfate operate as an oxidant, allowing H_2SO_4 to intercalate into the gallery of graphite interlayers. During the intercalation process of H_2SO_4, some of the excessive sodium peroxydisulfate may be drawn into the graphite's layers gallery. Chemically, the sodium peroxydisulfate forming an unstable compound when it reacts with the high concentration H_2SO_4 (B. Hou et al., 2020). Due to the chemical instability in an acidic medium, sodium peroxydisulfate may decompose and generate O_2 gas, causing an instantaneous pressure rise within the graphite interlayer gallery, causing graphite to expand. As the released gas is responsible for the graphite expansion, which raises the instantaneous pressure, it should generate more gas to get a larger expansion rate as showing in Figure 2.6.

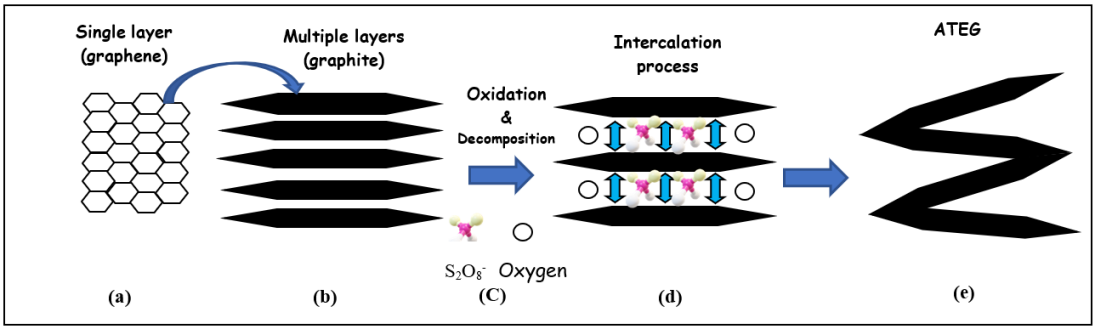

Figure 2.6: The mechanism scheme of graphite expansion (a) Single layer (b) Multi layers (c) Oxidation and decomposition (d) Intercalation (e) Expansion (worm-like structure)
(Elbidi et al., 2023)

Nevertheless, the mechanism behind this efficient process is yet understood entirely, and more research is needed. According to some studies, $S_2O_8^{2-}$ is strongly oxidizable and unstable in acidic medium, causing it to decompose and release oxygen (Kolthoff & Miller, 1951; Parvez et al., 2014; L. K. Wu et al., 2008). The proposed and modified reaction mechanisms of the decomposition for $Na_2S_2O_8$ mixed with the concentrated H_2SO_4 could be expressed as the following equations:

$$S_2O_8^- + H_2O \rightarrow 2HSO_4^- + {}^1/_2\, O_2 \qquad (2.2)$$

$$H_2S_2O_8 + H_2O \rightarrow H_2SO_5 + H_2SO_4 \qquad (2.3)$$

$$H_2SO_5 + H_2O \rightarrow H_2O_2 + H_2SO_4 \qquad (2.4)$$

$$\frac{d(S_2O_8^-)}{dt} = k_1[S_2O_8^-] + k_2[H^+][S_2O_8^-] \qquad (2.5)$$

The values of k_1 and k_2, respectively, are 6.0 X 10-5 $m.k^{-1}$ and 3.5 $X10^{-3}$ (min^{-1}) $(m/L)^{-1}$ at an ionic strength of 0.4 at 50 °C (Kolthoff & Miller, 1951). The $H_2SO_4^-$ shifted to $H_2S_2O_8$ and H_2O. The $H_2S_2O_8$ shifted to $S_2O_8^{2-}$ and H_2O in a moment (B. Hou et al., 2020; L. K. Wu et al., 2008). The ($S_2O_8^{2-}$) can be thermally activated to produce a powerful oxidant known as the sulfate free radical (SO_4^{2-}) (Bruell et al., 2003).

$$S_2O_8^{2-} \rightarrow 2SO_4^{2-} \quad (2.6)$$

$$2SO_4^{-} + 2H_2O \rightarrow 2HSO_4^{-} + 2HO \quad (2.7)$$

$$2HO \rightarrow H_2O + \frac{1}{2}O_2 \quad (2.8)$$

The standard oxidation- reduction potential for the reaction is 2.1V, compared 1.8V for hydrogen peroxide (H_2O_2) and 1.4V for the peroxy-monosulfate anion (HSO_5^-). This potential is greater than that of the permanganate anion (MnO_4^-), which is 1.7V, but slightly less than that of ozone, which is 2.2V (Block et al., 2004).

Mixing $Na_2S_2O_8$ with H_2SO_4 could result in a violent heat decomposition and pressure rise. Attention was focused on the $Na_2S_2O_8$ forming an unstable compound when it reacted with the high concentration of H_2SO_4, which had a great quantity of H_2SO_4 and with increasing the mass of $Na_2S_2O_8$ shifted quickly to $Na_2S_2O_8$ decomposition reaction.

2.2.2.2 Mechanism of HTEG

The expansion of expandable graphite results from disjoining pressure which is formed during its heating process. The process as shown in Figure 2.7 may be simply modeled as: intercalating species in expandable graphite can be considered as a liquid or solid phase which is fixed between the graphite sheets. Heating expandable graphite leads to conversion of the intercalating species from a liquid or solid phase to a gas phase. The formation of gas results in an increase in volume of the intercalating species of about 1000-fold. The pressure formed by this volume increase forces the adjacent graphite layers to separate, thereby resulting in the expansion of expandable graphite

(B. Hou et al., 2020; T. Liu et al., 2018). Therefore, the expansion ratio is affected strongly by the disjoining pressure which is derived from the gas. In order to increase expansion ratio, therefore, we should prevent gas from escaping through the edges of graphite flakes (M. Wang & Ji, 2012). The mechanism of graphite expansion at the micro-level can be described as follows:

In the initial stage, the oxidant agent causes oxidation of the edges of the graphite layers, resulting in the loss of electrons and the generation of positive charges. These positive charges are transferred to all layers due to the conjugate structure of carbon atoms. Graphite intercalation compounds (GICs) then enter the interlayer space, and certain anions are attracted to and adsorbed onto the layers through electrostatic attraction. During the decomposition of the GICs, gaseous products are formed. These gases create high pressure between the interlayer graphene sheets, exerting a force that pushes the graphite layers apart. The release of gases generates a driving force between the graphite sheets. This driving force overcomes the Van der Waals forces that hold the graphite sheets together, promoting the expansion of the particles from the edges towards the center of the sheets (Dai et al., 2019).

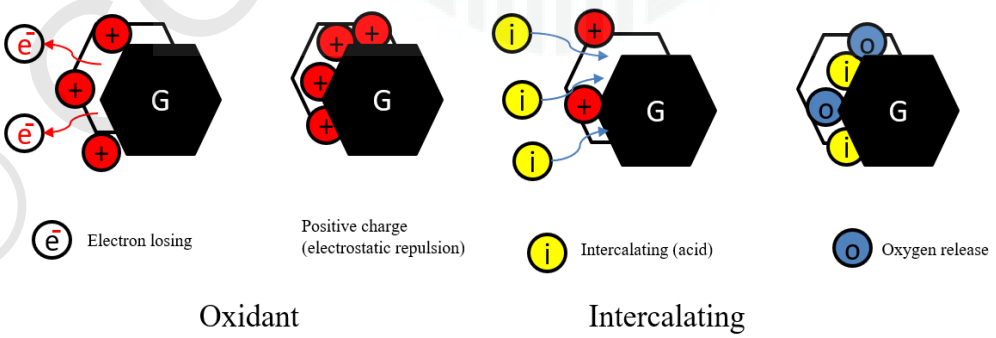

Figure 2.7: The mechanism scheme of graphite expansion of HETG

2.2.3 Characterizations

The expanded graphite has a unique structure and properties. Therefore, identifying crystal structures and functional groups is essential for future applications. There are different characterization techniques for the identification of expanded graphite.

In this regard, the structures of the natural graphite flakes and expanded graphite samples were analyzed by X-ray diffraction (XRD, Shimadzu, XED 6000).

X-ray diffraction (XRD) analysis is a widely used technique to determine the crystal structure and properties of materials. It provides information about the arrangement of atoms or molecules in a material by analyzing the diffraction pattern produced when a crystalline sample is exposed to X-rays. The basic principle behind XRD analysis is that when X-rays interact with a crystal, they undergo constructive interference, resulting in the generation of a diffraction pattern. This pattern consists of a series of distinct spots or peaks corresponding to the scattering of X-rays by the crystal lattice planes (Dresselhaus & Dresselhaus, 2002; Murugan et al., 2021).

In graphite expansion, X-ray diffraction (XRD) analysis can be used to investigate the expansion of graphite through measurements of its crystal structure. When graphite undergoes expansion, the interlayer spacing between the graphene layers increases. This change in interlayer spacing can be detected and quantified using XRD. By analyzing the XRD data, it is possible to determine the interlayer spacing in the expanded graphite and quantify the extent of expansion. This information can be used to study the effects of different processing conditions or intercalating agents on the

expansion behavior of graphite. XRD analysis provides valuable insights into the structural changes occurring in graphite during expansion, allowing for a better understanding of its properties and potential applications (Dresselhaus & Dresselhaus, 2002; Malard et al., 2009).

The surface functional groups of EG were analyzed by Fourier transform infrared spectroscopy (Nicolet FT-IR 6700, Thermo Fisher Scientific).

Fourier Transform Infrared (FTIR) analysis is a widely used spectroscopic technique that provides information about the chemical composition and molecular structure of a sample. It involves the measurement of the absorption, transmission, or reflection of infrared radiation by the sample. The basic principle behind FTIR analysis is that different chemical bonds within a molecule vibrate at specific frequencies, known as vibrational frequencies, in the infrared region of the electromagnetic spectrum. By measuring the absorption or transmission of infrared light across a range of frequencies, FTIR spectroscopy can identify the functional groups present in a sample and provide information about molecular structure, chemical bonding, and the presence of specific compounds (P. Wang et al., 2015).

FTIR analysis can be used to investigate the expansion or intercalation of graphite by studying the changes in its infrared absorption spectrum. Specifically, in the context of graphite expansion, FTIR analysis can provide information on the intercalation of molecules or ions between the graphene layers. It can detect the presence of intercalated species by changes in absorption bands related to the vibrational modes of the intercalated molecules or ions. By comparing the FTIR spectrum of expanded

graphite with that of the pristine graphite, one can identify new peaks or changes in peak intensity, which indicate the presence of intercalated species. The analysis can also provide insights into the type of intercalated species and the bonding interactions between them and the graphite layers. FTIR analysis is a valuable tool to study the structural changes in graphite due to intercalation or expansion and can help in understanding the intercalation mechanisms, optimizing intercalation processes, and developing new functional materials based on expanded graphite (Dresselhaus & Dresselhaus, 2002; Tarango-Rivero et al., 2022).

The micro-morphologies were viewed by field emission scanning electron microscopy (LEO 1445 VP scanning electron microscope). Generally, SEM analysis is a powerful imaging technique used to examine the surface morphology and topography of materials at high magnification. It provides detailed information about the sample's surface features, such as shape, size, texture, and composition. It provides valuable insights into the microstructure and surface properties of materials, allowing researchers and scientists to study, understand, and optimize material behavior and performance.

SEM analysis can be used to examine the surface morphology and structural changes in graphite due to expansion or intercalation. SEM analysis provides valuable visual information about the surface structure and morphology of expanded graphite. It can help in understanding the effects of expansion processes, intercalation agents, or other factors on the graphite structure (Tarango-Rivero et al., 2022).

2.3 Preparation Process of Expanded Graphite

The graphite expansion process refers to the controlled expansion of graphite, which involves increasing the spacing between the layers of graphene within the graphite structure. This expansion results in the formation of expanded graphite, which exhibits unique properties and enhanced functionalities compared to natural graphite (Chung, 2016; Dresselhaus & Dresselhaus, 2002; Saikam et al., 2022; Tarango-Rivero et al., 2022).

Currently, the preparation methods for producing expanded graphite are primarily based on the principle of intercalation expansion. The chemical oxidation method and electrochemical method are the most prominent and widely used approaches, and they have practical applications in various industries (Murugan et al., 2021). Alongside these methods, other techniques such as the microwave method, explosion method, and gas phase volatilization methods are utilized, each with its distinct approach for introducing intercalants and inducing expansion as shown in Figure 2.8 below. These methods provide alternative options depending on the desired degree of expansion, scalability, and specific properties required for particular applications (Dong et al., 2021).

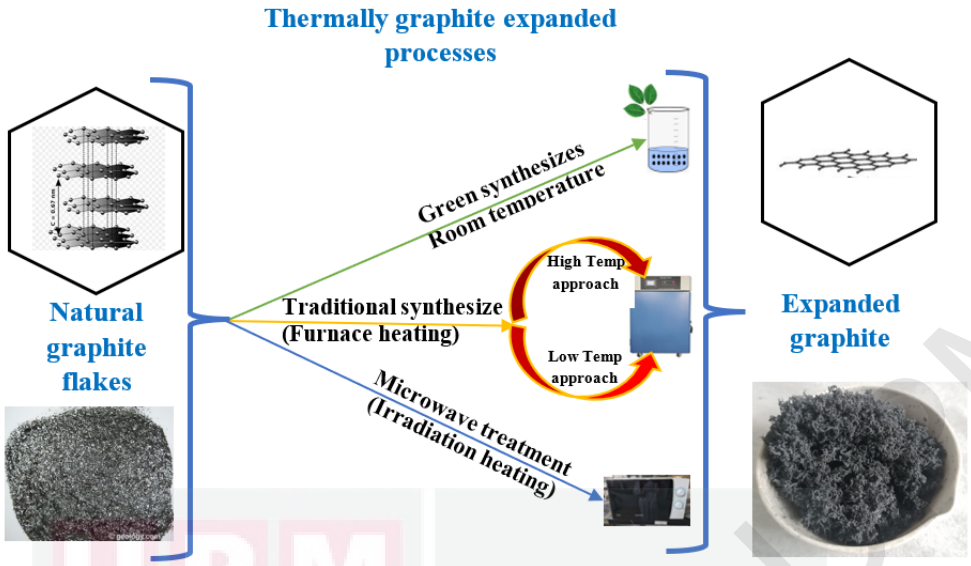

Figure 2.8: Graphite expansion techniques

2.3.1 Thermally expanded graphite

TEG, or thermally expanded graphite, is a type of graphite that has been thermally processed to increase its volume and create a highly porous structure. Some of the main features of TEG include a highly porous structure: TEG has a very open, sponge-like structure, which makes it useful in applications where high surface area is desired. Lightweight: TEG has a very low apparent density, typically between 0.002 and 0.02 g. cm^{-3}, which makes it an attractive material for lightweight applications. High mechanical properties: Despite its low density, TEG has excellent mechanical properties, with a tensile strength of around 10 MPa. Thermal conductivity: TEG has high thermal conductivity, typically between 25 and 470 W m^{-1} K^{-1}, making it useful in applications where heat needs to be transferred efficiently. High electrical conductivity: TEG also has high electrical conductivity, typically between 106 and 108 S m^{-1}, making it useful in electrical applications. Low-cost: TEG is relatively inexpensive to produce compared to other high-performance materials, making it

attractive for cost-sensitive applications (Mukhopadhyay & Gupta, 2012; Murugan et al., 2021).

Numerous researchers have dedicated their efforts to investigating different preparation methods for expanded graphite. They have explored various factors such as the choice of oxidant agent, intercalation agent, and heating duration in order to achieve specific goals such as maximizing surface area or minimizing bulk density. The objective is to find the optimal conditions that result in expanded graphite with desirable properties. In general, researchers have found that optimum conditions for preparing expanded graphite involve using either muffle or tubular furnaces with a temperature of around 900 °C or alternatively, irradiation techniques such as microwave heating have also been explored, with a heating time ranging from 5 to 30 seconds for both techniques. These conditions have been identified as effective in achieving the desired expansion and properties of the graphite material (Goudarzi & Hashemi Motlagh, 2019; Murugan et al., 2021).

2.3.1.1 TEG at room temperature

The impact of energy requirements on the overall cost of the expansion process is widely recognized. Methods that require high temperatures or extensive heating may consume more energy and increase operational costs. Energy-efficient preparation methods can help minimize costs and improve the economic viability of the process.
Liu et al. (T. Liu et al., 2017) presented a one-step method for the production of expanded graphite (EG) at room temperature as shown in Figure 2.9. In this method, the graphite material was intercalated by using concentrated sulfuric acid and

ammonium persulfate as the intercalating agents. The process involved the addition of the intercalating agents to the graphite, followed by sonication stirring to facilitate the mixing and intercalation process. Moreover, the amount of oxidant considered high compared to the intercalating agent and the graphite. The resulting expanded graphite exhibited a specific volume expansion of 225 mL/g, indicating a significant increase in volume compared to the original graphite material. However, it is important to note that this process did not involve any washing steps, which means that the expanded graphite produced may require additional treatment or purification steps before it can be used in applications. The one-step method described by Liu et al. offers a convenient approach for the production of expanded graphite, but the use of special techniques such as sonication stirring and the relatively high amount of oxidant used may have certain implications for the overall process and the quality of the final product.

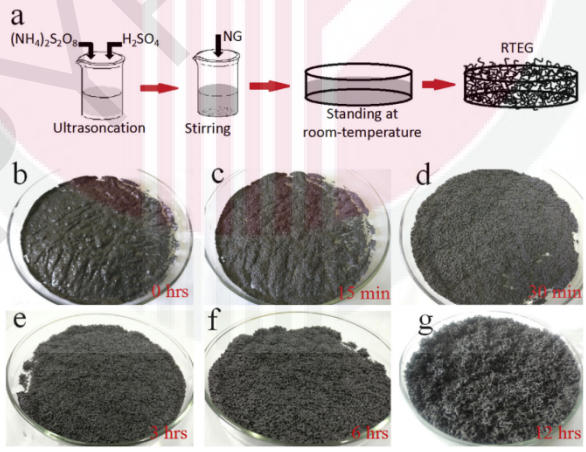

Figure 2.9: (a) The schematic diagram of thermally synthesis by the one-step room-temperature method. (b–g) Optical images of the graphite intercalation and morphological evolutions with time from 0 to 12 h
(T. Liu et al., 2017)

In a recent study by Ardestani et al. (Ardestani et al., 2022), expanded graphite was successfully developed with an expansion volume of 250 mL/g at room temperature. The process involved the use of a tricomponent system comprising potassium permanganate, sulfuric acid, and hydrogen peroxide for the reaction and intercalation of flake graphite. While the study provided details about the reaction and intercalation steps, it did not specifically mention the drying process for the resulting graphite intercalation compounds (GICs). The entire process, from GIC preparation to graphite expansion, took more than two days, indicating that it required a considerable amount of time. This extended duration is likely due to the need for sufficient intercalation and reaction time to achieve the desired expansion volume. Finally, the study by Ardestani et al. demonstrated the successful production of expanded graphite at room temperature using a tricomponent system. However, further information regarding the drying process and the specific conditions used for intercalation and expansion would be required for a more comprehensive understanding of the methodology.

Table 2.1: Summary of graphite expansion at room temperature

Strarting materials	Synthesis Temp. (°C) and special technique	EV (mL/g)	Ref.
Natural flake graphite (50mesh), H_2SO_4 (intercalator) and ammonium persulfate (oxidant)	Mixing by sonication for 5 min Intercalating time 30 s standing time 12 h Room temperature	225	(T. Liu et al., 2017)
Natural graphite flake (100 mesh); H_2SO_4 (intercalator); $KMnO_4$ and H_2O_2 (oxidants)	Intercalating 25.5 h Drying didn't mention Room temperature	250	(Ardestani et al., 2022)

2.3.1.2 TEG at low temperature

Graphite expansion at low temperatures refers to the process of inducing the expansion of graphite at temperatures below the typical high-temperature range used in thermal expansion methods. As presented in Figure 2.10 the low-temperature expansion allows

for the modification of graphite without subjecting it to extreme heat, providing certain advantages in terms of energy consumption and process control. These low-temperature expansion techniques offer advantages such as reduced energy consumption, enhanced process control, and the ability to modify graphite without compromising its structure or properties. However, it's important to note that the specific parameters, intercalating agents, and conditions required for low-temperature graphite expansion can vary depending on the desired degree of expansion and the targeted application (B. Hou et al., 2020; S. Hou et al., 2021).

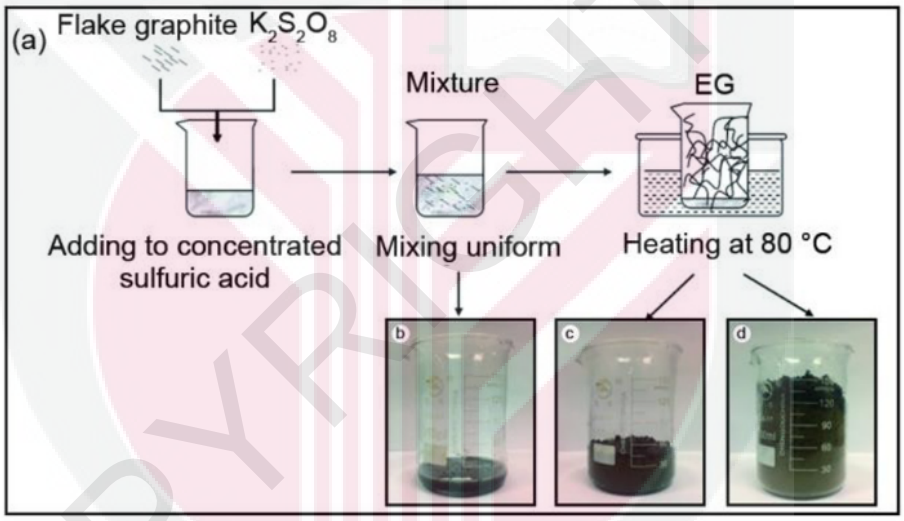

Figure 2.10: (a) An illustration of thermally synthesis of EG, (b) Heating for 0-30 s, (c) Heating for 1 min, and (d) Heating for 2 min at 80 ℃
(B. Hou et al., 2020)

S. Hou and his team (S. Hou et al., 2022) successfully prepared expanded graphite (EG) blocks using ultra-large flakes of graphite. They achieved this by intercalating the graphite with H_2SO_4 and utilizing a significant amount of H_2O_2 as an intercalating agent. The intercalation process involved reaching a maximum temperature of up to 80 ℃. Subsequently, the intercalated graphite underwent expansion within a closed container, resulting in the successful preparation of EG blocks with bulk densities

ranging from 0.008 to 0.024 g/cm^3. S. Hou, S. He, T. Zhu, and other researchers (S. Hou et al., 2021) proposed an environmentally friendly method for preparing expanded graphite using a binary system of sulfuric acid and hydrogen peroxide. Through this method, they were able to achieve an expansion volume of up to 320 mL per gram at a temperature of 60 ℃ for a duration of 4.5 to 9.5 hours. Bo Hou et al. (B. Hou et al., 2020) prepared EG using concentrated sulfuric acid and potassium persulfate. The process involved heating the mixture at 80 °C for 5 minutes, followed by vacuum filtration. The resulting material was then dried in an oven at 60 °C for 5 hours, resulting in the production of expanded graphite. The volume of EG obtained through this method reached 150 mL per gram. G. Zhao and his team (G. Zhao et al., 2019) employed a multi-step process to obtain expanded graphite with a 10-fold expansion volume. Before usage, they effectively eliminated moisture from the graphite through vacuuming and drying. Furthermore, they employed a sophisticated technique involving four chemicals and numerous intricate steps. J. Huang et al. (Huang et al., 2017) produced expandable graphite with an expansion volume of 282 mL per gram. This was achieved by utilizing two intercalating agents, sulfuric acid and phosphoric acid, along with hydrogen peroxide. The process took approximately 15 hours at a temperature of 60 ℃. The following table, Table 2.2, summarizes the low-temperature methods for EG production.

Table 2.2: Summary of graphite expansion at low-temperature

Strarting materials	T (℃) or IR (W)	Time	EV (mL/g) or density (g/cc)	Application	Ref.
NGF: H_2SO_4 (i) : H_2O_2 (ox)	Ti: 5℃, Td:80℃	ti = 30 min ts = 10 h td = 2 h	0.008–0.024 g/cc	Oil sorption	(S. Hou et al., 2022)
NGF (300 μm): H_2SO_4 (i): H_2O_2 (ox)	Ti: 5℃, Ts: 40 ℃, Td: 60 ℃	ti = 30 min ts = 4 h td = 5 h	320 mL/g	Oil sorbents	(S. Hou et al., 2021)
NGF (300 μm): H_2SO_4 (i): $K_2S_2O_8$ (ox)	Ti: 80°C, Td: 60 ℃	ti =5 min td = 5 h	150 mL/g	recommended use is graphene preparation	(B. Hou et al., 2020)
NGF (300 μm): $HClO_4$ (i): NH_2SO_3H: $NaNO_3$: $KMnO_4$: H_3PO_4: NaOH: (ox)	Ti: 40°C, Td: 60°C,	ti = 90 min td = 6 h	10 times	steam channelling control in heavy oil reservoirs	(G. Zhao et al., 2019)
NGF (50 m): $HClO_4$ (i): H_2O_2 (ox): $KMnO_4$ (ox): Hac (ox)	Ti: Tr, Ts:RT,40°C, Td: 60 °C	ti = 12 min ts = 6, 1 h td = 8 h	273 mL/g	steam plugging agent in heavy oil reservoirs	(Dai et al., 2019)
NGF (300 μm): H_2SO_4 (i): H_3PO_4: H_2O_2 (ox)	Ti: 40°C, Td: 65°C	ti = 3 h td = 12 h	282 mL/g	Flame-resistance	(Huang et al., 2017)

m: mesh, i: intercalator, ox: oxidant, Ti: intercalating temperature, Ts: standing temperature, Td: drying temperature, RT: room temperature, ti = intercalation time, ts: standing temperature, td = drying time, te: expansion time,

2.3.1.3 TEG at high temperature

Graphite expansion at high temperatures refers to the process of inducing the expansion of graphite by subjecting it to elevated temperatures as shown in Figure 2.11. This high-temperature treatment allows for the modification of graphite by promoting the separation and expansion of the graphene layers within the structure. Graphite is heated to temperatures typically exceeding 1000 ℃ in a controlled environment. As the temperature increases, the thermal energy disrupts the interlayer bonding forces, causing the graphene layers to separate and expand. The expansion can be controlled by adjusting the temperature and duration of heating (Z. X. Liu et al., 2022; L. Wang et al., 2020).

The high-temperature expansion methods provide greater control over the degree of expansion and allow for modifications to the graphite structure. However, it's important to note that the specific parameters, heating rates, and temperature ranges required for high-temperature graphite expansion can vary depending on the desired outcome and application (Çalın et al., 2020).

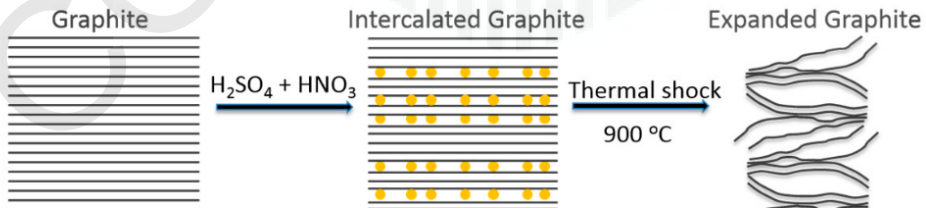

Figure 2.11: Schematic showing the expansion of graphite at high temperature (Seredych et al., 2018)

G. Yin et al. (2021) produced expanded graphite at an expansion temperature of 900 ◦C. The specific surface area of EG was found to be approximately 120 times larger

than that of NFG (non-expanded graphite). Additionally, they observed that the pores in EGs were predominantly distributed within the pore size range of 3.0–10 nm. This indicates that the EGs prepared in their study can be classified as mesoporous carbon materials (Yin et al., 2021).

Bannov et al. (2021) synthesized expanded graphite using the programmable heating technique, employing heating with a constant rate of 20 ◦C/min from room temperature to 400–700 ℃. They compared this method with thermal shock as methods of producing expanded graphite and found that the programmable heating technique demonstrated greater efficiency, particularly at a temperature of 400 ℃. The resulting expanded graphite exhibited surface areas of 699 and 184 m^2/g, respectively. The researchers also discovered that their novel method of production, involving intercalated graphite, enabled them to achieve a relatively higher yield ranging from 78% to 90% (Bannov et al., 2021).

Nirwan et al. (2021) conducted a study where they prepared expanded graphite utilizing graphite flakes with a mesh size of +100. They employed $KMnO_4$ as an oxidizing agent and H_2SO_4 as intercalates. Under optimized conditions, they achieved a high expansion volume of 375 ml per gram and a good surface area of 100 m^2 per gram. The optimized ratios of graphite flakes, $KMnO_4$, and H_2SO_4 were 1:0.15:2.5, respectively, with a 65% mass concentration. The reaction time was optimized to 3 hours (Nirwan et al., 2021).

K. H. Wu et al. (2021) conducted a study to produce expanded graphite with a high expansion volume. They used a mixture of sulfuric acid and nitric acid as the

intercalating agents and natural flake graphite as the starting material. The intercalation process involved mixing the acids with the graphite for a duration of 4 hours. This allowed the acids to penetrate between the layers of the graphite and form graphite intercalation compounds (GICs). Subsequently, the GICs were dried for 24 hours at a temperature of 60 ℃ to remove any residual moisture. Finally, the GICs heated up to 1150 ℃ to obtain the expanded graphite (K. H. Wu et al., 2021).

Calin et al. (2020) conducted an investigation to examine the relationship between the expansion ratio and the pore structure of expanded graphite. They achieved this by modifying the expansion conditions of expandable graphite with different flake sizes. The highest expansion ratio of 80 ml/g was obtained for the 10-mesh sample when exposed to a temperature of 1150 ℃. In contrast, the +50 mesh (>300μm) commercial expandable graphite demonstrated an expansion ratio of 400 ml/g at the same temperature (1150 ℃) within a closed-lid crucible (Çalın et al., 2020).

Wang et al. (2020) carried out the preparation of expanded graphite through a series of steps. Initially, they converted graphite into intercalated graphite by subjecting it to chemical oxidation using a mixture of sulfuric and nitric acid. The resulting intercalated graphite was then dried in a vacuum oven at 65 °C for 24 hours. Subsequently, it underwent heat treatment at 900 °C for 60 seconds. The porous graphite sheets obtained from this process were further compressed to form bulk expanded graphite. The density of the bulk expanded graphite was increased by applying higher pressure (X. L. Wang et al., 2020).

Z. Liu et al. (2018) produced expanded graphite with an expansion ratio of up to 100 times that of ordinary graphite. They achieved this by utilizing a rarely large flake graphite, specifically a 9-mesh graphite (Z. Liu et al., 2018).

Tingkai Zhao et al. (2018) produced expanded graphite through a series of steps, including stirring, filtering, washing, and drying. Subsequently, they achieved the expansion of graphite by subjecting it to rapid expansion in a muffle furnace at a temperature of 800 ◦C for a duration of 10 seconds (T. Zhao et al., 2018).

Peng et al. (2018) conducted a study on the preparation of expandable graphite at a low temperature of 400 ℃. They utilized natural flake graphite as the raw material and employed potassium permanganate, perchloric acid, and ammonium nitrate as oxidative intercalants. Through the oxidation and intercalation process, the intercalation reagents introduced oxygen-containing groups onto the edges and within the layers of the graphite product. This led to an expansion of the interlayer spacing (Peng et al., 2018).

Trivedi et al. (2018) made an observation regarding the oxidation of graphite by potassium permanganate in concentrated sulfuric acid compared to a potassium dichromate-concentrated sulfuric acid mixture. They found that potassium permanganate in concentrated sulfuric acid more efficiently oxidizes the sp^2 carbon atoms in graphite, resulting in the formation of graphite bisulfate. Furthermore, they investigated the impact of varying heat treatment temperatures ranging from 400 ℃ to 1030 ℃ on expandable graphite treated with $KMnO_4$ in concentrated sulfuric acid and graphite treated with $K_2Cr_2O_7$ in concentrated sulfuric acid. Their findings indicated

that the expandable graphite treated with $KMnO_4$ in concentrated sulfuric acid exhibited superior expansion compared to the graphite treated with $K_2Cr_2O_7$ in concentrated sulfuric acid (Trivedi et al., 2018).

J. He et al. (2017) successfully prepared sulfur-free expanded graphite using a two-step chemical oxidation process. They utilized natural flake graphite as the precursor material. The resulting expanded graphite exhibited an expansion volume of 420 mL/g (He et al., 2017).

Table 2.3: Summary of graphite expansion at high-temperature

Strarting materials	T (°C) or IR (W)	Time	EV (mL/g) or density (g/cc)	Application	Ref.
NGF: H_2SO_4(i): HNO_3(ox)	Ti: RT, Td: 60°C 1150°C	ti = 4 h td = 24 h	300 mL/g 34.8 m^2/g	Oil sorption	(K. H. Wu et al., 2021)
NFG (50-60) m: $HClO_4$(i) : $K_2Cr_2O_7$: CH_3COOH: HNO_3: (ox)	Ti: RT, Td: 80°C 900 °C 5s	ti = 40 min td = 40 min	120 mL/g 124 m^2/g	Adsorption	(Yin et al., 2021)
NGF (+100) m: H_2SO_4 (i): $KMnO_4$ (ox)	Ti: RT, Ts: 120°C 900 °C	ti = 3 h ts = overnight	375 mL/g	Oil spills application	(Nirwan et al., 2021)
NGF (+50 and 10) m: H_2SO_4 (i): HNO_3(ox)	Ti: RT, Td: 100°C 1150 °C 2min	ti = 130 min td = 24 h	400mL/g 4.63 m^2/g 80mL/g 41m^2/g	Study different flake sizes on EG production	(Çalın et al., 2020)
NGF: H_2SO_4 (i): HNO_3(ox)	Ti: --, Td: 65 °C 900 °C 60s	ti = -- td = 24 h	0.21 g/cc	Phase change materials	(X. L. Wang et al., 2020)
NGF >1.25 mm: $HClO_4$(i): H_2O_2 (ox)	Ti: RT, Td: 80 °C 1100°C 60s	ti = 50min td = --	178.3 mL/g 100.97 m^2/g	Oil sorption	(Pham et al., 2019)
NGF (+100) m: H_2SO_4 (i): $KMnO_4$: $K_2Cr_2O_7$ (ox)	Ts: RT, Td: 120°C 700°C --min	ts = 21 h td = 1 h	130 mL/g	Study the effect of oxidizing agents	(Trivedi et al., 2018)
NFG 50 m: $HClO_4$(i): $KMnO_4$: NH_4NO_3 (ox)	Ti: 30°C, Td: 70°C 900°C 5min	ti = 10 min td = 4 h	480 mL/g	Recommended use in flame retardant	(Peng et al., 2018)
NFG: H_2SO_4(i): HNO_3(i): $KMnO_4$ (ox)	Ti:RT, Td: 90°C 800°C 10 s	ti = 30 min td --	Pore volume 0.0185 cc/g.nm	Super-capacitors	(T. Zhao et al., 2018)
NFG 9 m: H_2SO_4(i): $KMnO_4$ (ox)	Ti: RT, Td: 70°C 1000°C 70s	ti = 1h td --	100 times	Wound dressing	(Z. Liu et al., 2018)
NGF (500µm): $HClO_4$(i)	Ti: RT, 1000°C 60s	ti = 10 s	375 mL/g	Adsorption	(Sykam et al., 2018)
NFG: $HClO_4$(i):KH_2PO_4: $KMnO_4$ (ox)	Ti: 30°C, Td: 65°C 950 °C 15s	ti = 50 min td = 24 h	420 mL/g 245 m^2/g	Adsorption	(He et al., 2017)

m: mesh, i: intercalator, ox: oxidant, Ti: intercalating temperature, Ts: standing temperature, Td: drying temperature, RT: room temperature, ti = intercalation time, ts: standing temperature, td = drying time, te: expansion time, Trs: thermal shock

2.3.1.4 TEG via microwave irradiation

Preparation of expanded graphite using the microwave irradiation technique involves subjecting graphite material to microwave radiation, which induces thermal energy and leads to the expansion of the graphite structure (Saikam et al., 2022). The microwave irradiation technique offers advantages such as rapid heating, uniform heating distribution, and potential energy efficiency compared to traditional thermal methods. It allows for the preparation of expanded graphite with unique structural and morphological properties (Dong et al., 2021; Murugan et al., 2021).

Microwave irradiation is a more promising method compared to conventional heating for several reasons. Firstly, it can be conducted at room temperature, eliminating the need for high-temperature environments. Secondly, microwave irradiation significantly reduces the processing time, allowing for faster production. Lastly, this method consumes less energy, making it a more energy-efficient option. Overall, the use of microwave irradiation offers advantages such as reduced processing time, lower energy consumption, and the ability to operate at room temperature, making it a favorable choice for the preparation of expanded graphite (Z. X. Liu et al., 2020; Zhou et al., 2018). Saikam et al used microwave irridaiton to expand graphite as shown in Figure 2.12.

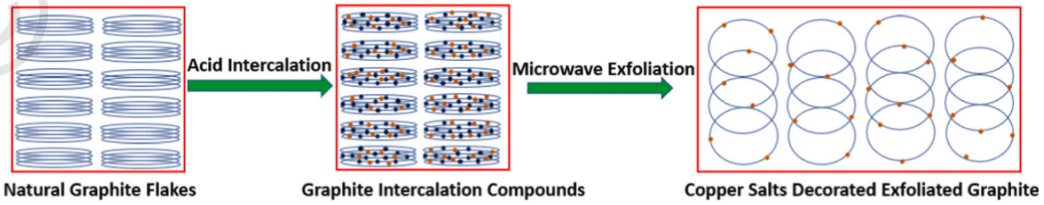

Figure 2.12: Schematic representation of the expansion of graphite via microwave technology
(Saikam et al., 2022)

Gabriela Tarango-Rivero et al. (2022) focused on developing alternative chemical routes for producing expanded graphite with reduced environmental impact, based on the principles of green chemistry. They proposed a process for expanded graphite production that employs only two intercalation chemicals, significantly reducing the consumption of sulfuric acid to just 10%. Additionally, they eliminated the use of strong oxidant salts, which are known to have negative environmental effects. During their study, the team evaluated three key process parameters: the effect of milling, peroxide concentration, and microwave expansion. These parameters were carefully examined to optimize the production process and achieve the desired expansion of the graphite material. The research carried out by Gabriela Tarango-Rivero and her team demonstrates a commitment to developing more sustainable methods for expanded graphite production, considering the principles of green chemistry and minimizing the environmental impact associated with traditional production approaches (Tarango-Rivero et al., 2022).

Siakam et al. (2022) developed EG by oxidizing natural graphite with perchloric acid and cupric nitrate. The mixture was stirred at ambient temperature for 20 s. During the mixing step, perchloric acid was intercalated between the layers of graphite, resulting in the formation of graphite intercalation compounds (GICs). After that, the mixture was transferred to a microwave oven and irradiated for 40 s at 800 W. The increase of the graphite layers was noticed at this time, along with fuming and lightning effects. SEM investigation revealed the worm-like structure of EG, and the surface morphology of EG revealed a well-expanded structure with expansion occurring along the direction of the c-axis (Saikam et al., 2022).

Zhen-Xue Liu et al. (2022) synthesized expanded graphite using two different chemical methods but the same technique. They referred to this expanded graphite as "SEG" or spitball expanded graphite. It is noteworthy that the two types of SEG exhibited significant differences compared to traditional expanded graphite. They lacked the characteristic worm-like structures and web-like pores typically found in traditional expanded graphite. However, these unique properties make SEG suitable as user-friendly, non-polar adsorbents in various engineering applications that do not rely on a homogeneous structure. SEG can be utilized for purposes such as adsorption or separation of aromatic compounds and graphene production (Z. X. Liu et al., 2022). Zhen-Xue Liu et al. (2020) conducted a study where they produced a slightly expanded graphite with an expansion ratio of only four times. The researchers used a microwave treatment with a power of 1000 W for 2 minutes, which is considered the highest microwave power used thus far in similar studies. The preparation method they employed involved an improved version of the Hummers method, which aimed to convert natural flake graphite into expanded graphite. The process involved a sophisticated procedure and the use of excessive chemicals, resulting in only a slight expansion volume being achieved (Z. X. Liu et al., 2020).

Van Pham et al. (2019) synthesized EG in two steps. First, graphite fakes, potassium permanganates, acetic anhydride, and perchloric acid were mixed for a few seconds in a ratio of 1: 0.5: 1: 0.4 (g/g), and the mixture was placed in a microwave oven at 360 W for 50 seconds to generate graphite sheet expansion (Pham et al., 2019).

Ngoc Bich Hoang et al. (2019) focused on the production of sulfur-free expanded graphite. They employed a specific method utilizing perchloric acid as a key

component. The expansion of graphite was achieved through the utilization of potassium permanganate as an oxidizing agent and perchloric acid as an intercalating agent. The process was facilitated by the application of a microwave-assisted technique. This approach allowed for the production of sulfur-free expanded graphite, which can have potential applications in various fields (Hoang et al., 2019).

Tianyu Zhou et al. (2018) developed a one-step synthesis process for the production of boron acid-modified expanded graphite (B-EG) with the assistance of microwave irradiation. The process involved the use of H_2SO_4 and H_3BO_3 as intercalating agents, while $KMnO_4$ served as the oxidizing agent. The resulting B-EG exhibited a unique structure characterized by a combination of worm-like and lamellar morphology, along with a significant presence of small dispersed particles throughout the material (Zhou et al., 2018).

Sykam, Jayram, and Rao (2018) conducted a study on the rapid and cost-effective production of expanded graphite using microwave irradiation and a binary system of NFG (natural flake graphite) and perchloric acid. The process involved intercalating the graphite flakes with perchloric acid, which quickly entered the layers and formed graphite intercalation compounds (GICs). The GICs were then rapidly expanded using microwave heating, resulting in the formation of highly porous EG materials with a unique worm-like structure. The expansion volume achieved was 524 mg/L, and the entire process took approximately one minute (60-70 seconds) to complete (Sykam et al., 2018).

Table 2.4: Summary of graphite expansion via microwave irradiation technique

Strarting materials	T (°C) or IR (W)	Time	EV (mL/g) or density (g/cc)	Application	Ref.
NGF >1.25 mm: $HClO_4$(i) $KMnO_4$: $(CH_3CO)_2O$ (ox)	Ti: RT, 360 W 50 s	ti =10 s 60 s	244 mL/g 147.5 m^2/g	Oil sorption	(Pham et al., 2019)
NGF >1.25 mm: $HClO_4$: $KMnO_4$: $(CH_3CO)_2O$ (ox)	Ti: RT, 720 W 40s	ti = 10 s	29.9523 m^2/g	Adsorption	(Hoang et al., 2019)
NGF: H_2SO_4(i): H_3BO_3: $KMnO_4$ (ox)	Ti: RT, 350 W 30s	ti = 3 min	--	Adsorption	(Zhou et al., 2018)
NGF granule size 1.25 mm: H_2SO_4(i): H_2O_2 (ox)	Ti: RT, 720 W 30s	ti = 100 min	196.67	--	(Thinh et al., 2018)
NGF (500µm): $HClO_4$(i)	Ti: RT, 800 W 60s	ti = 10 s	524 mL/g	Adsorption	(Sykam et al., 2018)
NGF: H_2SO_4(i): H_3PO_4(i): $KMnO_4$ (ox)	Ti: RT, Td: 80°C 350 W 30s	ti = 3 min td = --	70 mL/g	Adsorption	(Fengshuang Zhang et al., 2015)
NGF (40µm): HNO_3(i): $KMnO_4$ (ox)	Ti: RT, 700 W 60s	ti = 5 min	212.33 mL/g	Recommended use are production of graphene and oil adsorption	(Kim et al., 2014)
NGF (510µm): $HClO_4$(i): $KMnO_4$: $(CH_3CO)_2O$ (ox)	Ti: RT, 600 W 50s	ti =10 s	565 mL/g	Oil sorption	(Sykam & Kar, 2014)

m: mesh, i: intercalator, ox: oxidant, Ti: intercalating temperature, Ts: standing temperature, Td: drying temperature, RT: room temperature, ti = intercalation time, ts: standing temperature, td = drying time, te: expansion time, Trs: thermal shock, IR: irradiation power

2.4 Applications of EG

Expanded graphite is a highly prospective material due to its unique properties including very low density with typical apparent densities of 0.002–0.01 g/cm^3, high aspect ratio, high porous structure, closest electrical/thermal conductivity and thermal/chemical stability to natural graphite and ease of preparation and low cost (Goudarzi & Hashemi Motlagh, 2019).

Demand for expandable natural flake graphite is also expected to increase, principally for use as a fire-retardant additive in foam, plastic and various construction materials. For this use, suitable flake graphite is intercalated with a chemical species (e.g., halogens, sulfate, nitrate, organic acids, ferric chloride) which will rapidly gasify at high temperatures causing the graphite to exfoliate/expand to between 80 and 300 times. Coarse flakes (>300 μm) show the highest expansion but finer sizes (<150 μm) are preferred for some applications. On expansion, graphite retards the spread of fire and minimizes the creation of toxic gases and fumes. Expanded graphite can also be interlocked and compressed to give an essentially flat, flexible, integrated graphite foil, which is widely used as gaskets and seals, with potential use also as a separation layer in fuel cells and redox flow batteries as shown in Figure 2.13 (Keeling, 2017).

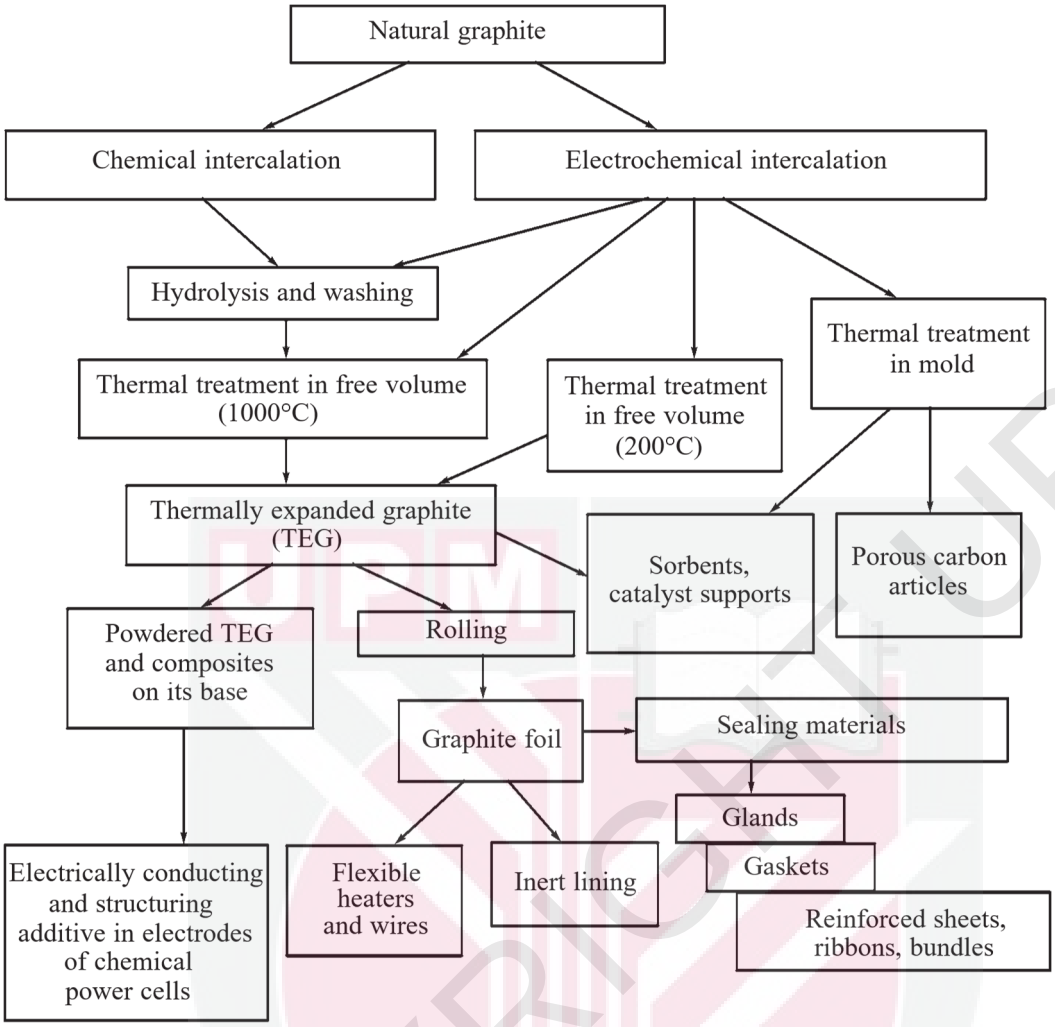

Figure 2.13: Expanded graphite applications
(Yakovlev et al., 2006)

2.5 Background of Oil Spills

An oil spill occurs when liquid petroleum hydrocarbons are released into the environment, either accidentally or intentionally, in significant amounts. Such spills can take place in various locations, including marine environments such as oceans, seas, or rivers, as well as on land from pipelines or storage sites. The impact of oil spills on ecosystems, wildlife, human well-being, and the economy makes them a major environmental issue (Tian et al., 2020).

Oil spills have harmful effects not only in marine environments but also in freshwater ecosystems, such as lakes, rivers, and wetlands. The term "aquatic" encompasses both marine and freshwater environments (M. B. Wu et al., 2021). When an oil spill occurs in an aquatic environment, it poses a threat to organisms residing on or near the water surface, as well as those living underwater. Additionally, the spill can disrupt the food chain, impacting valuable resources for human consumption. The severity of the spill's impact is influenced by several factors, including the characteristics of the oil itself and natural conditions such as water temperature and weather. Different types of habitats exhibit varying sensitivities to oil spills (Mahmoud, 2020; K. H. Wu et al., 2021).

Oil spills pose severe environmental catastrophes, resulting in substantial and long-term consequences for the affected ecosystems, socio-economic activities, and the overall environment. The long-term impact of environmental pollution emphasizes the urgency to enhance measures for the protection of coastlines and marine ecosystems. Various materials have been employed in endeavors to restore marine and wildlife habitats, although with varying degrees of success, in the context of oil spill cleanup and recovery (Kartel et al., 2023; Tarango-Rivero et al., 2022).

2.5.1 Oil sorption technique

According to the reviewed literature, conventional treatment methods exhibit poor performance and have other significant drawbacks, including lengthy treatment times, extensive land requirements, and high capital costs. Even though these techniques are employed for oil spill remediation, adsorption is considered the most suitable method

(Soliman et al., 2020). The process of oil sorption using absorbents is a practical method for addressing oil slicks in areas affected by spills. Adsorption has been viewed as a promising technique due to its simplicity, ease of use, high removal capacity, and rapid removal of pollutants (He et al., 2017; Soliman et al., 2020).

Generally, the process of oil adsorption in sorbents consists of three chemical stages. The first stage is diffusion, where oil molecules penetrate the surface of the sorbent. The second stage involves the trapping of oil within the structure of the sorbent through capillary action. In the final stage, oil droplets accumulate within the porous and rough structures of the sorbent (Hadela et al., 2020; Wahi et al., 2013).

An excellent absorbent material possesses unique characteristics that make it highly effective in absorbing liquids. These characteristics include a high absorption capacity, which allows it to absorb and retain a significant amount of oil relative to its own weight. It also has a fast absorption rate, quickly drawing in the oil upon contact, minimizing the spread of the spilled substance and reducing further contamination. Additionally, it has good retention properties, ensuring that the absorbed liquid is contained within the material without significant leakage or release (Al-Majed et al., 2012; Soliman et al., 2020).

Furthermore, an excellent absorbent material is environmentally friendly and biodegradable. It does not introduce additional harm to the environment and naturally degrades over time. Cost-effectiveness is another important factor, as the material should provide a balance between performance and affordability. It should offer a reasonable cost per unit of absorbency, making it a practical choice for spill

management. Lastly, recyclability is a desirable characteristic, as it promotes sustainability and reduces waste (Hadela et al., 2020; Rozi et al., 2017; K. H. Wu et al., 2021). By meeting these specifications, an absorbent material can be considered excellent in terms of its effectiveness, efficiency, and suitability for managing spills across various industries and applications.

2.5.2 Adsorbent used to treat oil spills

Shokry et al. (2020) prepared and tested the absorption of nano-magnetic activated carbon hybrid material, and the result demonstrated of oil adsorption capacity of 30.2 g/g (Shokry et al., 2020). Soliman et al. (2020) conducted a study on the absorption capacity of wood sawdust-coated magnetite nanoparticles that were functionalized with stearic acid. In their research, they determined that the maximum absorption capacity reached 41.22 g/g of crude oil (Soliman et al., 2020). Mahmoud et al. (2020) modified of raw flax fiber through acetylation and microwave energy enhances its hydrophobic properties, resulting in improved oil sorption capacity (24.54 g/g) compared to raw (13.75 g/g) and microwave fiber (17.42 g/g) (Mahmoud, 2020). Table 2.5 illustrates the oil absorption capacity of different sorbents.

Table 2.5: Comparison of adsorption capacity of various adsorbent materials

Grade	Sorbent	Sorption capacity (g/g)	Oil type	References
High capacity, >50 g/g	Carbon fiber aerogel from bamboo	70 – 85	Diesel oil – crude oil	(Yang et al., 2015)
	Graphene sponge	68.5	Lubricating oil	(Bi et al., 2012)
	Exfoliated graphite by microwave irradiation	56	Engine oil	(T. Wei et al., 2008)
	Functional graphite sheets	47 - 63	Diesel oil - Engine oil	(S. Hou et al., 2021)
Med-capacity 25 – 50 g/g	TiO_2-coated nanocellulose	40	organic solvents	(Korhonen et al., 2011)
	Polyimide/graphene aerogel	37.44	Motor oil	(Ren et al., 2019)
	Nanofibril Aerogels	24 - 46	Heavy oil	(Mulyadi et al., 2016)
	Magnetic cellulose aerogel/TiO_2 aerogel	28	Diesel oil (paraffin oil)	(Chin et al., 2014)
	Magnetic graphene/CNT foam	27	Motor oil	(Yang et al., 2014)
Low capacity, <50 g/g	Polysulfone/$NiFe_2O_4$ nanostructured fibrous	15.11	Motor oil	(Cojocaru et al., 2017)
	Expanded perlite	3.5	Light crude	(Al-Majed et al., 2012)
	Magnetic cobalt ferrite nanoparticles	3.6	Used motor oil	(Hadela et al., 2020)
	Palm Fatty Acid Functionalized Fe_3O_4 Nanoparticles	3.5	Lubricant oil	(Rozi et al., 2017)

Sorbents can be divided into synthetic and natural types. Currently, in developed countries, the most effective sorbents are made of foamed synthetic materials. Various materials have been proposed as adsorption agents, including nanomaterials, nanocomposites, nanoparticles, clays, biopolymers, metal-organic frameworks, and zeolites. Among carbon-based materials, porous carbon materials are commonly used in wastewater treatment due to their micropores and excellent adsorption capacity. Activated carbon, in particular, has been recommended as an ideal agent for removing contaminants from water. However, its production and regeneration can be quite expensive (Tarango-Rivero et al., 2022). Similarly, special molecules such as carbon nanotubes and graphene have demonstrated exceptional performance, but their current cost renders them impractical for utilization in oil spill remediation (Al-Majed et al., 2012).

The intrinsic properties of expanded graphite, including its low density, high porosity, and electrical conductivity, have received significant global attention for their potential applications. This material shows promise in various fields, including fuel cells, electromagnetic interference shielding, catalysts, vibration damping, supercapacitors, biomedical materials, and as a spilled oil adsorbent (Eltaweil et al., 2022; Kartel et al., 2023).

2.5.3 Potential use of EG in oil sorption

Expanded graphite has indeed gained significant attention as a promising material for adsorption applications, particularly in the field of oil sorption. Many interesting articles have been published so far on expanded graphite for oil spill recovery this is

evident from the increasing number of publications focused on expanded graphite as an adsorbent between 2010 and 2020, as shown in Figure 2.14 (Singh et al., 2020).

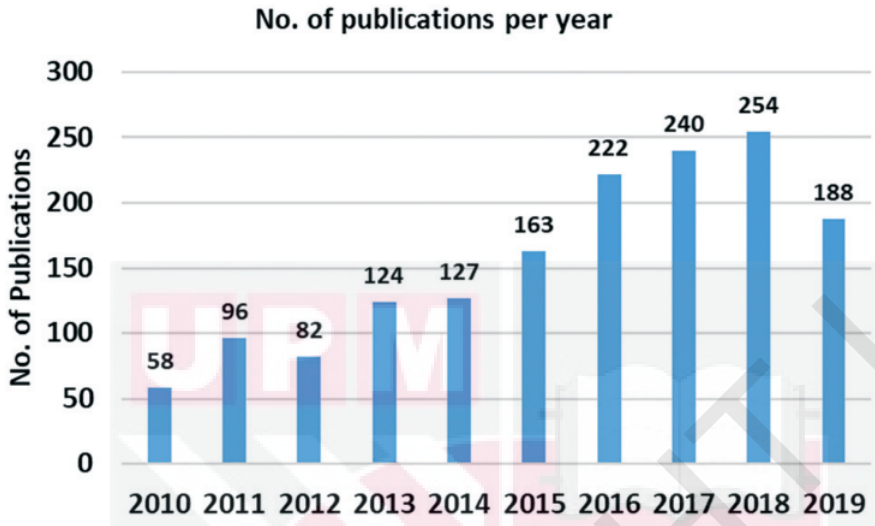

Figure 2.14: Statistical plot for the number of publications per year on materials for oil recovery applications. The keyword used for the search is "material in oil spill application."
(Singh et al., 2020)

The growing interest in expanded graphite as an adsorbent can be attributed to its unique properties, such as high porosity, large surface area, and excellent adsorption capacity. The expanded structure of graphite provides numerous interconnected pores and channels, enabling efficient adsorption of various substances, including oils and hydrocarbons.

Figure 2.14 likely depicts a graphical representation or trend analysis showing the rising trend of publications related to the use of expanded graphite as an adsorbent during the specified time period. This indicates the increasing recognition and exploration of expanded graphite's potential in addressing environmental challenges related to oil spills and contamination. The extensive research and development in this

area highlight the growing importance of expanded graphite as a versatile and effective adsorbent material with promising applications in oil sorption and environmental remediation.

The first work on the application of expanded graphite for oil sorption was reported by Robert L. Morgan and Ronald G. Schmidt in 1975. The patent titled "Oil Sorbent" (US Patent No. 3,877,945) describes a method for preparing an oil sorbent material using expanded graphite. This patent provides insight into the early development of expanded graphite-based materials for oil sorption applications.

Inagaki and Toyoda were indeed early pioneers in recognizing the high effectiveness of expanded graphite for oil sorption applications. Their work conducted two decades ago, shed light on the remarkable oil sorption capabilities of expanded graphite. Their research likely demonstrated that expanded graphite exhibits a strong affinity for oils, allowing for efficient sorption of oil from water or when in direct contact with pure oil. This characteristic makes expanded graphite a promising material for oil spill cleanup, environmental remediation, and other oil sorption applications. The ability of expanded graphite to selectively adsorb and retain oils while repelling water is attributed to its unique structure and surface properties. The expanded structure creates a highly porous material with a large surface area, providing ample space for oil molecules to be adsorbed and trapped within its interconnected pores. The early work by Inagaki and Toyoda played a significant role in establishing the foundation for further research and development in utilizing expanded graphite as an effective sorbent material for oil spills and related environmental challenges. Their findings have since paved the way for continued exploration and optimization of expanded graphite-based

sorbents for efficient oil sorption and environmental remediation (Toyoda & Inagaki, 2000).

In addition, Thinh and his team (Thinh et al., 2016) prepared magnetic of expanded graphite by coating $CoFe_2O_4$ particles on expanded graphite (EG) using the sol-gel method, researchers aimed to develop magnetic expanded graphite with enhanced sorption capacities for oil spill treatment. The results of the study demonstrated successful deposition of $CoFe_2O_4$ particles onto the surface of EG, indicating uniform and effective coating. The as-synthesized magnetic EG-$CoFe_2O_4$ composite exhibited high sorption capacities for different types of oils, namely Fuel oil (FO), Diesel oil (DO), and Crude oil (CO). Among these oils, the highest sorption capacity was observed for Fuel oil. This finding suggests that the EG-CoFe2O4 composite has great potential as a promising material for oil spill treatment, where the sorption of Fuel oil is of particular interest. The sorption capacities of the EG-$CoFe_2O_4$ composite were quantified, with the highest sorption capacity observed for Fuel oil at 54.13 g/g. Although slightly lower, the composite also exhibited considerable sorption capacities for Crude oil (50.79 g/g) and Diesel oil (42.12 g/g). These results highlight the potential of the magnetic expanded graphite composite, EG-$CoFe_2O_4$, as an efficient sorbent for the removal of different types of oils from water or other environments. The magnetic properties of the composite, along with its high sorption capacities, make it a promising candidate for oil spill treatment and environmental remediation applications.

In a comparative study conducted by Pham et al, (Pham et al., 2019) two different approaches, conventional thermal heating and microwave irradiation methods, were

investigated for the fabrication of expanded graphite from locally available flake graphite sources in Vietnam. The objective of the study was to evaluate the effectiveness of these methods in producing expanded graphite for the purification of oil-contaminated water. The results of the study revealed that expanded graphite obtained from both methods exhibited multilevel pore structures, indicating the presence of various pore sizes and interconnected voids. The specific surface area, which is an important parameter influencing adsorption capacity, was measured for the expanded graphite samples. Under optimal processing conditions, the surface area of expanded graphite obtained from the microwave irradiation method was found to be 147.5 m^2/g, while the surface area of expanded graphite produced through conventional heating was 100.97 m^2/g. Furthermore, the as-synthesized expanded graphite obtained from the microwave irradiation method demonstrated higher adsorption capacities for diesel oil, crude oil, and fuel oil compared to the expanded graphite obtained through the conventional heating method. This suggests that the microwave irradiation method resulted in expanded graphite with improved adsorption performance for hydrocarbon pollutants. The findings of this study highlight the potential of microwave irradiation as an effective technique for the fabrication of expanded graphite with enhanced adsorption properties. The higher surface area and superior adsorption capacities of the microwave-synthesized expanded graphite make it a promising material for the purification of oil-contaminated water, offering potential applications in environmental remediation and oil spill cleanup efforts.

K. H. Wu et al. (K. H. Wu et al., 2021) conducted a study where they synthesized a magnetic expanded graphite (MEG) composite using the explosive combustion method and black powder. The expanded graphite obtained from this process exhibited

an expansion volume of 300.0 ml/g and a specific surface area (SBET) of 34.8 m2/g. The researchers investigated the sorption behavior of the EG/Fe3O4 composite for the removal of heavy oil, engine oil, and diesel oil from water. The results revealed that the composite exhibited high sorption capacities for these oils. Specifically, the sorption capacity for heavy oil was measured at 87.70 g/g, while engine oil and diesel oil showed sorption capacities of 53.20 g/g and 44.22 g/g, respectively. These findings indicate that the EG/Fe3O4 composite possesses excellent sorption properties, making it a promising material for the removal of heavy oil, engine oil, and diesel oil from water. The magnetic properties of the composite, coupled with its high sorption capacities, offer potential applications in oil spill remediation and environmental cleanup processes.

A recent work by Tarango-Rivero et al. (Tarango-Rivero et al., 2022) proposed a process for the production of expanded graphite that aimed to reduce the consumption of sulfuric acid by utilizing only two intercalation chemicals. They conducted experiments to evaluate the effects of milling, peroxide concentration, and microwave expansion on the process. The results of their study demonstrated that the proposed route led to the production of expanded graphite with high specific volumes and elevated oil adsorption rates. The expanded graphite exhibited a high selectivity for oil-water separation and demonstrated rapid adsorption capabilities. Among the samples tested, the 0-2 and 0-1 samples showed the highest oil adsorption capacities, reaching values of 111.8 ± 5.6 (g/g) and 95.3 ± 3.8 (g/g), respectively. These findings highlight the effectiveness of the proposed process in producing expanded graphite with excellent oil adsorption properties, indicating its potential for applications in oil spill cleanup and water purification.

Indeed, the expansion temperature plays a crucial role in determining the oil sorption capacities of expanded graphite. According to Goudarzi and Hashemi (Goudarzi & Hashemi Motlagh, 2019) higher expansion temperatures lead to increased sorption capacity due to the higher porosity achieved during the expansion process as shown in Figure 2.15. When graphite is subjected to high temperatures, the intercalation agents used to expand the graphite, such as sulfuric acid or other oxidants, generate gases that cause the interlayer spacing of the graphite to increase. This expansion results in the formation of a highly porous structure with interconnected voids and channels. The porosity of the expanded graphite is directly related to its ability to sorb oil. Larger pores and voids provide more space for oil molecules to penetrate and be trapped within the structure. Consequently, EG specimens prepared at higher temperatures tend to have a higher porosity, allowing for greater oil sorption capacity. On the other hand, if the pore size distribution of the EG specimens is too small, large oil molecules may face difficulty diffusing into these restricted pores. Therefore, it is desirable to have a suitable range of pore sizes in the expanded graphite structure to facilitate the effective sorption of oil molecules of varying sizes. By optimizing the expansion temperature, researchers can control the porosity and pore size distribution of the expanded graphite, tailoring its sorption capacity for specific applications. This knowledge helps in designing EG materials with enhanced oil sorption capabilities, making them efficient and effective for oil spill cleanup and other oil sorption scenarios.

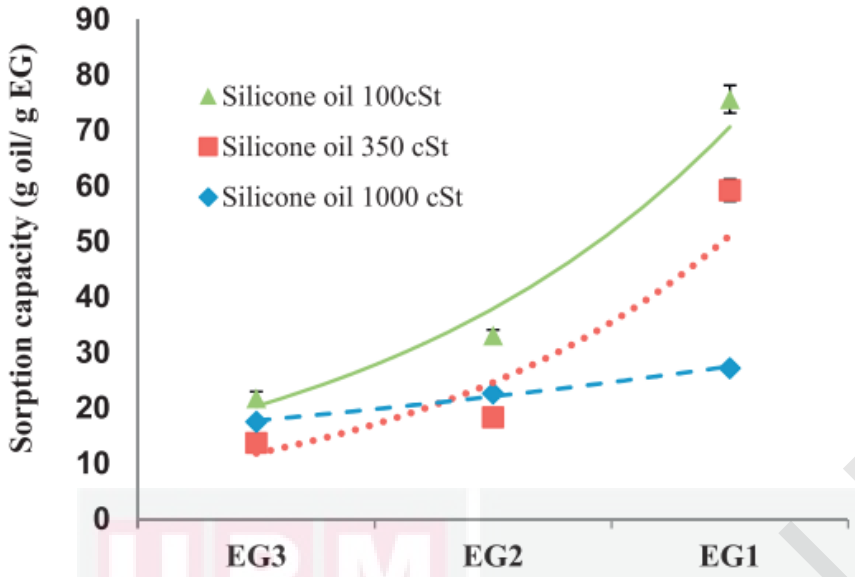

Figure 2.15: The oil sorption capacities of EGs prepared at different expansion temperatures
(Goudarzi & Hashemi Motlagh, 2019)

CHAPTER 3

MATERIALS AND METHODS

3.1 Introduction

This chapter provides the methodologies for the synthesis of expanded graphite by two different approaches as illustrated by the framework in Figure 3.1. The primary objective of this study was to synthesize two different expanded graphite, taking into account environmental and economic considerations. Two methods are used in the production of EG: a one-step method that emphasizes reducing energy consumption to achieve economic efficiency, and a two-step method that avoids the use of strong acids, making it more environmentally friendly. After that, a description of the procedures used to synthesize expanded graphite and the justification for these procedures. Followed by testing a process parameter along with the morphological and structural characterization of both types produced expanded graphite is given in this chapter. Finally, application of expanded graphite of oil sorption are given in this chapter.

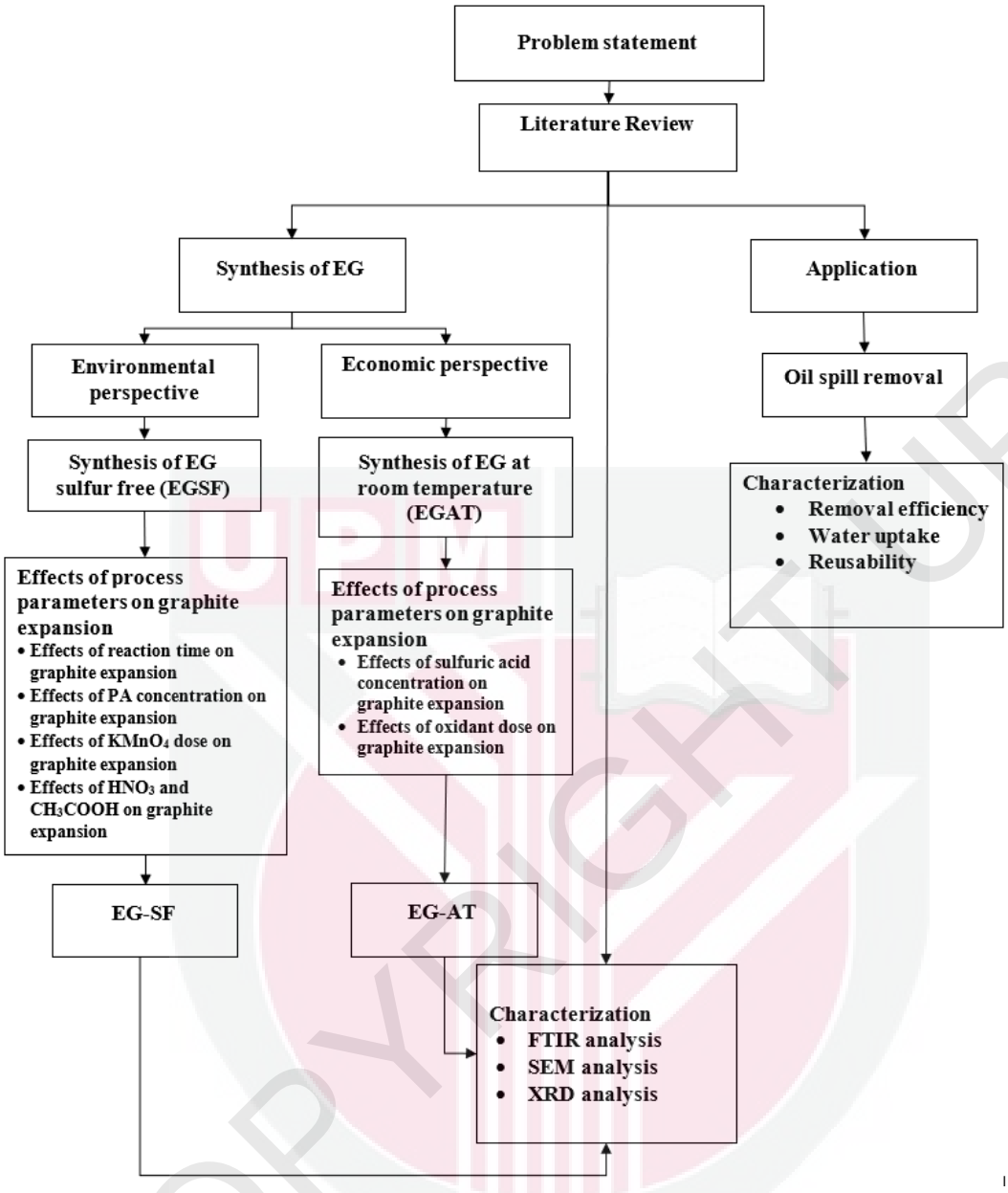

Figure 3.1: Flow chart of methodology

3.2 Materials

The materials used in the first scope were; natural graphite flakes with a carbon content of (99%) and a 50-mesh particle size were obtained from Sigma-Aldrich, acetic acid (99.5%) and potassium permanganates (99.5%) were obtained from Evergreen Engineering & Resources Sdn. Bhd. (Semenyih, SGR, Malaysia). Palmitic acid

(hexadecanoic acid) was obtained from Chemiz (M) Sdn. Bhd (Shah Alam, Malaysia). Phosphoric acid (95-98 %) and nitric acid (65 %) were obtained from R & M Chemicals, Malaysia.

In the second scope, in addition to the natural graphite flakes used in the first scope, concentrated sulfuric acid (98%) and sodium peroxydisulfate were used, which were obtained from the Evergreen Engineering & Resources Sdn. Bhd (Semenyih, SGR, Malaysia).

In the third scope, the expanded graphites as fabricated in the first and second scopes used and Perodua semi-synthetic engine oil. All chemicals were used as received as shown in Figure D1.

3.3 Apparatus

Electronic scale was used to weigh the materials accurately and burette was used to measure the liquids. The materials were weighed carefully to ensure the results are reliable and accurately. Furthermore, in first experiment after the materials were added to the beaker the ultrasonic was used for stirring, and in the second objective the magnetic stirrer was used for mixing. After the GICs were prepared, the drier was used to dry the pH-neutral GICs, while filter paper was employed to dry the wet GICs in the drier. Finally, the expanded graphite was prepared after GIC was placed into a microwave oven (SAMSUNG ME711K) operated at 200W for 5s. In addition, measuring cylinder was used to measure the volume of the EG. For the oil sorption study, engine oil was used as the oil sample. All the materials were ready-to-use and

the experiments was carried out at the Environmental Lab, Faculty of Engineering, UPM. Moreover, the structures of the natural graphite flakes and expanded graphite samples were analyzed by X-ray diffraction (XRD, Shimadzu, XED6000). The surface functional groups of EG were analyzed by Fourier transform infrared spectroscopy (Nicolet FT-IR 6700, Thermo Fisher Scientific). The micro-morphologies were viewed by field emission scanning electron microscopy (LEO 1445 VP scanning electron microscope). All characterizations were conducted at the Material Characterization Lab, Faculty of Engineering, UPM.

3.4 Preparation of Expanded Graphite

In this thesis, two different types of expanded graphite were prepared by two different techniques and completely with different chemicals. The first type of expanded graphite was prepared in an economical manner at room temperature in order to reduce energy consumption and this is called EG-AT. The second type of expanded graphite was prepared in the environmental manner in which EG was prepared by using palmitic acid with the aid of phosphoric acid in two steps process, whereas traditional expanded graphite preparation processes depend mainly on sulfuric acid, which is related to various environmental problems. Sulfuric acid-free expanded graphite is an eco-friendly and sustainable alternative to traditional expanded graphite that contains sulfuric acid. Sulfuric acid is often used as an intercalating agent in the preparation of expanded graphite, but its use can result in the emission of sulfuric dioxide (SO_2) and other harmful sulfuric compounds during the production process. The use of sulfuric acid-free expanded graphite can reduce the environmental impact of expanded graphite production and offer sustainable alternatives for various industrial applications.

3.5 Preparation of ATEG

As shown in Figure 3.2. First, 1 g of natural graphite flakes was added to a certain amount of concentrated sulfuric acid (98%) (6 - 14) mL and stirred until evenly mixed. Next, (3-10) g sodium peroxydisulfate was added to the mixture and left at ambient temperature for 30 min. Then, the obtained acid GICs were washed with ultrapure water to neutral under vacuum filtration and left for 24 hours. The EG that is prepared by this method is referred to as **ATEG**.

In comparison, a typical high-temperature expansion procedure was used to prepare EG. The same process was used to synthesize the GICs, with the exception that only 1 g of sodium peroxydisulfate was added to the mixture of sulfuric acid and graphite. Then the precipitates were washed with distilled water to neutral under vacuum filtration and then dried at 55 °C, where no expansion of the host graphite was observed even after drying. The precipitates were converted to EG after the microwave oven (SAMSUNG ME711K) operated at 200 W for a few seconds. The item was referred to be high quality expanded graphite at high temperature **HTEG** (B. Hou et al., 2020).

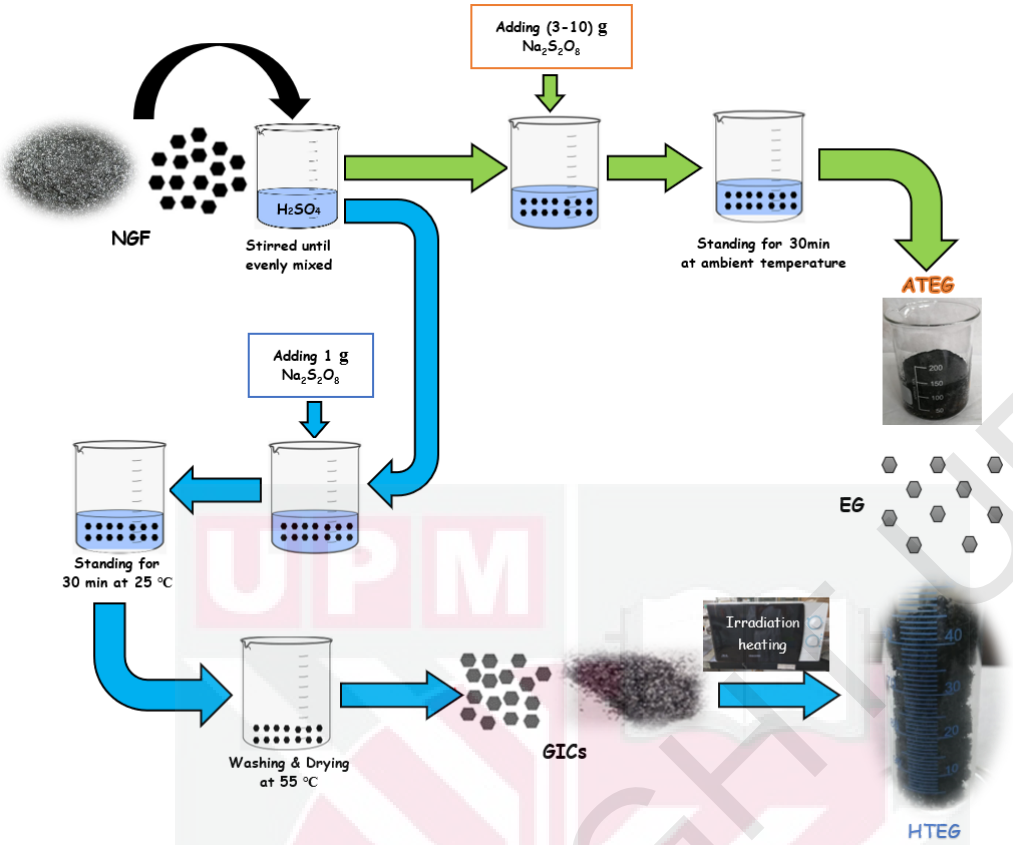

Figure 3.2: Schematic illustrates the preparation process of ATEG and HTEG.

3.5.1 Study the effect of sulfuric acid concentration on graphite expansion volume

Sulfuric acid can cause graphite to expand due to its ability to intercalate or insert molecules between the layers of graphite. However, the extent of expansion is dependent on the concentration of sulfuric acid used. At low concentrations, sulfuric acid can cause a small amount of expansion in graphite. As the concentration of sulfuric acid increases, so does the amount of expansion. However, there is a limit to how much the graphite can expand, and the expansion will eventually level off as the acid concentration continues to increase. Additionally, the rate of expansion will also be affected by the concentration of sulfuric acid. At higher concentrations, the rate of expansion will be faster, but the overall amount of expansion may be less due to the graphite reaching its maximum expansion limit more quickly. It is worth noting that

sulfuric acid is a highly corrosive substance and can be dangerous to handle without proper safety precautions. Therefore, any experiments involving sulfuric acid and graphite should be conducted with caution and under the guidance of a trained professional.

To inspect the effect of sulfuric acid amount on graphite expansion volume, a series of graphite-sulfuric acid solutions were prepared with solid-liquid mass ratios of 1%, 2%, 3%, 5%, 7%, 10%, and 13% (B. Hou et al., 2020). Graphite samples were introduced into separate beakers, and different amounts of sulfuric acid were added to each beaker, ensuring a range of sulfuric acid concentrations. The volume of sulfuric acid added was sufficient to fully immerse the graphite samples. The mixture of graphite-sulfuric acid was stirred until evenly mixed, and then the optimum amount of sodium peroxydisulfate was added. Afterward, the graphite samples were carefully removed and thoroughly rinsed with distilled water to eliminate any residual sulfuric acid and sodium peroxydisulfate. The expansion volume of each graphite sample was measured by comparing the dimensions (e.g., thickness or height) of the expanded graphite with the original dimensions of the graphite before the expansion. Expansion volumes for each sulfuric acid amount were recorded, and the data obtained to determine the relationship between sulfuric acid amount and graphite expansion volume were analysed.

3.5.2 Study of the effect of sodium peroxydisulfate dosage on graphite expansion volume

The use of an oxidant can also cause graphite to expand due to its ability to intercalate between the graphite layers and create a space between them. The amount of expansion will depend on the dosage of the oxidant used. As the dosage of the oxidant increases,

the amount of expansion in the graphite will also increase. However, like with sulfuric acid, there is a limit to how much the graphite can expand, and the expansion will eventually level off as the oxidant dosage continues to increase. The rate of expansion will also be affected by the dosage of the oxidant. At higher dosages, the rate of expansion will be faster, but the overall amount of expansion may be less due to the graphite reaching its maximum expansion limit more quickly. It is important to note that different oxidants may have varying effects on the expansion of graphite, and the optimal dosage may differ depending on the specific oxidant being used. Additionally, the type and quality of the graphite may also affect the expansion volume. Therefore, it is important to conduct experiments with different dosages and oxidants to determine the optimal conditions for achieving the desired expansion volume in graphite.

To investigate the effect of the amount of sodium peroxydisulfate on the expansion volume of graphite, the following steps were followed: A series of sodium peroxydisulfate samples with different amounts were weighted starting from 1 g, 2 g, 3 g, 5 g, 7 g, 10 g, and 13 g. The optimum amount of sulfuric acid-graphite ratio which was estimated before was added into separate beakers. Sodium peroxydisulfate was added to each beaker, ensuring that each beaker contains a different amount of sodium peroxydisulfate. The volume sulfuric acid graphite ratio should be sufficient to fully immerse the sodium peroxydisulfate samples. The sulfuric acid-graphite mixture allowed to react with the sodium peroxydisulfate for 30 min. Afterward, the graphite samples were carefully removed and rinsed thoroughly with distilled water to eliminate any residual sulfuric acid and sodium peroxydisulfate. The expansion volume of each graphite sample was measured. This can be done by comparing the dimensions (e.g., thickness or height) of the expanded graphite with the original

dimensions of the graphite before the reaction. Expansion volumes for each of sodium peroxydisulfate amount were recorded. The data obtained to determine the relationship between sodium peroxydisulfate and graphite expansion volume were analysed.

3.6 Preparation of EG-SF Modified with PA/H_3PO_4

The sulfuric acid-free expanded graphite preparation process consisted of two stages. Figure 3.3 shows an overview of the entire procedure. In the first stage, known as the 'pre-oxidation' stage, 1 g of natural graphite flakes was added to a flask containing 6 mL palmitic acid, 10 mL phosphoric acid, and 0.2 g potassium permanganate. The reaction mixture was continuously stirred in an ultrasonic bath at a temperature below 40 ℃ for 30 minutes. Afterward, the reaction product was washed with distilled water until it became clear and transparent, with a pH range of 5-7. The resulting solution was then filtered using a vacuum filter and dried in an oven at 55 ℃ for 30 minutes. This process resulted in the production of acidized graphite (AG). In the second stage, referred to as 'deep oxidation,' 1 g of acidized graphite (prepared in the first stage, i.e., pre-oxidized graphite), 1.5 mL of nitric acid, 6 mL of acetic acid, and 0.1 g of potassium permanganate were stirred for 30 minutes. The resulting mixture was then washed close to neutrality with distilled water using a vacuum filter and dried at 55 ℃ for 30 minutes, resulting in the synthesis of the graphite intercalation compound (GIC). Finally, the expanded graphite was prepared by placing the GIC into a Samsung ME711K microwave oven operated at 200W for 5 seconds (J. J. Zhao et al., 2014).

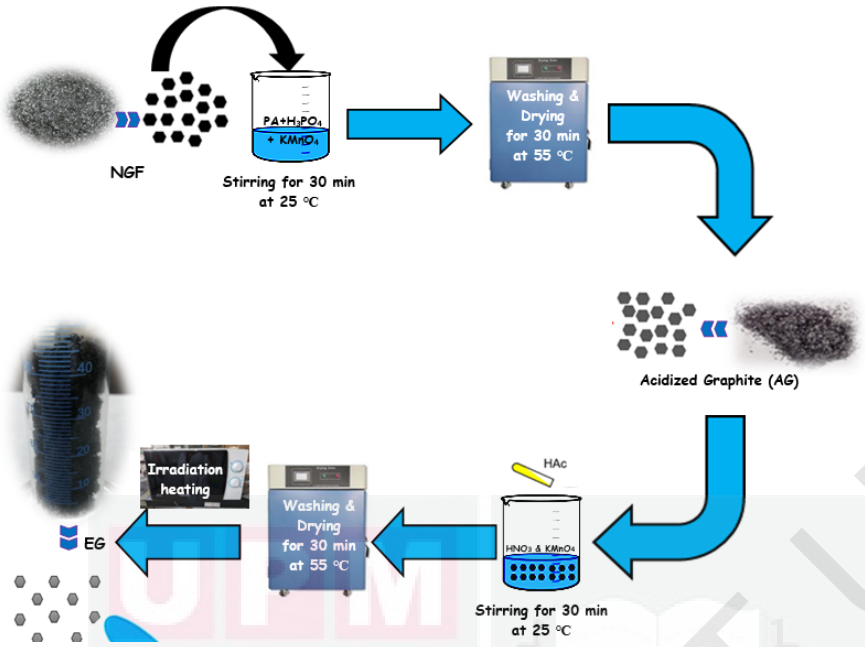

Figure 3.3: Schematic illustrates the preparation process of EG-SF

3.6.1 Investigating the effects of reaction time on the graphite expansion volume

The reaction time during the synthesis of expanded graphite can affect the expansion volume of the final product. The longer the reaction time, the more time the intercalating agent (such as sulfuric acid) has to penetrate and expand the layers of the graphite. At shorter reaction times, the expansion volume of the graphite may be less, as the intercalating agent may not have had sufficient time to fully expand the graphite layers. However, a shorter reaction time may be desirable in some cases where a lower expansion volume is required. Conversely, longer reaction times may result in a higher expansion volume, as the intercalating agent has more time to penetrate and expand the graphite layers. However, an excessively long reaction time may result in over-expansion or chemical degradation of the graphite material, leading to a decrease in its quality. The optimal reaction time for synthesizing expanded graphite will depend on various factors, including the type and quality of the graphite, the type and

concentration of the intercalating agent, and the desired expansion volume. It is important to carefully control the reaction time to achieve the desired expansion volume while maintaining the quality of the final product. To examine the effect of reaction time on the graphite expansion volume, the following steps were performed: Different graphite samples were prepared with optimum conditions. A series of reaction beakers with different reaction times were set up (10 min, 20 min, 30 min, 40 min, 50 min, and 60 min). Each beaker represented a different reaction time. The graphite samples were introduced into the reaction beakers, ensuring that the reaction temperature remained constant. The reactions were started simultaneously and allowed to proceed for the specified duration according to each beaker. After the designated reaction time elapsed, the reactions stopped. The resulting solution was then filtered using a vacuum filter and dried in an oven at 55 ℃ for 30 minutes. The previous steps were repeated in both stages, but there was a significant difference. In the first stage, acidic graphite was prepared, while in the second stage, GICs were prepared. The expanded graphite was prepared by placing the GICs into a Samsung ME711K microwave oven operated at 200W for 5 seconds. Expanded graphite was transferred lightly into the cylinder, and the volume and mass of expanded graphite were recorded. Finally, the relationship is obtained by plotting the expansion volume vs reaction time.

3.6.2 Investigating the effects of palmitic acid concentration on the graphite expansion volume

The concentration of the palmitic acid used in the synthesis of expanded graphite can significantly affect the expansion volume of the final product. Generally, a higher concentration of acid will lead to a higher expansion volume in the graphite. As the PA concentration increases, more protons are available to react with the graphite and

generate more intercalation compounds. This results in an increase in the space between the graphite layers, leading to a higher expansion volume. However, as the acid concentration becomes too high, the expansion volume may plateau or even decrease due to excessive chemical degradation of the graphite material. On the other hand, a lower concentration of PA may lead to a lower expansion volume in the graphite. The intercalation reaction may not occur to the same extent, resulting in less space between the graphite layers. The optimal PA concentration for synthesizing expanded graphite depends on various factors, including the type and quality of the graphite, the desired expansion volume, and the specific acid used. It is important to carefully control the PA concentration to achieve the desired expansion volume while maintaining the quality of the final product.

To investigate the effects of palmitic acid on the graphite expansion volume, the next steps were followed: a series of palmitic acid amounts were prepared as 4mL, 5mL, 6mL, 7mL, and 8mL. Then, 1g of graphite, 10 mL phosphoric acid, and 0.2 grams of potassium permanganates as the optimum conditions were introduced into separate beakers. The different palmitic acid amounts were added to each beaker, ensuring that each beaker contains a different amount of palmitic acid. The volume of palmitic acid added was sufficient to fully immerse the graphite samples. The reaction mixture was continuously stirred in an ultrasonic bath at a temperature below 40 ℃ for 30 minutes. Afterward, the reaction product was washed with distilled water until it became clear and transparent, with a pH range of 5-7. The resulting solution was then filtered using a vacuum filter and dried in an oven at 55 ℃ for 30 minutes. The steps mentioned above were repeated in both stages, with a notable distinction. In the initial stage, acidic graphite was synthesized, whereas, in the second stage, the preparation of GICs

took place. The procedure for obtaining expanded graphite involved the introduction of the GICs into a Samsung ME711K microwave oven, set at an operating power of 200W for 5 seconds. The expanded graphite was gently transferred into the cylinder, and measurements were taken for both the volume and mass of the expanded graphite. The correlation can be established by graphing the expansion volume against the palmitic acid amount.

3.6.3 Investigating the effects of potassium permanganate dosage on the graphite expansion volume

The dosage of the potassium permanganate used during the synthesis of expanded graphite can also have a significant effect on the expansion volume of the final product. Generally, a higher dosage of potassium permanganate will lead to a higher expansion volume in the graphite. As the potassium permanganate dosage increases, more oxidizing agents are available to react with the graphite and generate more intercalation compounds. This results in an increase in the space between the graphite layers, leading to a higher expansion volume. However, as the potassium permanganate dosage becomes too high, the expansion volume may plateau or even decrease due to excessive chemical degradation of the graphite material. On the other hand, a lower dosage of potassium permanganate may lead to a lower expansion volume in the graphite. The intercalation reaction may not occur to the same extent, resulting in less space between the graphite layers. The optimal potassium permanganate dosage for synthesizing expanded graphite depends on various factors, including the type and quality of the graphite, the desired expansion volume, and the specific oxidant used. It is important to carefully control the oxidant dosage to achieve the desired expansion volume while maintaining the quality of the final product.

In the case of potassium permanganate, its contribution varied in both stages, with different amounts. To investigate the effect of the potassium permanganate quantity on the expansion volume of graphite, the following steps were implemented: In the first stage, potassium permanganate was used in varying weights: 0.1g, 0.15g, 0.2g, 0.25g, and 0.3g. In the second stage, the weights used were 0.01g, 0.05g, 0.1g, 0.15g, and 0.2g. The optimum conditions were introduced into separate beakers. In the first stage, the reaction mixture was continuously stirred in an ultrasonic bath at a temperature below 40 ℃ for 30 minutes. while in the second stage, magnetically stirred for 30 minutes. Afterward, the reaction product was washed with distilled water until it became clear and transparent, with a pH range of 5-7. The resulting solution was then filtered using a vacuum filter and dried in an oven at 55 ℃ for 30 minutes. The steps mentioned above were repeated in both stages, with a notable distinction. In the initial stage, acidic graphite was synthesized, whereas, in the second stage, the preparation of GICs took place. The procedure for obtaining expanded graphite involved the introduction of the GICs into a Samsung ME711K microwave oven, set at an operating power of 200W for 5 seconds. The expanded graphite was gently transferred into the cylinder, and measurements were taken for both the volume and mass of the expanded graphite. Finally, the relationship is obtained by plotting the expansion volume vs potassium permanganate amount for each stage.

3.6.4 Investigating the effects of nitric acid and acetic acid on the graphite expansion volume

In the two-step method of graphite expansion, an assistant oxidant is typically used during the second step to further expand the graphite. The addition of an assistant oxidant can have a significant effect on the expansion volume of the synthesized

expanded graphite. The assistant oxidant typically reacts with the intercalation compound generated during the first step, leading to the formation of gas that causes the expansion of the graphite. A higher concentration of the assistant oxidant can lead to a higher expansion volume in the graphite. However, as the concentration of the assistant oxidant becomes too high, the expansion volume may plateau or even decrease due to excessive chemical degradation of the graphite material. On the other hand, a lower concentration of the assistant oxidant may lead to a lower expansion volume in the graphite. The reaction with the intercalation compound may not occur to the same extent, resulting in less space between the graphite layers and a lower expansion volume. The specific assistant oxidant used can also affect the expansion volume of the synthesized expanded graphite. Different oxidants have different reactivity and can produce different amounts of gas during the reaction, leading to different expansion volumes. Therefore, it is important to carefully choose the appropriate assistant oxidant and concentration to achieve the desired expansion volume while maintaining the quality of the final product. In summary, the addition of an assistant oxidant in the two-step method of graphite expansion can have a significant effect on the expansion volume of the synthesized expanded graphite. The concentration and type of assistant oxidant used should be carefully controlled to achieve the desired expansion volume while maintaining the quality of the final product.

To investigate the effects of the assistant intercalating agents used in the second stage, namely nitric acid and acetic acid, on the graphite expansion volume, the following steps were followed: A series of reaction beakers were prepared that contain the desired amounts of nitric acid 0.5 mL, 1 mL,1.5 mL, 2 mL, and 2.5 mL and acetic acid

2 mL, 4 mL, 6 mL, 8 mL, and 10 mL were added to each beaker, ensuring different concentrations or ratios. The acidic graphite samples that were prepared in the first stage were introduced into the reaction beakers. The reactions were started simultaneously and allowed to proceed for a specified duration. After the designated reaction time had elapsed, the graphite samples were removed from the reaction beaker and thoroughly rinsed with distilled water to remove any residual acids. The expansion volume of each graphite sample was recorded by measuring its dimensions or weight. The data was analysed, and the relationship between the concentrations or ratios of nitric acid and acetic acid and the expansion volume of the graphite was observed.

3.7 Estimate the expansion rate of the expanded graphite

The expanded volume (EV) of expanded graphite was measured using a graduate cylinder that had a capacity of 100 ml. The EG was synthesized after heating 0.1 g of GICs in the microwave. EG was transferred lightly into the cylinder, and the volume and mass of EG were recorded, respectively. The EV was then calculated by the following equation (3.1) (Sykam et al., 2018):

$$EV\ \left(mL/g\right)=\frac{V}{m} \qquad (3.1)$$

Where:

EV is the expanded volume,

V is the volume measured in (*mL*),

and m is the mass quantity of the sample measured in (*g*).

To ensure the reliability of the result, the expanded volume is recorded by taking the mean of three different batches obtained by microwave irradiation (J. J. Zhao et al., 2014).

3.8 Morphological and Structural Characterization

The morphological and structural characterization of expanded graphite is important to understand its physical and chemical properties and to optimize its performance in various applications. Here are some common methods used for the morphological and structural characterization of expanded graphite:

3.8.1 SEM Analysis

Scanning Electron Microscopy (SEM): SEM is a commonly used method to visualize the morphology of expanded graphite at high resolution. SEM images can reveal the surface morphology and structure of the expanded graphite, including the size and shape of the expanded flakes, the thickness of the expanded layers, and the presence of any defects or impurities (B. Hou et al., 2020; Ting & Xuesha, 2017).

The morphological and compositional studies of raw, intercalated, and expanded graphite powders were carried out via scanning electron microscopy (SEM) using Hitachi SU35000and a JSM-7401 F field emission microscopes. Wet route chemical analyses were performed with a Thermo Scientific Flash Smart Element Analyzer and a spectrometer model iCAP 6500 Series (ICO).

3.8.2 XRD Analysis

X-ray Diffraction (XRD): XRD is a powerful technique to determine the crystal structure of expanded graphite. By analysing the diffraction patterns of X-rays scattered from the expanded graphite, XRD can identify the interlayer spacing between the graphite layers, as well as any crystallographic changes that may have occurred during the expansion process (Çalın et al., 2020; Goudarzi & Hashemi Motlagh, 2019). Structural and phase identification studies were performed through X-ray diffraction (XRD) using a Panalytical X'pert PRO diffractometer with Cu Ka radiation (λ=1.5405Å) operated at 40 kV and 30 mA; the diffractograms were obtained using a scanning 2θ ranged from 5 to 60◦ with a 0.008◦ /step and 60 s/step.

3.8.3 FT-IR Analysis

Fourier Transform Infrared (FTIR) Spectroscopy: FTIR spectroscopy is used to identify functional groups on the surface of the expanded graphite. By analysing the absorption peaks in the FTIR spectrum, FTIR can provide information on the chemical composition of the surface of the expanded graphite, including the presence of surface functional groups (T. Liu et al., 2017; Saikam et al., 2022).

The identification of functional groups and structure elucidation was made in a Shimadzu IR spectrophotometer model Affinity 1S. Spectrum 100, Perkin Elmer by method of attenuated total reflection (ATR) detector with scanning 4000 cm^{-1} to 650 cm^{-1} number 16 scanning units %T resolution 4.00 cm^{-1}.

3.9 Statistical Analysis

Two-way ANOVA was conducted to examine the effects of different variables (such as palmitic acid concentration, potassium permanganate dosage, nitric acid concentration, and acetic acid concentration) on the expanded volume of the synthesized sulfur-free expanded graphite. Also, a two-way ANOVA was conducted to examine the effects of the solid-liquid ratio and sodium peroxydisulfate on the volume expansion of the room temperature expanded graphite. The ANOVA allowed us to determine whether there were significant differences in the expanded volume among the different levels of each variable.

Furthermore, post hoc tests were also conducted, specifically the LSD (Least Significant Difference) test, to determine specific pairwise differences between the levels of each variable. The post hoc tests allowed us to identify which specific pairs of levels showed significant differences in the expanded volume.

3.10 Oil Sorption

In the oil sorption studies, two types of expanded graphite namely expanded graphite at ambient temperature (EG-AT) and expanded graphite sulfur-free (EG-SF), developed in this research, were used in the oil sorption experiment.

3.10.1 Application study for removal of engine oil by EGs

The sorption of crude oil from an aqueous medium was conducted in a batch system according to ASTM F726-99 as described (Alassod et al., 2022; Soliman et al., 2020). A weighed portion (0.1 g) of the EG was contacted with 50 g/L of Perodua semi-

synthetic engine oil at room temperature. After 5 min of sorption time, with a little agitation, a sieve net was used to remove the EG sorbent from the beaker, and the excess oil was allowed to drain. The oil-loaded sorbent was then weighed and the oil sorption capacity, q (g/g), was calculated using equation (**3.2**) (He et al., 2017; Ifeyinwa Obi et al., 2023; Soliman et al., 2020). The mixture was shaken for 1 min and allowed to settle for 5 min (Iqbal & Abdala, 2013).

$$\text{Oil sorption capacity } \left({}^{g}/_{g}\right) = \frac{w_1 - w_o}{w_o} \qquad (3.2)$$

Where w_0 is a mass of the dry sorbent before sorption (g), w_1 is the total mass of wetted sorbent after oil drain out (g).

The sorbent was removed from the oil surface by raising the basket until no more oil dropped down after 1 h (K. H. Wu et al., 2021). C_0 = 5 g of oil in 100 mL of water = 50 g of oil in 1 L of water.

Expanded graphite has been shown to have high oil sorption capacities (He et al., 2017; Sykam & Kar, 2014; K. H. Wu et al., 2021). As shown in Figure 3.4.

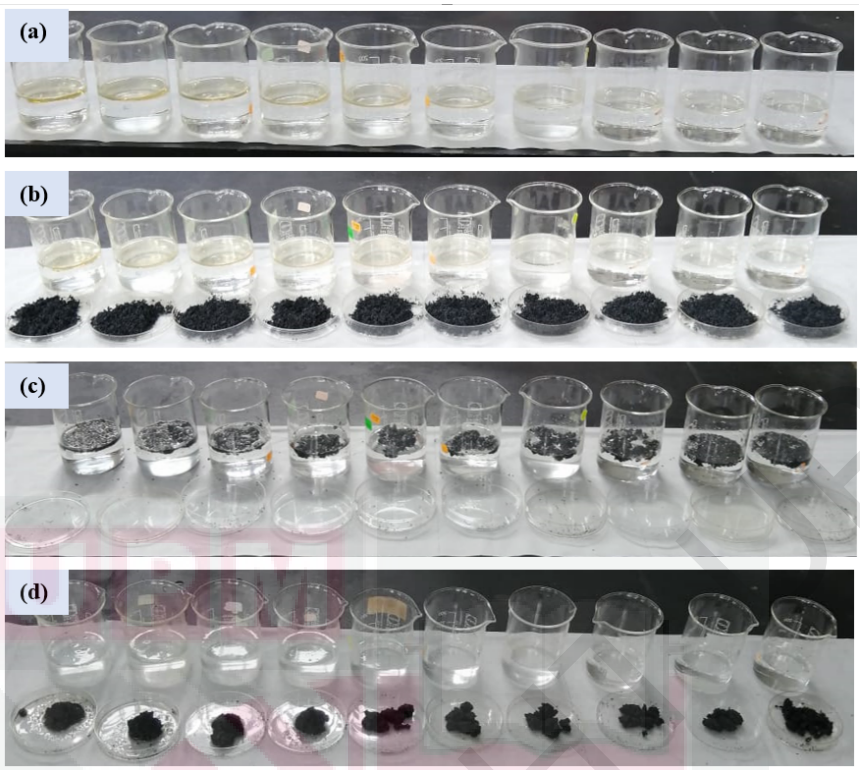

Figure 3.4: Optical images of (a) oil–water mixture (b) 1 g of EG (c) after the addition of EG amount yielding an oil/EG ratio equivalent to the sorption capacity and (d) after removal of the oil-saturated

3.10.2 Effects of contact time on the sorption capacity of the EGs

The equilibrium adsorption capacity is important in the design of adsorption systems. Equilibrium studies in adsorption indicate the potential maximum capacity of the adsorbent during the treatment process. In order to find the optimum equilibrium and contact time for maximum uptake of oil spill under studying from oil spilled sample by EG, experiments were conducted at different contact times ranging from 1, 2, 3, 4, 5, 6, 7, 8, 9, and 10 min. The two other parameters including adsorbent dosage (0.1 g) and initial oil concentration (50 g/L) were kept constant. The adsorption capacity in different time was obtained from the weight increase before and after adsorption. The adsorption capacity of oil at certain time was calculated via equation (**3.2**) (He et al., 2017) where q is the adsorption capacity of EG at certain time (g/g); w and w_0 (g) are

the weights of EG before and after the oil adsorption. In order to ensure the accuracy, measurements were carried out in triplicate, and the average value was adopted.

3.10.3 Water uptake study

The water uptake behavior of expanded graphite is measured by the water volume retained by 1 g ($M_{initial}$) of the dry EG was soaked in distilled water for 2 h at room temperature for two hours. After that, the inflated samples were separated, dried for 30 minutes at 50 ℃ in an oven with air circulation, and then reweighed (M_{final}). The water uptake (WU) percentage was then calculated using following (3.3) (Eltaweil et al., 2022):

$$WU\ (\%) = \frac{\text{final mass } (M_f) - \text{initial mass}(M_i)}{\text{initial mass}(M_i)} \times 100 \qquad (3.3)$$

3.10.4 Recyclability

Recycling of adsorbent materials in oil sorption is an important aspect of sustainable waste management. Adsorbent materials, such as expanded graphite, are commonly used for the removal of oil and other hydrocarbons from water. After use, expanded graphite can become contaminated with oil and other pollutants, and it is important to recycle or dispose of them properly. One method of recycling adsorbent materials is through thermal desorption. This involves heating the adsorbent material to a high temperature, which causes the adsorbed oil to vaporize and be recovered as a liquid or gas. The regenerated adsorbent material can then be reused for further oil sorption. Another method of recycling adsorbent materials is through solvent extraction. This

involves using a solvent, such as ethanol or hexane, to dissolve the adsorbed oil and recover it as a liquid. The solvent can then be recovered and reused, while the adsorbent material can be reused for further oil sorption. In some cases, adsorbent materials can be biodegraded by microorganisms, which break down the adsorbed oil and convert it into harmless substances. This can be a sustainable approach to recycling adsorbent materials, as it does not require the use of additional chemicals or energy. Proper recycling of adsorbent materials can help reduce waste and pollution, while also providing a cost-effective solution for oil spill cleanup and other environmental remediation projects.

To evaluate the ability of EG to be recycled and reused several times, EG was utilized for oil removal in three successive cycles as follows: after the absorption run, EG was washed with hexane to desorb the oil and dried in oven at 90 °C for 24 hours (Rozi et al., 2017). The utilized EG was then evaluated during the subsequent adsorption/desorption cycle.

CHAPTER 4

RESULTS AND DISCUSSION

4.1 Introduction

This chapter presents the results of the research described in the chapter on methodology. Firstly, an efficient and energy-conserving preparation process to synthesis EG, in which flake graphite is intercalated and expanded at room temperature. The flake graphite was expanded using a simple and effective method in which graphite intercalation and expansion are accomplished using a binary system of concentrated sulfuric acid (H_2SO_4) and inorganic salts, specifically sodium peroxydisulfate ($Na_2S_2O_8$). The optimal conditions were examined. XRD, SEM, FT-IR, and Raman spectroscopy were used to characterize the expanded graphite's microstructures, morphology, and functional groups. Secondly, an eco-friendly EG was prepared using natural flake graphite as a precursor in a two-step chemical oxidation method. Effects of process parameters on eco-friendly, mesoporous, sulfur-free, expanded graphite were studied. Then, XRD, SEM, FT-IR, and Raman spectroscopy were used to examine the microstructures, morphology, and functional groups of the EG. Finally, the ability of expanded graphite by oil sorption experiment was carried out using engine oil.

4.2 Study the Parameters Influencing the Rapid Preparation of Expanded Graphite at Ambient Temperature

The focus of the study is to investigate the various parameters that effected the efficient and fast preparation of expanded graphite at ambient temperature. This could involve exploring factors such as the choice of intercalation agents, processing conditions,

reaction times, and other variables that influence the expansion process. The objective is to identify the key parameters that can lead to the rapid and effective production of expanded graphite without the need for high temperatures.

4.2.1 Study the effect of sulfuric acid concentration on graphite expansion volume

It is really important to disclose the amount of concentrated sulfuric acid in the system of the expanded graphite formation in order to limit the effluent and mitigate the environmentally harmful effects caused by the excessive usage of concentrated sulfuric acid.

To investigate the effects of concentration of sulfuric acid, it was tested at a fixed mass friction of graphite and sodium peroxydisulfate, which was 1: 7, as shown in the Figure 4.1. As can be observed, the amount of concentrated sulfuric acid has a significant effect on the expanded volume value. Initially, the expansion volume increased gradually with a reduction in the graphite to the sulfuric acid ratio between 1% and 3%. An excessively increased amount of H_2SO_4 may cause severe oxidation of graphite layers, resulting in a reduction in ATEG (T. Wei et al., 2008). It is also because the acidity has changed the nature of the graphite, which led to the change in the chemical process, hence the expansion volume decreased (Trivedi et al., 2018). Besides, when excessive acid was added, it would envelop the graphite and lead to additional pressure on the graphite which prevents the expansion of graphite and result in lower expansion volume (T. Liu et al., 2017). When the ratio of graphite to sulfuric acid reached 5%, the maximum expansion volume of ATEG was achieved. On the other hand, the expansion volume dropped when the ratio of graphite to sulfuric acid rose by more than 5%. This was due to the fact that the concentration of the oxidant

reduced as the acid level increased. In addition, reducing the acid dosage can slow down the reaction between persulfate and acid, which will reduce gas production and, consequently, the graphite expansion volume (Dai et al., 2019). Hence, this finding will give a great motivation to use expandable graphite in various applications that will be affordable and mitigate environmental pollution.

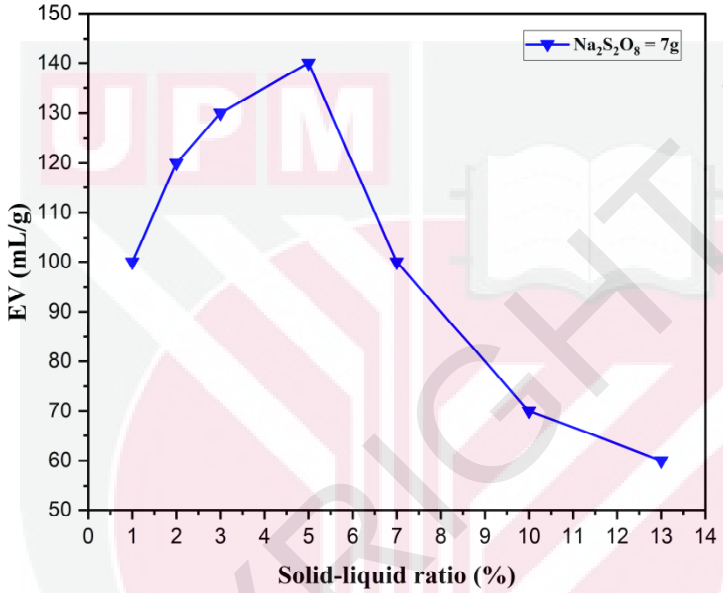

Figure 4.1: Effects of sulfuric acid concentration on graphite expansion volume at optimum condition

4.2.2 Study the effect of sodium peroxydisulfate on graphite expansion volume

In order to investigate the effects of sodium peroxydisulfate on graphite expansion volume, further experiments were performed to obtain better expansion effects using the optimized ratio that was employed in subsequent experiments. As shown in Figure 4.2 when the amount of sodium peroxydisulfate increased at a fixed amount of graphite and concentrated sulfuric acid, the expansion volume of graphite gradually increased until it reached 140 mL/g at 7 g of $Na_2S_2O_8$. When the amount of sodium

peroxydisulfate was below 7 g (3 g, 4 g, 5 g, or 6 g), the dosage of sodium peroxydisulfate was insufficient. As a result, the edges of the graphite layers were not fully oxidized, and the complete opening of the layers was hindered. This incomplete oxidation prevented the concentrated sulfuric acid from fully penetrating between the graphite layers. In contrast, when the dose of sodium peroxydisulfate was very high, exceeding 7 g (8 g, 9 g, or 10 g), the graphite layers underwent excessive oxidation. This led to the opening of the layers becoming too wide, causing intercalated molecules to leak out from the edges (T. Liu et al., 2017; Trivedi et al., 2018). Both of these circumstances had an impact on the expandable graphite's expansion volume, implying that a perfect sodium peroxydisulfate was required. Conversely, a reagent with a poor decomposition speed is unable to produce sufficient force to fully open the layers. Furthermore, during the slow decomposition process, the gas gradually leaks from the edges of the layers, leading to unexpended graphite or weak expansion.

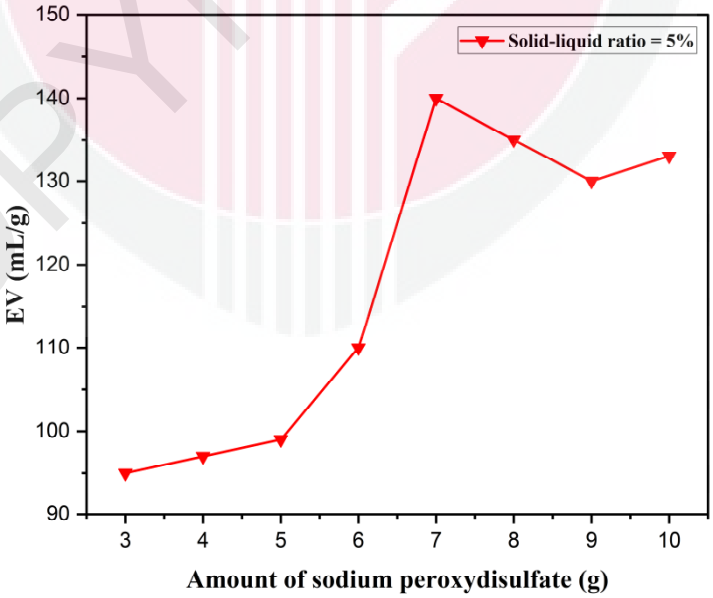

Figure 4.2: Effects of sodium peroxydisulfate dosage on graphite expansion volume at optimum condition

4.2.3 Morphological and structural characterization

Morphological and structural characterization of expanded graphite involves the analysis of the physical and chemical properties of the material at different scales, from the macroscopic level to the atomic level. The following are some common techniques used to characterize the morphology and structure of expanded graphite:

4.2.3.1 SEM Analysis

The morphology of natural graphite flake and expanded graphite was analyzed using SEM, and SEM micrographs of both are presented in Figure 4.3 and Figure 4.4. Figure 4.3 illustrates the morphology of natural graphite flakes, indicating a rough surface with a multilayered crystalline structure. In contrast, the morphology of expanded graphite exhibited significant differences compared to graphite. The expansion process transformed the lamellar structure of natural graphite flakes into a worm-like structure, expanding along the c-axis of the graphite crystal. Figure 4.4 presents an enlarged SEM micrograph of the expanded graphite morphology. In an effort to achieve a worm-like fluffy shape, the basic structure of graphite was disrupted. The breakdown of sodium peroxydisulfate resulted in the generation of gases. The increased gas pressure was able to overcome the van der Waals forces between the interlayers, leading to a rapid expansion of graphite along the c-axis direction.

In fact, Figure 4.4 illustrate the changes in the morphology of the expanded graphite particles at a higher magnification. The results demonstrate that initially, the distance between the graphite sheets is relatively close. As the intercalation compounds in the

EG particles decompose, gas expansion occurs, creating a driving force. When the gas reaches the free interface of the EG particles, it acts as a driving force, leading to the separation of the graphite sheets. This separation results in a significant expansion of the EG particles. Although there are numerous large pores between the graphite sheets, some parts of the sheets remain attached at their edges due to weak Van der Waals forces. These characteristics contribute to the retention of certain strengths in the EG particles even after being subjected to high temperatures (G. Zhao et al., 2019).

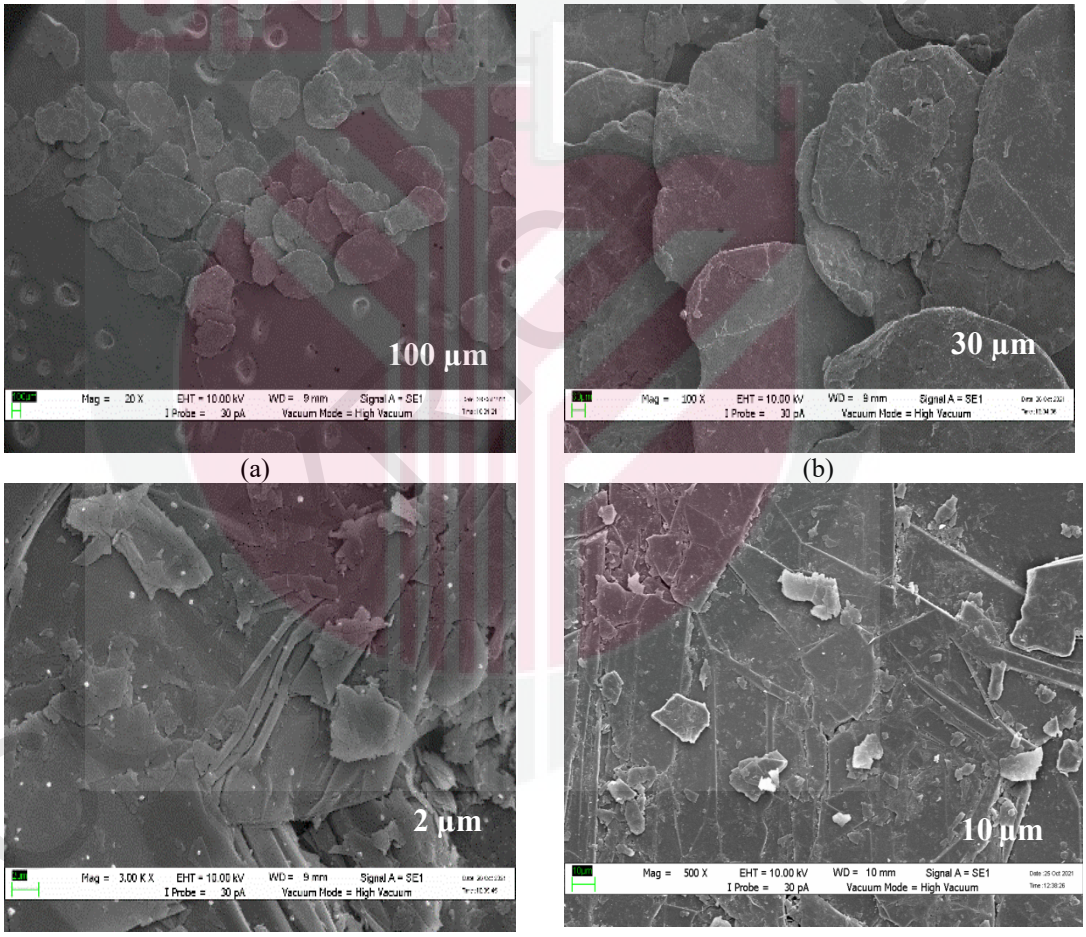

(a) (b)

(c) (d)

Figure 4.3: SEM image of NFG

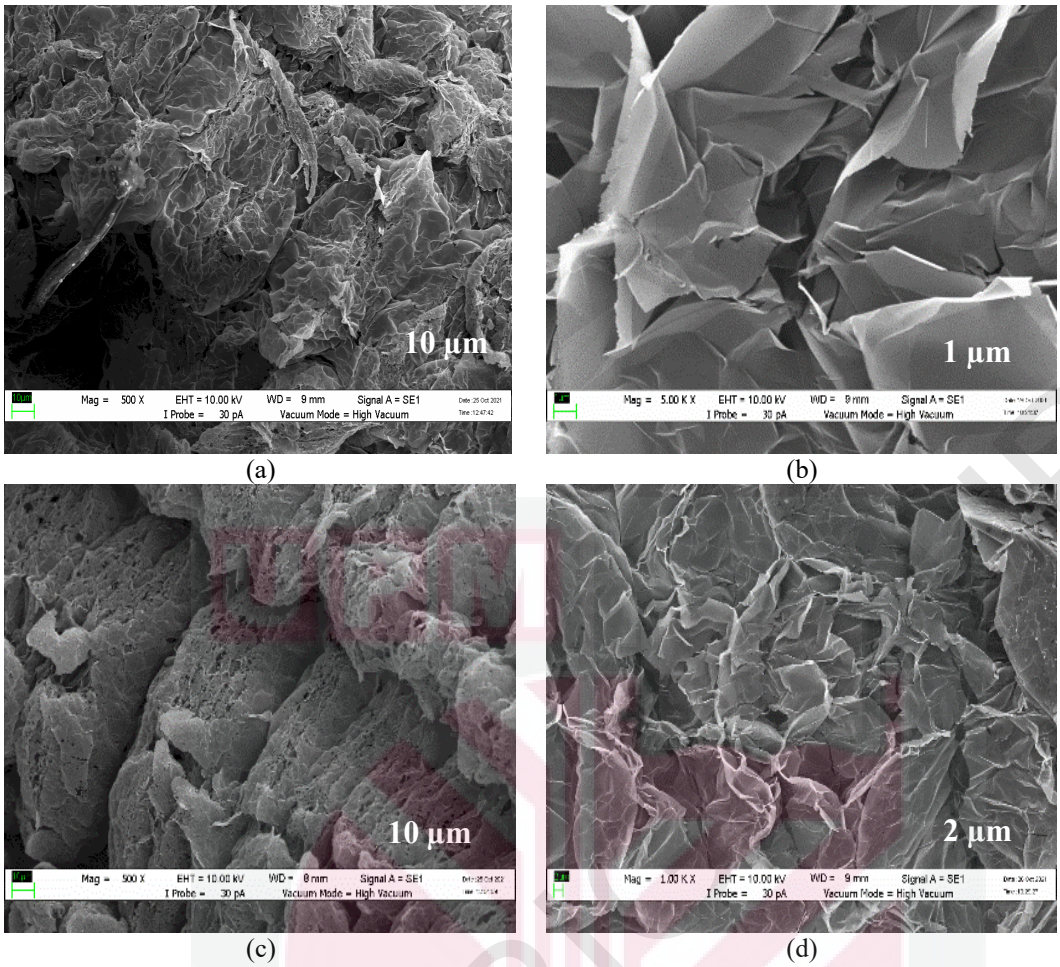

Figure 4.4: SEM images EG

4.2.3.2 XRD Analysis

The crystal structures of NG and ATEG were characterized using XRD powder X-ray diffraction Figure 4.5. NG exhibits a sharp peak at 2θ° = 26.6, which corresponds to the diffraction of (002) plane with an interlayer distance of (0.34 nm) (Zhou et al., 2018). Upon oxidation, the released oxygen will attach to single graphene plane, causing distortion of the interlayer structure. When comparing natural graphite to EG, it can be noted that the intensity of 002 reflections is lower. This is because acid intercalation increases the interplanar distance of graphite, causing a decrease in 2θ° when compared to pristine graphite (Marcano et al., 2010; Trivedi et al., 2018).

According to XRD patterns, the basal spacing of expanded graphite is increased as a result of graphite expansion. Due to some destruction to graphite's crystal structure, the intensity of the characteristic diffraction peaks of NG and EG decreased significantly. This showed that the full width at half maximum (FWHM) slightly increased from 0.386 to 0.417.

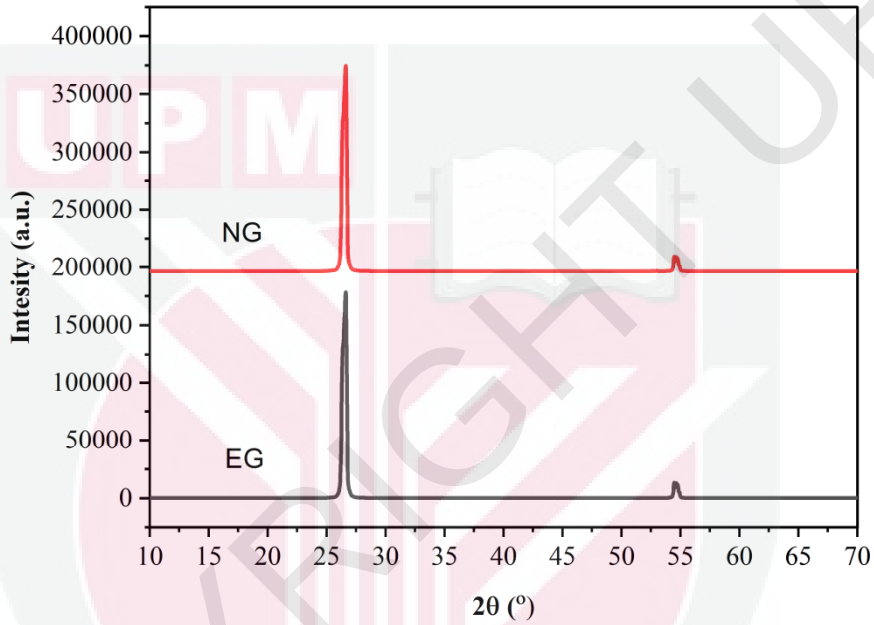

Figure 4.5: XRD patterns of NG and ATEG

4.2.3.3 FT-IR Analysis

Fourier Transform Infra-Red (FTIR) is used to depict a variety of oxygenated functional groups of EG as shown in Figure 4.6. The characteristic bands around 3378.24 cm^{-1}, 2927.02 cm^{-1}, 1745.72 cm^{-1}, and 1158.92 cm^{-1} corresponds to the O–H, C–H, C=O and C–C stretch vibration of ATEG, respectively (Dhakate et al., 2009; Goudarzi & Hashemi Motlagh, 2019; Yao et al., 2016). The EG particle peaks demonstrated in Figure 4.6 confirm that the intercalating agents were successfully

inserted into the NG particles. The presence of hydroxyl, carboxyl, and epoxyl groups on the surface of EG was clearly evident using FTIR analysis.

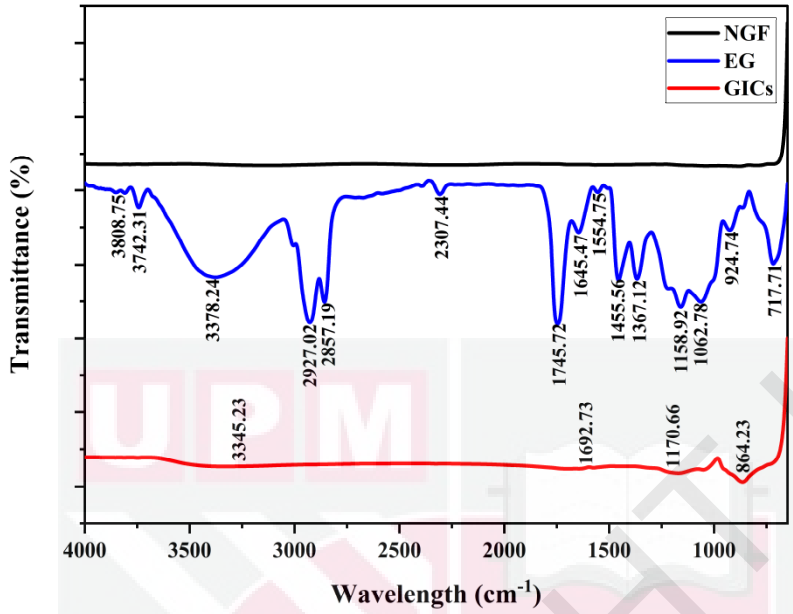

Figure 4.6: FT-IR spectra of expanded graphite

4.3 Study Parameters Affecting the EG-SF

The crucial stage in the chemical method of preparing expanded graphite is oxidation. The carbon atoms of adjacent interlayers on the edges were independent of each other due to the effect of the oxidant, and the interlayer space increased. Therefore, the energy required in the intercalation reaction was reduced, resulting in an easier intercalation reaction.

The optimum conditions for the first stage intercalation to synthesize acidized graphite (oxidized graphite) AG depend on the oxidation capacity of potassium permanganate, which is affected by the pH value of the solution, which is related to the mass concentration of palmitic acid (PA). Similarly, the optimum conditions for the second

stage intercalation of nitric and acetic acids have a great contribution to the oxidation process as they provide an acid environment, as well as act as intercalation aids to release more gas and help push the graphite layers (T. Liu et al., 2017). The impacts of different reagents on the volume expansion of graphite flakes were investigated, and the results are presented below:

4.3.1 Study the effects of reaction time on the graphite expansion volume

The reaction time is critical in the graphite expansion process as shown in Figure 4.7. During the mixing process, $KMnO_4$ acted as the oxidant to oxidize the natural graphite edge, creating a space between the graphite layers. As a result, it enables acid to enter the graphite interlayers. Besides, the oxidant is unstable and decomposed easily in acid solutions, leading to the symmetrical rupture of the O-O bond, hence the gas production during the mixing process (T. Liu et al., 2017). When the reaction time is short less than 20 min, the graphite edge does not fully oxidize because the acid could not intercalate between the graphite layers. The value of EV rises from 310 to 470 mL/g as the reaction time grows from 20 to 30 min, then decreases significantly as time passes. When the reaction time is less than 20 min, the intercalating reaction cannot be complete, and the longer time will aid in the oxidant's destruction of the graphite edge layer. As a result of the extended time, more intercalating reagents will penetrate the layer of graphite, which is favourable to reaching optimum EV. However, the EV is decreased after the mixing time exceeded 30 min, especially after 40 min of mixing time, the EV of the EG would drop dramatically. This scenario happened because part of the intercalated acid had been vaporized which led to less acid molecules existing in the mixture (Trivedi et al., 2018). Therefore, the optimum reaction time of 30 min was determined for the preparation of EG.

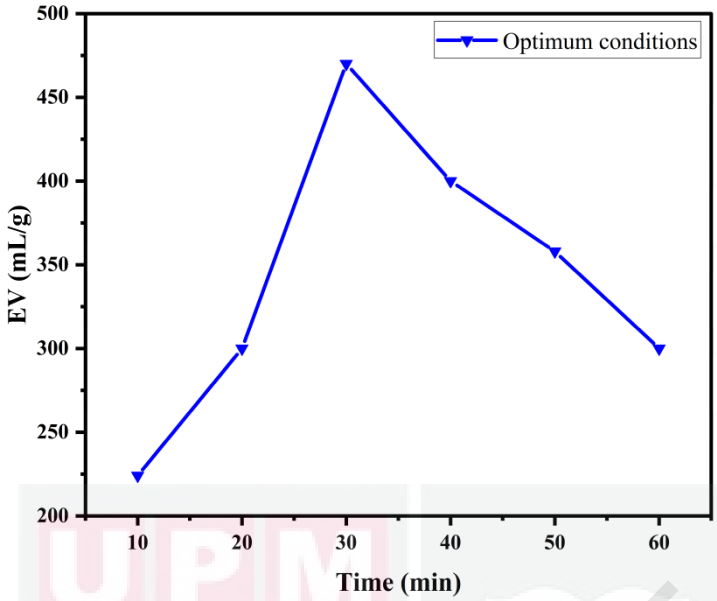

Figure 4.7: Effects of reaction time on graphite expansion volume

4.3.2 Effects of palmitic acid concentration on the on the graphite expansion volume

The expanded volume (EV) was a criterion to judge whether the expandable graphite was formed. Under normal temperatures and pressures, the chemical property of graphite is stable, so only strong acids can intercalate the natural flake graphite and break the graphite edge (Chung, 2016). To determine the effect of PA on the EV of EG Figure 4.8 is investigated with various amounts of PA, under the condition of graphite: G: $KMnO_4$ (mass ratio) = 1: 0.2. It can be clearly seen that the EV of EG is increased when the amount of PA is increased from 5-6 mL. It is due to the increasing acid content, which is PA, since it increases the gas production during the intercalation process and hence increases the expanded volume of the natural graphite flake (Dai et al., 2019). However, the EV of graphite increases first and then decreases when the amount of PA is increased from 7-8 mL, because when the intercalating agent exceeds 8 mL, it affects the ability of the graphite to expand. An excessively increased amount of PA may cause severe oxidation of graphite layers, resulting in a reduction in EG (T.

Wei et al., 2008). It is also because the acidity has changed the nature of the graphite, which has led to a change in the chemical process, hence the EV decreases (Trivedi et al., 2018). Besides, when the excessive acid is added, it would envelope the GICs and lead to additional pressure on the GICs. It inhibits the expansion of GICs and results in a lower EV (T. Liu et al., 2017).

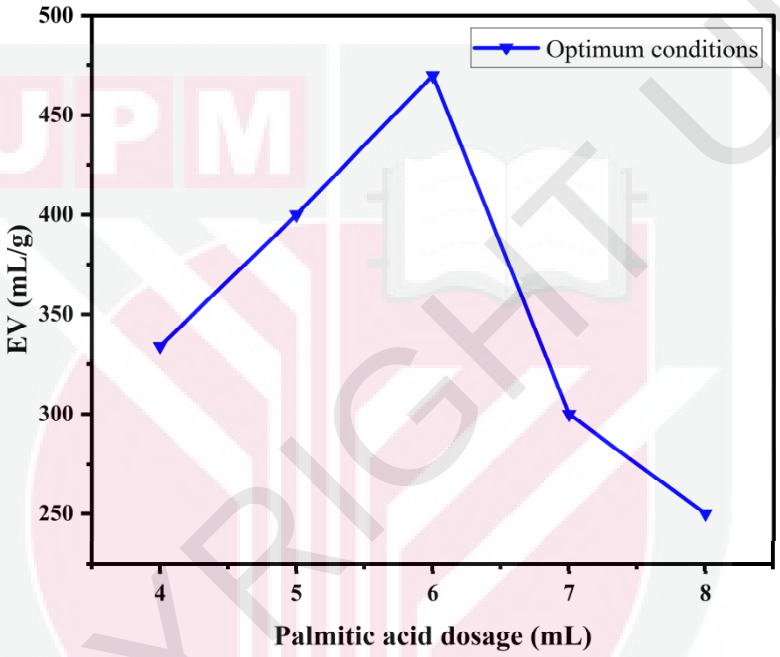

Figure 4.8: Effects of palmitic acid concentration on graphite expansion volume

4.3.3 Effects of potassium permanganate dosage on the graphite expansion volume

$KMnO_4$ plays a crucial role in the graphite expansion process as a principal oxidizer. If the $KMnO_4$ amount is insufficient, the edges of the graphite layers are neither fully oxidized nor entirely opened, preventing the intercalation agent molecules from entering completely between the graphite layers. When the $KMnO_4$ dosage was very high, the graphite layers were overly oxidized, allowing intercalated molecules to seep from the edges of the very open layers. The effect of the $KMnO_4$ dosage of the first

stage intercalation on the expanded volume value was investigated, as shown in Figure 4.9**.** As the $KMnO_4$ dosage increases, the expanded volume value obviously increases, showing that a higher $KMnO_4$ amount is preferable for achieving a higher expanded volume value. Furthermore, when the amount of $KMnO_4$ was increased from 0.1g to 0.15g, the expansion volume of EG increased significantly, but plateaued at 470 mL/g when the amount of $KMnO_4$ was increased from 0.15g to 0.2g. The amount of $KMnO_4$ is excessive, consequently, severe oxidation would damage the structure of the graphite layers., and the EV would be decreased. As a result, $KMnO_4$ should play a significant role in expanded graphite production. According to studies, $KMnO_4$ is chemically unstable and breaks rapidly in acidic environments, causing the oxygen bond to break symmetrically and oxygen to be generated.

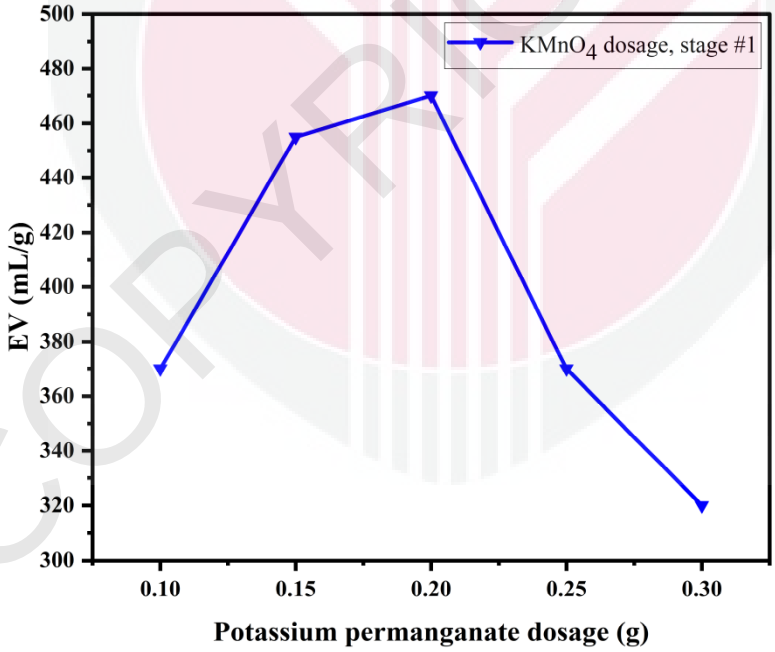

Figure 4.9: Effects of oxidant dosage of first step on graphite expansion volume

Likewise, adding $KMnO_4$ in the second stage of intercalation will cause GICs to be oxidized. Consequently, more graphite edges are oxidized, and this insertion of

oxygen-containing functional groups in the graphene basal plane leads to dramatic changes in the basal dimension (P. Wang et al., 2015). Figure 4.10 demonstrates that the amount of $KMnO_4$ used for intercalation in the second stage has a significant effect on EV. When the $KMnO_4$ was less than 0.1 g, it could not fully open the layers of graphite due to its lack, and the EV was small. When there is more than 0.1 g in the reaction system, graphite layers over oxidation occurs. The interaction force between graphite layers and the intercalating agent has been destroyed, so that the intercalating agent cannot be effectively bound among the interlayers and the EV is not at its maximum. Thus, the optimum amount of $KMnO_4$ found was 0.1 g.

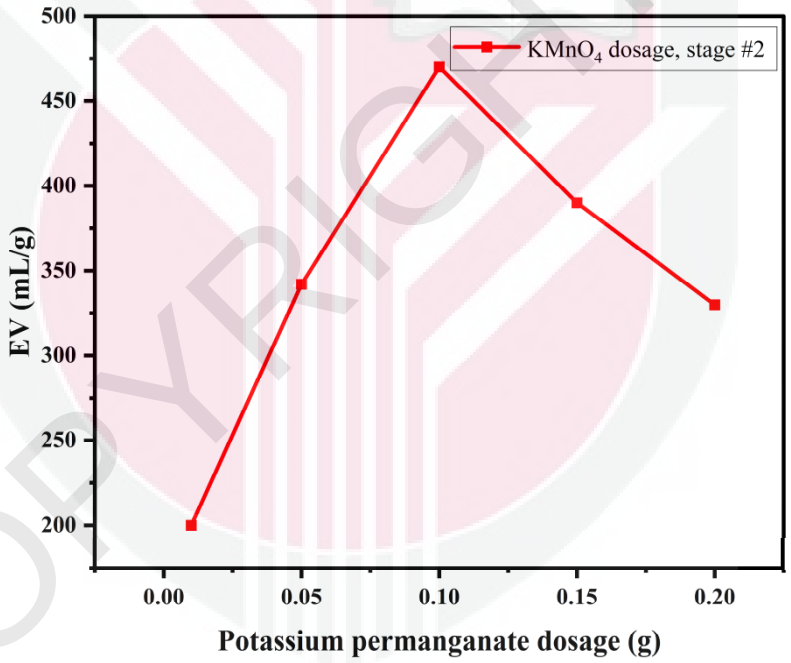

Figure 4.10: Effects of oxidant dosage of second step on graphite expansion volume

4.3.4 Study the effects of nitric acid and acetic acid on the graphite expansion volume

The HNO_3 and CH_3COOH were used as intercalation-assisted agents in the second-stage intercalation, and they were the last two reagents to be added to the reaction

systems. $KMnO_4$ requires an acid environment to work, and the two acids provide an acid environment. In addition, HNO_3 and CH_3COOH act as intercalation aids to release more gas and help push the graphite layers. The expansion effect was shown to be worse when PA, HNO_3, and CH_3COOH were simultaneously added into the reaction systems. This was due to the fact that the intercalation of PA, the primary agent, was inhibited by the competitive intercalation of these different agents. After conducting the first-stage intercalation for 30 min, the acidity of the reaction system was enhanced by the addition of both acids (HNO_3 and CH_3COOH). Therefore, HNO_3 and CH_3COOH could enhance the oxidation effect of KMnO4 and promote the intercalation process of PA. As intercalation agents, HNO_3 and CH_3COOH also entered the graphite layers and enhanced the EV. Figure 4.11 and Figure 4.12 shows that the best amounts of HNO_3 and CH_3COOH for increasing the EV are 1.5 and 6 mL, respectively. Conversely, the excessive amounts of HNO_3 and CH_3COOH reduce the concentrations of PA and $KMnO_4$, which ultimately cause the EV to decrease.

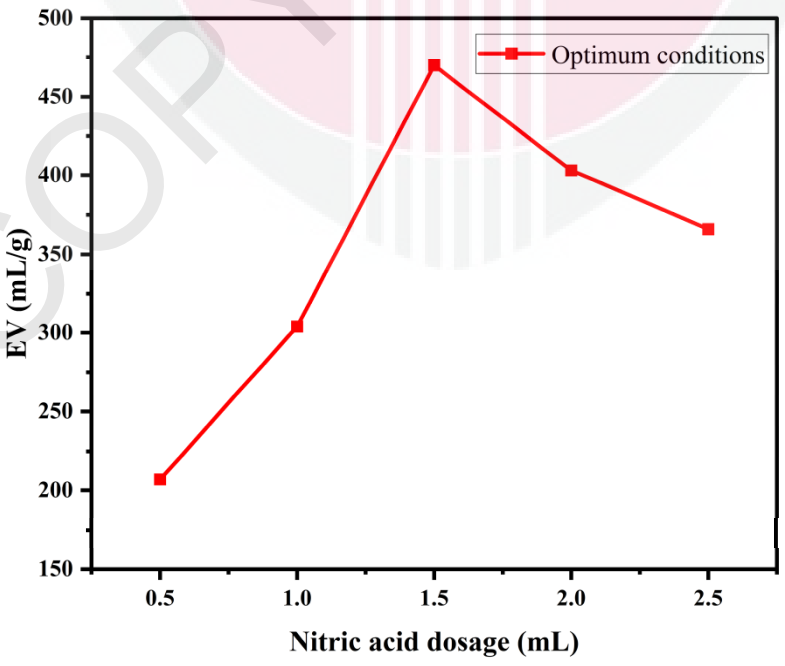

Figure 4.11: Effects of nitric acid on graphite expansion volume

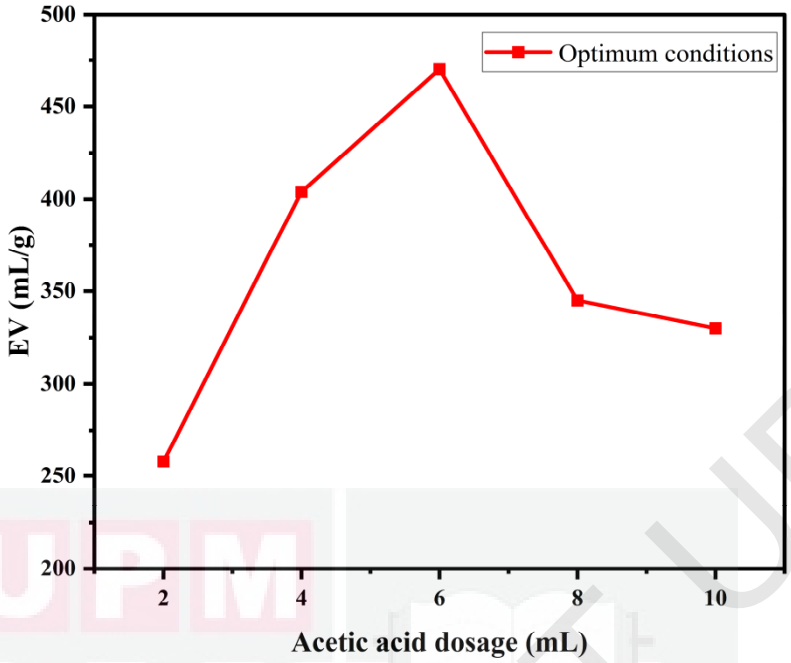

Figure 4.12: Effects of acetic acid on graphite expansion volume

4.3.5 Morphological and structural characterization of EG-SF

4.3.5.1 SEM Analysis

SEM was used to examine the morphology of natural graphite flake and expanded graphite, and SEM micrographs of both are presented in Figure 4.13 and Figure 4.15. The morphology of natural graphite flakes is depicted in Figure 4.13, which reveals that the morphology of natural graphite presents a rough surface with a multilayered crystalline structure. Furthermore, Figure 4.14 showed that the structure of GICs consists of layers of graphite stacked on top of each other, with intercalated species inserted between the layers. The layers of graphite are composed of hexagonal rings of carbon atoms arranged in a two-dimensional honeycomb lattice. The intercalated species are usually arranged in a specific way between the graphite layers (Chung, 2015; Dresselhaus & Dresselhaus, 1981). Compared to graphite, EG has a very distinct

morphology. The lamellar structure of natural graphite flakes was expanded along the graphite crystal's c-axis, changing it from a lamellar structure to a worm-like shape. An expanded SEM micrograph of such a legume can be shown in Figure 4.15. The expanded domain clearly exhibits a honeycomb substructure. The basic structure was disrupted in an attempt to develop a worm-like fluffy shape. Gases are created in graphite layers by the breakdown of oxidants. The van der Waals forces present in the interlayers are overcome by the rising gas pressure, pushing and rapidly expanding the graphite in the direction of the c-axis (Chung, 2016).

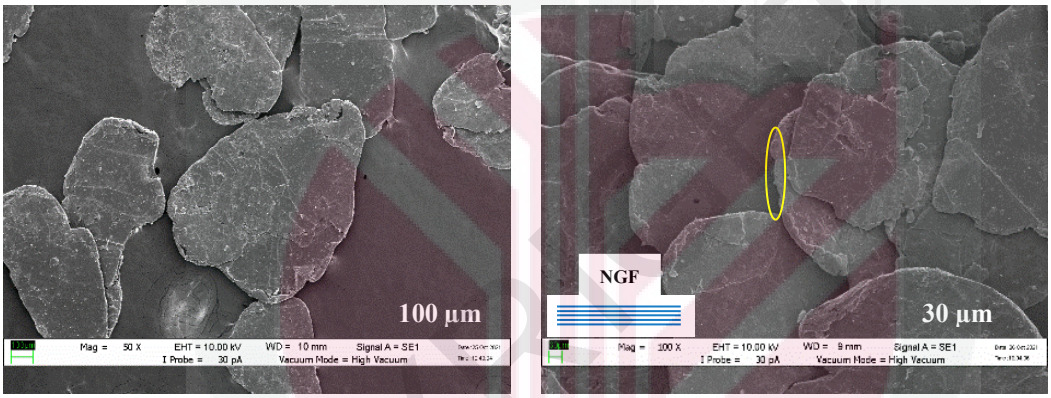

(a) (b)

Figure 4.13: SEM images of NFG

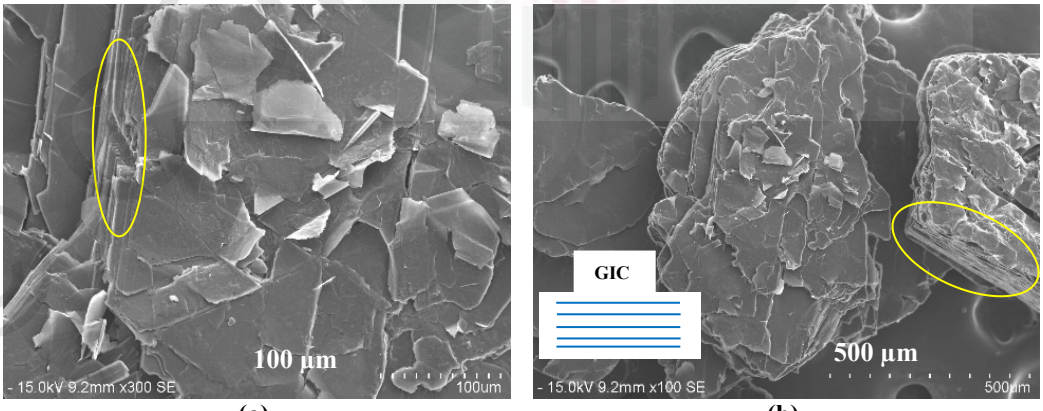

(a) (b)

Figure 4.14: SEM images GICs

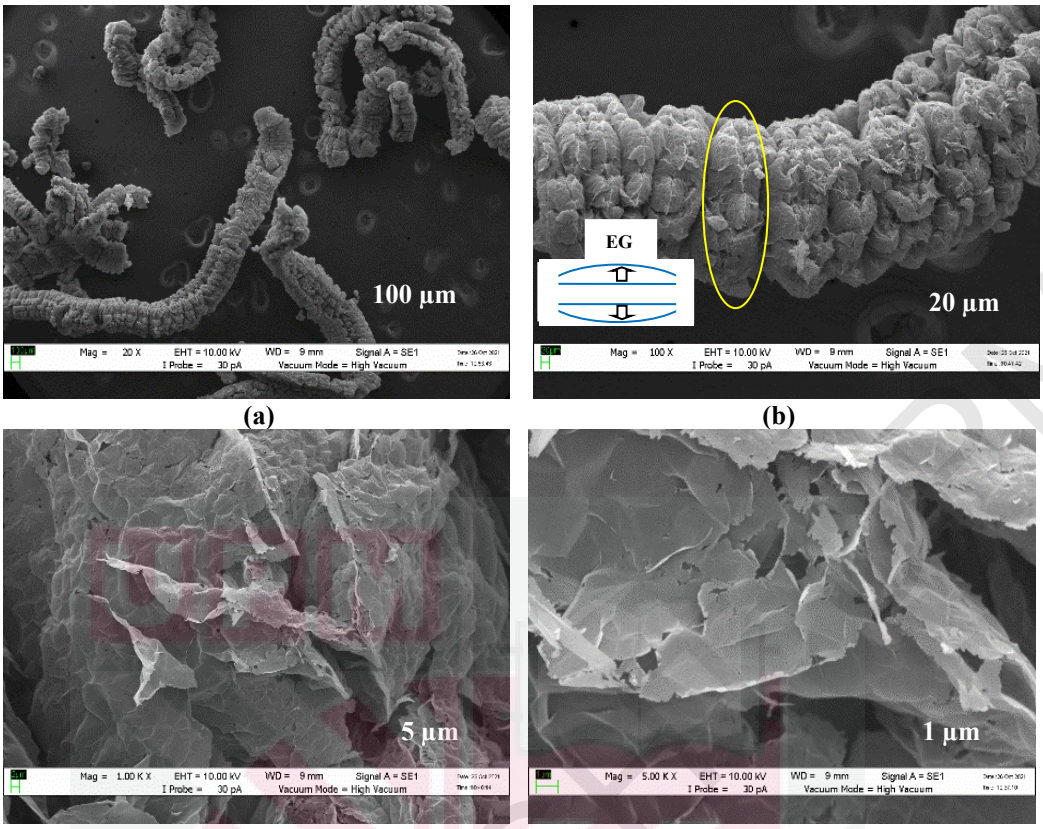

Figure 4.15: SEM images EG-SF

4.3.5.2 XRD Analysis

The X-ray diffraction (XRD) morphologies of NG and EG were represented in Figure 4.16. During the intercalation process that occurs along the EG, the combination of nitric acid, acetic acid, and potassium permanganate decomposes into ions. As shown in Figure 4.16 (a), the XRD patterns of EG materials exhibit two prominent peaks at 26.48 and 54.5, which correspond to the (002) and (004) reflections plane with an interlayer distance of (0.34 nm) (Saikam et al., 2022; Zhou et al., 2018). This is because acid intercalation increases the interplanar distance of graphite, causing a decrease in 2θ° when compared to pristine graphite (Dimiev & Tour, 2014; Malard et al., 2009). According to XRD patterns, the basal spacing of expanded graphite is increased as a result of graphite expansion.

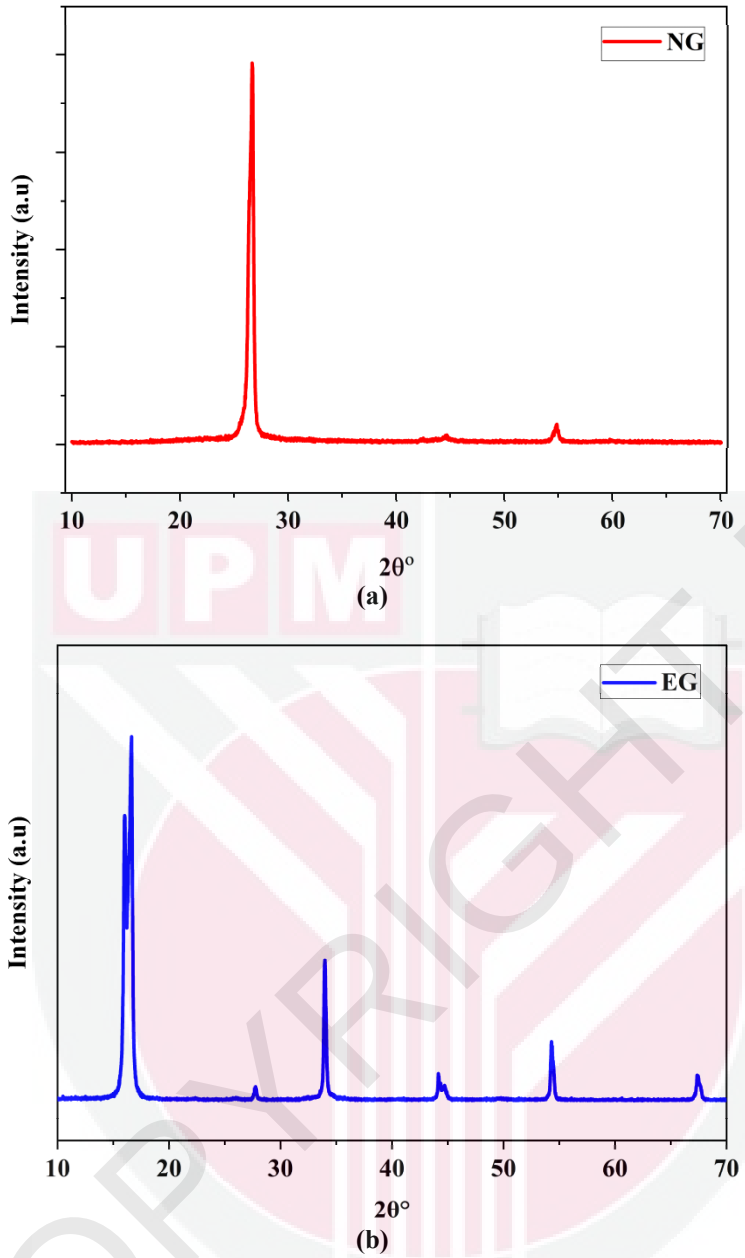

Figure 4.16: XRD images; (a) NFG and (b) EG-SF

4.3.5.3 FT-IR Analysis

To confirm the structural variation and represent a variety of oxygenated functional groups of the as-prepared EG, Fourier Transform Infra-Red (FTIR) were obtained, as shown in Figure 4.17. Also, Figure 4.17 demonstrated the EG particle peaks, confirming that the intercalating agents were successfully inserted into the NG. The

O-H stretch vibration of EG is located at 3742.99, 3621 and 3461.96 cm^{-1} (J. Chen et al., 2013; Dhakate et al., 2009; Eltaweil et al., 2022; Lowe et al., 2019; Marcano et al., 2010; Saikam et al., 2022; Tarango-Rivero et al., 2022), the C-H stretch vibration at 3014.8 cm^{-1} (Eltaweil et al., 2022; Gale et al., 2021; Subrahmanyam et al., 2008; Tarango-Rivero et al., 2022), the C-C stretch vibration at 2355.94 cm^{-1} (Saikam et al., 2022), the C=O stretch vibration at 1739.60 and 1538.79 cm^{-1} (Eltaweil et al., 2022; Marcano et al., 2010; Ren et al., 2019; Tarango-Rivero et al., 2022; Toh et al., 2014), and the C-O stretch vibration at 1367.27 and 1217.4 cm^{-1} (J. Chen et al., 2013; C. Liu et al., 2011; Lowe et al., 2019; Marcano et al., 2010). Furthermore, the C-O-C symmetric and stretching band at 899.76–693.79 cm^{-1} (Tarango-Rivero et al., 2022), and that at 1445.66 cm^{-1} to different motions of the oxygenated groups C-OH bending (Eltaweil et al., 2022; C. Liu et al., 2011). FTIR analysis clearly revealed the presence of hydroxyl, carboxyl, and epoxyl groups on the surface of EG (Dhakate et al., 2009; Eltaweil et al., 2022; Ren et al., 2019; Saikam et al., 2022; Toh et al., 2014; Yao et al., 2016; Y. Zhang et al., 2017).

The stretching observed at 3400-3900 cm^{-1} in FTIR analysis typically corresponds to the O−H (hydroxyl) stretching vibration in organic molecules. This absorption band is typically broad and strong, indicating the presence of an alcohol, or carboxylic acid functional group. However, the stretching observed at 3000 cm^{-1} in FTIR analysis typically corresponds to the C−H stretching vibration in organic molecules. This absorption band is generally broad and strong, indicating the presence of carbon-hydrogen functional groups in the sample being analyzed. In addition, the stretching observed at 2000 cm^{-1} in FTIR analysis can correspond to several different functional groups depending on their exact position and shape. Most common possibilities

include C−C. Furthermore, the stretching observed at 1700 cm^{-1} in FTIR analysis typically corresponds to the C=O (carbonyl) stretching vibration in organic molecules. This absorption band is typically sharp and strong, indicating the presence of a carbonyl functional group in the sample being analyzed. Some common functional groups that exhibit a C=O stretching band at around 1700 cm^{-1} include ketones, and carboxylic acids. The stretching observed at 1600 cm^{-1} in FTIR analysis typically corresponds to the C=C stretching vibration in organic molecules. This absorption band is typically medium to strong and can indicate the presence of a carbon functional group in the sample being analyzed. The stretching observed at 1400 cm^{-1} in FTIR analysis typically corresponds to the bending vibration of the C-H (carbon-hydrogen) bond in organic molecules. This absorption band is usually weak to medium and can indicate the presence of several different functional groups, including alkane, alkene, and aromatic compounds. Moreover, the stretching observed at 1367.27 and 1217.4 cm^{-1} in FTIR analysis typically corresponds to several different functional groups, depending on the exact position and shape of the band. Some common possibilities include C-O stretching in ethers, esters, and some alcohols, and C-C stretching in some aromatic compounds and alkanes. Finally, the stretching observed at 900 cm^{-1} in FTIR analysis typically corresponds to the C-O-C out-of-plane bending vibration.

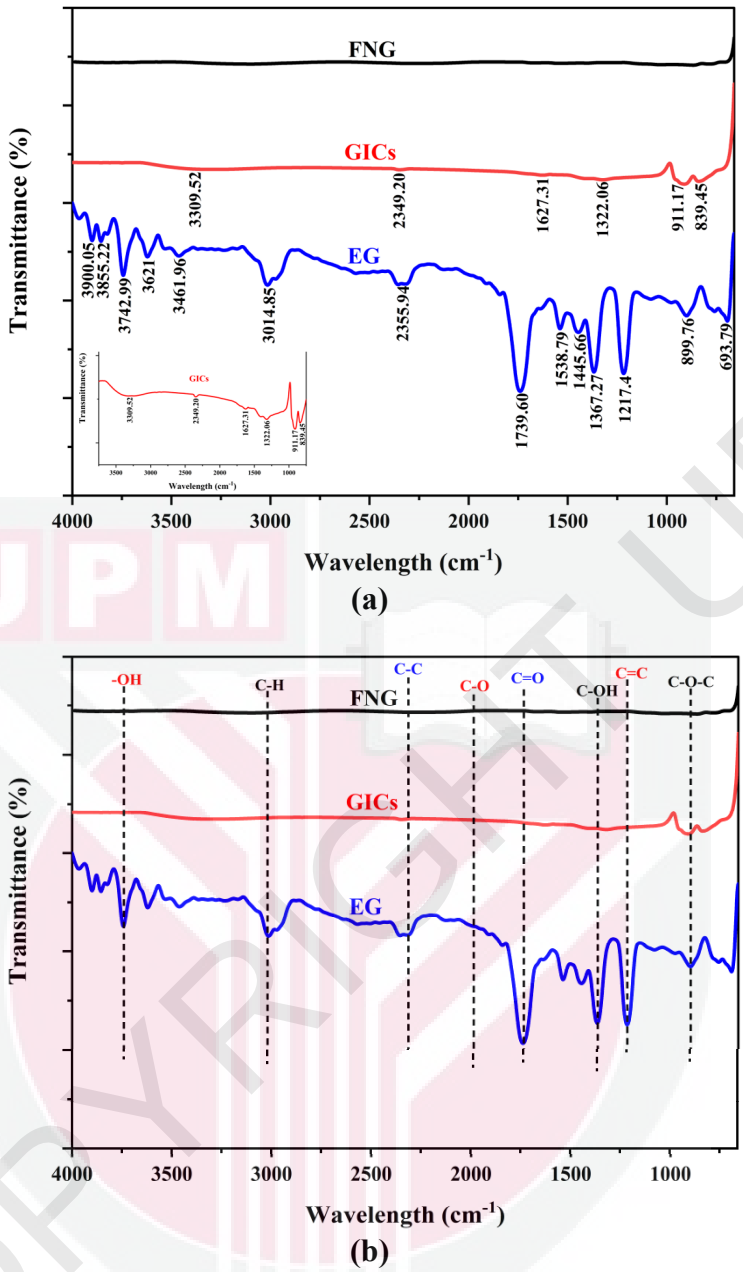

Figure 4.17: FT-IR spectra of (a) FNG, GICs and EG-SF and (b) the functional groups regions

4.4 Sorption Performance of Expanded Graphite on Engine Oil

The study evaluated the sorption abilities of the expanded graphite produced and examined the impact of various synthesis methods on the preparation process of expanded graphite. Additionally, although manipulating the engine oil may not be

practical in real operations, it can provide valuable insights into the optimal working conditions for the prepared materials.

4.4.1 Effect of expanded graphite type

Explore and assess the capability of the prepared two types of expanded graphite prepared in this research in sorbing oil. The morphology analyses and images that the two prepared of expanded graphite produced in this work have low density and high porosities. This porous structure should give them the ability to absorb hydrocarbons. It has been demonstrated that expanded graphite possesses significant oil-sorption capabilities (Saikam et al., 2022; Tarango-Rivero et al., 2022; K. H. Wu et al., 2021). The addition of EG to the oily upper layer results in the instant formation of a carbonaceous material agglomeration attached to the oil. Because of the several absorbing spaces generated by EG stacking on each other and pores located in each worm-like fluffy shape (Goudarzi & Hashemi Motlagh, 2019; M. Zhao & Liu, 2009). The maximum oil sorption capacity of the all type of expanded graphite was expressed by weight ratio of engine oil per 1 g of EG (g/g) as shown Figure 4.18 both ATEG and HTEG have the highest sorption capacity for oil 89 g/g and 27 g/g, respectively. Compared to its expanded volume, the oil absorbed by ATEG is higher than that absorbed by HTEG. These results indicate that the methods used to prepare EG have a significant impact on its adsorption capacity for oils.

When EG-SF absorbed between 1 g to 8.5 g of oil, some EG remained unused and the water's surface was clear after the oil was removed. However, when EG tried to absorb more than 9 g of oil, it was no longer effective. In this study, the maximum sorption capacity of EG for engine oil for sulfur free was determined which was 85 g/g. It is

because the water surface after extracting the oil was clear and all the EG had sorbed the oil effectively. Besides, there was no oil drop was observed when EG was extracted from the beaker. Thus, highest oil sorption capacity reached was 85 (g/g), demonstrating outstanding performance. For an adsorbent to be considered good, it should have a large sorption capacity, perform rapidly, and exhibit high selectivity.

Obviously, the surface structure has a significant impact on oil sorption performance, as shown in the SEM analysis. As the expanded volume increases, the oil sorption increases accordingly. The highly hydrophobic nature of EG allows it to selectively absorb oil and repel water, thereby improving the effectiveness of separating oil and water. When expanded graphite is arranged in a layered structure, it exhibits a significant presence of conjugated delocalized π-electrons on its surface, attributed to the sp^2 hybridization of carbon atoms. These π -electrons attract other π and σ electrons, resulting in the formation of π - π coupling. In the case of aromatic compounds, there is the formation of π - π electron coupling or stacking interaction. In hydrocarbons like engine oil, the σ electrons within the absorbed molecules can couple with the π -electrons on EG, thereby enhancing the oil absorption capability (Saikam et al., 2022; Toyoda & Inagaki, 2000; Yin et al., 2021).

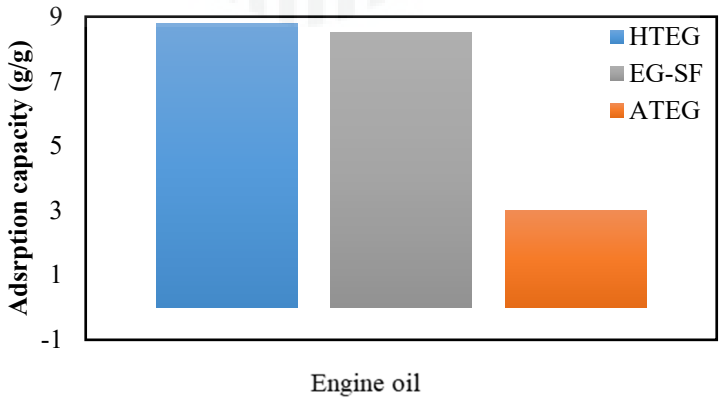

Figure 4.18: Adsorption capacity of ATEG and HTEG

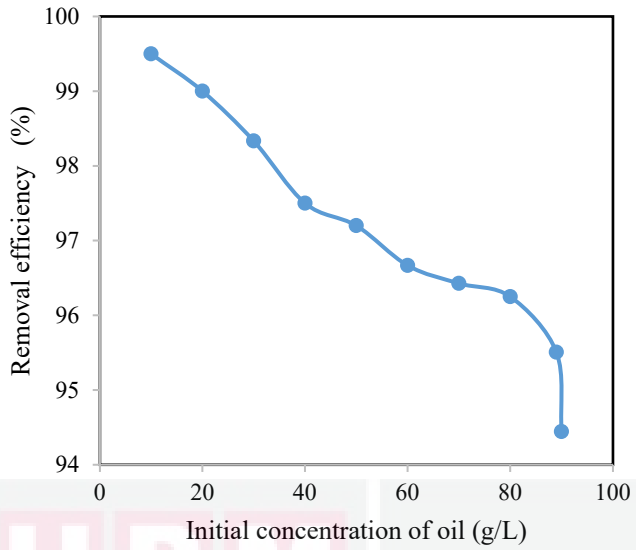

Figure 4.19: The effect of initial concentration on the removal efficiency

4.4.2 Effect of absorption time of the EGs

To examine the relationship between sorption uptake and time, the engine oil sorption on EGs was analyzed as a function of contact time. The absorption profile, illustrated in Figure 4.20, shows the weight changes recorded over the observation period.

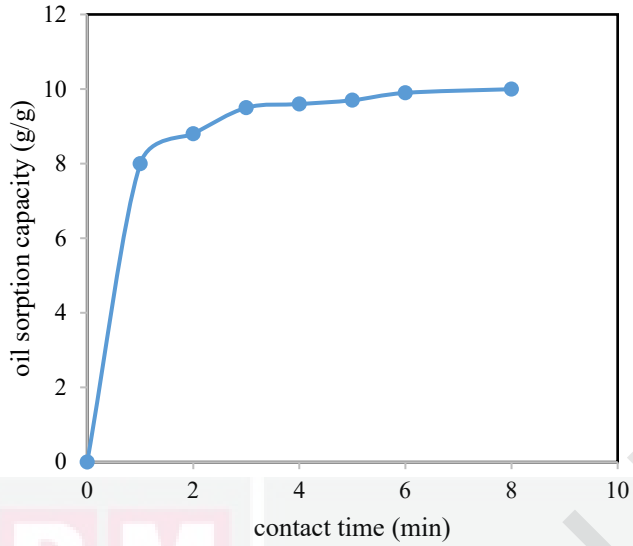

Figure 4.20: Effect of time on sorption capacity

4.4.3 Water uptake study

Water uptake is used to evaluate the water resistance or hydrophilicity of a material. Water uptake is a crucial behavior that is mostly dependent on the presence of hydrophilic functional groups. From the result, the EG-PA content water uptake value is 40.2 % due to the hydrophobic nature of EG-PA. Notably, the increase in the water uptake of the EG-PA increase in the number of the hydrophilic groups (OH and COOH), which induces the hydrophilicity of EG-PA (Eltaweil et al., 2022).

4.4.4 Recyclability

The main drawback associated with the adsorption technique is the cost of the adsorbent materials, which elevates the overall treatment process cost. Thus, recycling and reusing the adsorbent makes it affordable, promotes sustainable development, and allows for green chemistry-based engineering processes. Not only must EG remove oil

from water efficiently, but both the oil and EG must be recovered and recycled properly; nevertheless, the porous structure of EG is readily damaged during the regeneration process (Coha et al., 2021; S. Hou et al., 2022; Iqbal & Abdala, 2013). Different techniques have suggested for separating oil from saturated EG; physical process including filtration (Toyoda & Inagaki, 2000), manual squeezing (Vocciante et al., 2022), heating (Tarango-Rivero et al., 2022) which are practical methods. One of the drawbacks of using the physical method is that the amount of oil recovered decreases significantly as the recycling times increase, due to the oil being trapped in the pores or on the surface of EG. Additionally, the structure and appearance of the particles can be altered, and there are energy costs associated with the process. Another practical separation method is chemical extraction, different solvents have been proposed to separate the oil from the saturated EG, hexane (Rozi et al., 2017), petroleum ether (K. H. Wu et al., 2021), ethanol (Eltaweil et al., 2022). As shown in Figure 4.21 presents the recyclability test from 85, 80, and 78 g/g. This finding demonstrates extended graphite's favorable recyclability, which in turn reflects the material's wide range of potential uses.

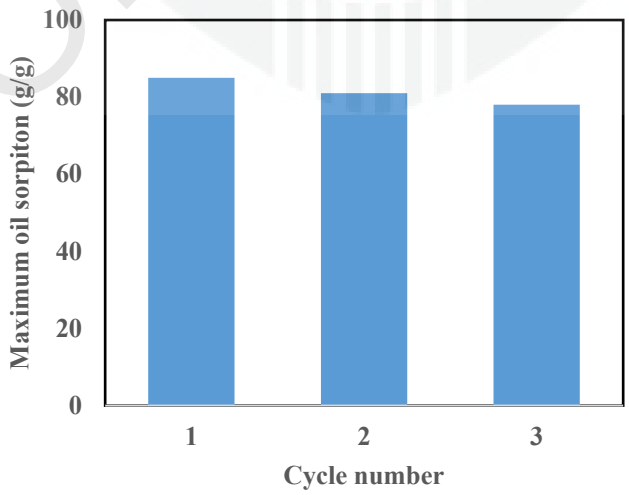

Figure 4.21: Recyclability test

4.5 Statistical Analysis

The effects of different variables on the volume expansion of both types of expanded graphite developed in this thesis were analyzed using ANOVA with multiple levels. Various factors such as reaction time, palmitic acid concentration, potassium permanganate amount, nitric acid concentration, and acetic acid were considered to evaluate the expansion of the eco-friendly sulfur-free expanded graphite. Similarly, sulfuric acid concentration and potassium peroxydisulfate amount were used to assess the expansion of the rapidly expanded graphite. The application of ANOVA in addressing the research objective is significant as it provides a statistical framework for testing the hypothesis related to expansion volume. By analyzing the variations among the mean expansion volumes, ANOVA helps identify the most influential factors that contribute to the optimal condition of expanded graphite. The following hypothesis is formulated to examine the impact of these parameters on the expansion volume:

4.5.1 Effects of sulfuric acid concentration on graphite expansion volume at optimum condition

In Table 4.1 the "Between Groups" section measures the variability between the groups, specifically the differences in means across the sulfuric acid concentration levels. It includes the sum of squares (SS), degrees of freedom (df), mean square (MS), F-ratio (F), and the associated p-value (Sig.). In this case, the sum of squares is 16240.571, the degrees of freedom are 6, and the mean square is 2706.762. The F-ratio is calculated as 931.836, and the p-value is reported as .000, which indicates a highly significant result.

In summary, the ANOVA results indicate a significant difference in the means of the expanded volume of graphite across the different concentrations of sulfuric acid. The between-group variability is much larger than the within-group variability, with a highly significant F-ratio. This suggests that the concentration of sulfuric acid has a significant effect on the expansion volume of graphite.

Null hypothesis (H0): The concentration of sulfuric acid does not have a significant effect on the expansion volume of graphite at the optimum condition.

Alternative hypothesis (H1): The concentration of sulfuric acid has a significant effect on the expansion volume of graphite at the optimum condition.

Table 4.1: Two-way ANOVA of the means of the expanded volume of graphite across the different concentrations of sulfuric acid

	Sum of Squares	df	Mean Square	F	Sig.
Between Groups	16240.571	6	2706.762	931.836	.000
Within Groups	40.667	14	2.905		
Total	16281.238	20			

Based on the significant results obtained from the ANOVA analysis Table 4.1, a post hoc test can be conducted to determine which specific pairs of the concentration of sulfuric acid ratio exhibit significant differences in the expanded volume of graphite. The post hoc test conducted for the expanded volume of graphite at different solid-liquid ratios reveals significant mean differences between various pairs of ratios. The least significant difference (LSD) test was employed to compare the means.

The table presents the mean differences (in mL/g) between different solid-liquid ratio pairs (I and J), along with the standard error, significance (p-value), and the 95% confidence interval of the difference. The significance is denoted by asterisks, indicating a significant difference at the 0.05 level.

The results show that for the 1% solid-liquid ratio, the mean difference is significant and negative when compared to the 2%, 3%, and 5% ratios. Similarly, the 2% ratio exhibits significant negative mean differences when compared to the 3% and 5% ratios. However, no significant differences were observed between the 7% and 1% ratios.

Furthermore, the 5% ratio displays significant positive mean differences when compared to the 7%, 10%, and 13% ratios. The 7% ratio also shows significant positive mean differences when compared to the 10% and 13% ratios. Moreover, the 10% ratio demonstrates significant positive mean differences when compared to the 13% ratio, also significant differences were observed between the 7% and 10% ratios, as well as between the 13% and 10%.

Table 4.2: Post-hoc results of mean differences (in mL/g) between different solid-liquid ratio pairs (I and J), along with the standard error, significance (p-value), and the 95% confidence interval of the difference

(I) Solid_liquid ratio	(J) Solid_liquid ratio	Mean Difference (I-J)	Std. Error	Sig.	95% Confidence Interval	
					Lower Bound	Upper Bound
1%	2%	-20.333*	1.392	.000	-23.32	-17.35
	3%	-31.000*	1.392	.000	-33.98	-28.02
	5%	-42.000*	1.392	.000	-44.98	-39.02
	7%	-2.000	1.392	.173	-4.98	.98
	10%	29.667*	1.392	.000	26.68	32.65
	13%	38.667*	1.392	.000	35.68	41.65
2%	3%	-10.667*	1.392	.000	-13.65	-7.68
	5%	-21.667*	1.392	.000	-24.65	-18.68
	7%	18.333*	1.392	.000	15.35	21.32
	10%	50.000*	1.392	.000	47.02	52.98
	13%	59.000*	1.392	.000	56.02	61.98
3%	5%	-11.000*	1.392	.000	-13.98	-8.02
	7%	29.000*	1.392	.000	26.02	31.98
	10%	60.667*	1.392	.000	57.68	63.65
	13%	69.667*	1.392	.000	66.68	72.65
5%	7%	40.000*	1.392	.000	37.02	42.98
	10%	71.667*	1.392	.000	68.68	74.65
	13%	80.667*	1.392	.000	77.68	83.65
7%	10%	31.667*	1.392	.000	28.68	34.65
	13%	40.667*	1.392	.000	37.68	43.65
13%	10%	-9.000*	1.392	.000	-11.98	-6.02

*. The mean difference is significant at the 0.05 level.

Figure 4.22 shows the significant differences in the expanded volume of graphite at different solid-liquid ratios. These findings suggest that the choice of solid-liquid ratio has a substantial impact on the expansion volume, with some ratios exhibiting significant differences in mean volume compared to others. Nevertheless, 5% seems to be the best solid-liquid among other ratios.

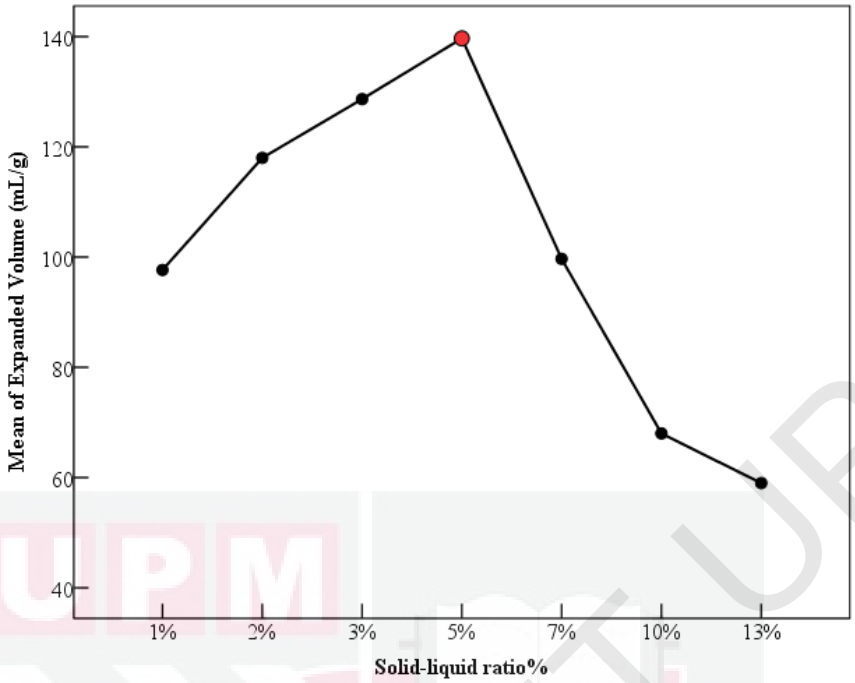

Figure 4.22: Mean of the expanded volume of graphite at different solid-liquid ratios

4.5.2 Effects of potassium peroxydisulfate on graphite expansion volume at optimum condition

The Table 4.3 provides a summary of the analysis of variance conducted on the expanded volume of graphite at different oxidant dosages at the optimum condition. The purpose of this statistical test is to determine if there are significant differences in the means of the expanded volume across the different dosage groups.

The "Between Groups" section measures the variability between the groups, specifically the differences in means across the oxidant dosage levels. It includes the sum of squares (SS), degrees of freedom (df), mean square (MS), F-ratio (F), and the associated p-value (Sig.). In this case, the sum of squares is 7818.625, the degrees of freedom are 7, and the mean square is 1116.946. The F-ratio is calculated as 837.710, and the p-value is reported as .000, indicating a highly significant result.

In summary, the ANOVA results indicate a significant difference in the means of the expanded volume of graphite across the different oxidant dosages at the optimum condition. The between-group variability is much larger than the within-group variability, with a highly significant F-ratio. This provides evidence to reject the null hypothesis and suggests that the oxidant dosage has a significant effect on the expansion volume of graphite at the optimum condition.

Null hypothesis (H0): The oxidant dosage does not have a significant effect on the expansion volume of graphite at the optimum condition.

Alternative hypothesis (H1): The oxidant dosage has a significant effect on the expansion volume of graphite at the optimum condition.

Table 4.3: Two-way ANOVA of the means of the expanded volume of graphite across the different sodium peroxydisulfate at the optimum condition

	Sum of Squares	df	Mean Square	F	Sig.
Between Groups	7818.625	7	1116.946	837.710	.000
Within Groups	21.333	16	1.333		
Total	7839.958	23			

Based on the significant results obtained from the ANOVA analysis Table 4.4, a post hoc test can be conducted to determine which specific pairs of oxidant dosage levels exhibit significant differences in the expanded volume of graphite.

The post hoc test conducted for the expanded volume of graphite at different amounts of oxidant reveals significant mean differences between various pairs of oxidant dosage levels. The least significant difference (LSD) test was employed to compare the means.

The Table 4.4 presents the mean differences in expanded volume (in mL/g) between different pairs of oxidant dosage levels (I and J), along with the standard error, significance (p-value), and the 95% confidence interval of the difference. The significance is denoted by asterisks, indicating a significant difference at the 0.05 level. The results show that there are significant mean differences between various pairs of oxidant dosage levels. For example, when comparing the 3 g oxidant dosage to other levels, significant negative mean differences are observed for all comparisons (4 g, 5 g, 6 g, 7 g, 8 g, 9 g, and 10 g).

Similarly, significant negative mean differences are observed when comparing the 4 g dosage to the 6 g, 7 g, 8 g, 9 g, and 10 g dosages. The 5 g dosage also shows significant negative mean differences when compared to the 6 g, 7 g, 8 g, 9 g, and 10 g dosages. Furthermore, significant negative mean differences are observed for comparisons between the 6 g dosage and the 7 g, 8 g, 9 g, and 10 g dosages. The 7 g dosage exhibits significant positive mean differences when compared to the 8 g, 9 g, and 10 g dosages. Moreover, the 8 g dosage shows significant positive mean differences when compared to the 9 g dosage. However, no significant differences are observed between the 8 g and 10 g dosages.

In summary, the post hoc analysis indicates significant differences in the expanded volume of graphite at different amounts of oxidant dosage. These findings suggest that the choice of oxidant dosage has a significant effect on the expansion volume of graphite, with some dosages exhibiting significant differences in mean volume compared to others.

Table 4.4: Post-hoc results of mean differences in expanded volume (in mL/g) between different pairs of sodium peroxydisulfate levels (I and J), along with the standard error, significance (p-value), and the 95% confidence interval of the difference

(I) Amount of Oxidant (g)	(J) Amount of Oxidant (g)	Mean Difference (I-J)	Std. Error	Sig.	95% Confidence Interval	
					Lower Bound	Upper Bound
3	4	-2.000*	.943	.050	-4.00	.00
	5	-3.000*	.943	.006	-5.00	-1.00
	6	-14.000*	.943	.000	-16.00	-12.00
	7	-45.000*	.943	.000	-47.00	-43.00
	8	-40.000*	.943	.000	-42.00	-38.00
	9	-35.333*	.943	.000	-37.33	-33.33
	10	-38.333*	.943	.000	-40.33	-36.33
4	5	-1.000	.943	.305	-3.00	1.00
	6	-12.000*	.943	.000	-14.00	-10.00
	7	-43.000*	.943	.000	-45.00	-41.00
	8	-38.000*	.943	.000	-40.00	-36.00
	9	-33.333*	.943	.000	-35.33	-31.33
	10	-36.333*	.943	.000	-38.33	-34.33
5	6	-11.000*	.943	.000	-13.00	-9.00
	7	-42.000*	.943	.000	-44.00	-40.00
	8	-37.000*	.943	.000	-39.00	-35.00
	9	-32.333*	.943	.000	-34.33	-30.33
	10	-35.333*	.943	.000	-37.33	-33.33
6	7	-31.000*	.943	.000	-33.00	-29.00
	8	-26.000*	.943	.000	-28.00	-24.00
	9	-21.333*	.943	.000	-23.33	-19.33
	10	-24.333*	.943	.000	-26.33	-22.33
7	8	5.000*	.943	.000	3.00	7.00
	9	9.667*	.943	.000	7.67	11.67
	10	6.667*	.943	.000	4.67	8.67
8	9	4.667*	.943	.000	2.67	6.67
	10	1.667	.943	.096	-.33	3.67
10	9	3.000*	.943	.006	1.00	5.00

*. The mean difference is significant at the 0.05 level.

Figure 4.23 would have the x-axis representing the amounts of oxidant (in g) and the y-axis representing the mean of the expanded volume (in mL/g). The points on the plot would represent the different amounts of oxidant, ranging from 3 g to 10 g, with corresponding mean values for the expanded volume.

Based on the information you provided, the highest amount of oxidant, 7 g, is associated with a mean expanded volume of 140 mL/g. Therefore, the point on the plot at the x-coordinate of 7 g would have a y-coordinate of 140.

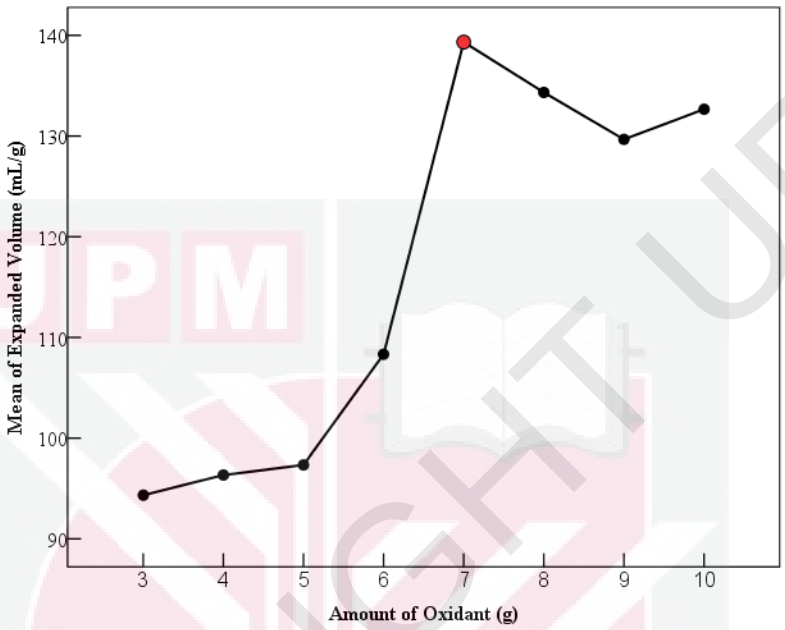

Figure 4.23: Mean of the expanded volume of graphite at different amount of sodium peroxydisulfate

4.5.3 Effects of reaction time on graphite expansion volume at optimum condition

Table 4.5 reveal a significant effect of reaction time on the expanded volume of the synthesized sulfur-free expanded graphite. The between groups sum of squares is 113,492.944, with 5 degrees of freedom, resulting in a mean square value of 22,698.589. The F-value of 1485.726 indicates a highly significant difference among the mean expanded volumes across different reaction times. The associated p-value (Sig.) is reported as 0.000, which is below the conventional significance threshold of 0.05.

In summary, based on the ANOVA results, we reject the null hypothesis (H0) that reaction time does not have a significant effect on the expanded volume of the synthesized sulfur-free expanded graphite. The analysis indicates a significant relationship between reaction time and the expanded volume, suggesting that the duration of the reaction process plays a crucial role in determining the volume expansion of the graphite material.

Null hypothesis (H0): The reaction time does not have a significant effect on the expanded volume of the synthesized sulfur-free expanded graphite.

Alternative hypothesis (H1): The reaction time has a significant effect on the expanded volume of the synthesized sulfur-free expanded graphite.

Table 4.5: Two-way ANOVA of the means of the expanded volume of graphite across different reaction times at optimum conditions

	Sum of Squares	df	Mean Square	F	Sig.
Between Groups	113492.944	5	22698.589	1485.726	.000
Within Groups	183.333	12	15.278		
Total	113676.278	17			

Based on the significant results obtained from the ANOVA analysis Table 4.6, a post hoc test can be conducted to determine which specific pairs of reaction times have significant differences in the expanded volume of the synthesized sulfur-free expanded graphite. This test allows for a more detailed comparison between individual groups to identify any significant variations.

The results of the post hoc test indicate significant differences between various pairs of reaction times. The mean differences, standard errors, significance levels (p-values), and 95% confidence intervals are provided for each pairwise comparison.

Comparing the expanded volume at 10 minutes to other time points, significant differences were observed. The expanded volume at 10 minutes was significantly lower compared to 20 minutes (-77.333 mL/g), 30 minutes (-245.667 mL/g), 40 minutes (-176.333 mL/g), 50 minutes (-135.667 mL/g), and 60 minutes (-70.667 mL/g).

Similarly, significant differences were found between 20 minutes and the subsequent time points, except for 60 minutes. The expanded volume at 20 minutes was significantly lower than at 30 minutes (-168.333 mL/g), 40 minutes (-99.000 mL/g), and 50 minutes (-58.333 mL/g). However, no significant difference was observed between 20 minutes and 60 minutes (6.667 mL/g).

Comparisons between 30 minutes and later time points revealed significant differences. The expanded volume at 30 minutes was significantly lower compared to 40 minutes (69.333 mL/g), 50 minutes (110.000 mL/g), and 60 minutes (175.000 mL/g).

At 40 minutes, a significant difference was found in expanded volume when compared to 50 minutes (40.667 mL/g) and 60 minutes (105.667 mL/g).

Lastly, comparing 60 minutes to 50 minutes revealed a significant difference, with the expanded volume at 60 minutes being significantly lower (-65.000 mL/g).

Overall, it should be noted that the significance levels (p-values) for almost all the observed differences were reported as 0.000, which is below the conventional significance threshold of 0.05. This indicates strong evidence of significant differences between the expanded volumes at different reaction times.

Table 4.6: Post-hoc results of mean differences in expanded volume (in mL/g) between different pairs of reaction time (I and J), along with the standard error, significance (p-value), and the 95% confidence interval of the difference

(I) Time (min)	(J) Time (min)	Mean Difference (I-J)	Std. Error	Sig.	95% Confidence Interval	
					Lower Bound	Upper Bound
10	20	-77.333*	3.191	.000	-84.29	-70.38
	30	-245.667*	3.191	.000	-252.62	-238.71
	40	-176.333*	3.191	.000	-183.29	-169.38
	50	-135.667*	3.191	.000	-142.62	-128.71
	60	-70.667*	3.191	.000	-77.62	-63.71
20	30	-168.333*	3.191	.000	-175.29	-161.38
	40	-99.000*	3.191	.000	-105.95	-92.05
	50	-58.333*	3.191	.000	-65.29	-51.38
	60	6.667	3.191	.059	-.29	13.62
30	40	69.333*	3.191	.000	62.38	76.29
	50	110.000*	3.191	.000	103.05	116.95
	60	175.000*	3.191	.000	168.05	181.95
40	50	40.667*	3.191	.000	33.71	47.62
	60	105.667*	3.191	.000	98.71	112.62
60	50	-65.000*	3.191	.000	-71.95	-58.05

*. The mean difference is significant at the 0.05 level.

Figure 4.24 help to identify the significant variations in expanded volume at different time points, providing insights into the optimal reaction time for synthesizing sulfur-free expanded graphite with the desired expanded volume characteristics. These findings provide valuable insights into the relationship between reaction time and the expanded volume of sulfur-free expanded graphite (EG), aiding in the understanding

of optimal reaction times which is 30 min for achieving desired expansion characteristics.

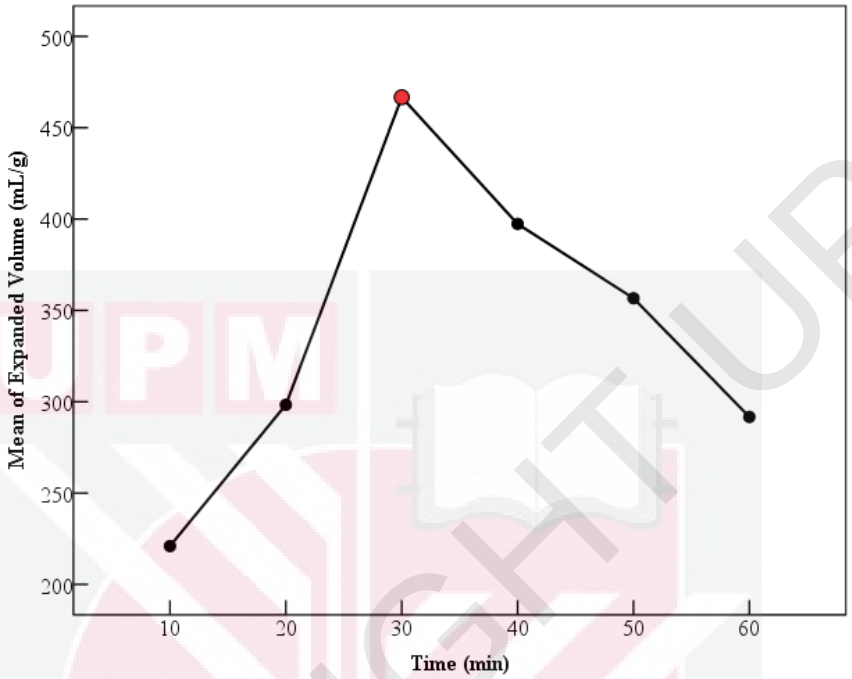

Figure 4.24: Mean of the expanded volume of graphite at different reaction time

4.5.4 Effects of palmitic acid concentration on graphite expansion volume at optimum condition

Based on the results of the ANOVA analysis Table 4.7, there is a significant effect of the concentration of palmitic acid on the expanded volume of the synthesized sulfur-free expanded graphite. The between-groups sum of squares is 90259.333, indicating substantial variability in the expanded volume across different PA concentrations. The degrees of freedom for the between-groups and within-groups factors are 4 and 10, respectively.

The mean square between groups is 22564.833, and the mean square within groups is 14.000. The F-statistic is calculated as 1611.774, which is obtained by dividing the mean square between groups by the mean square within groups. The obtained F-value is highly significant with a p-value of 0.000, indicating strong evidence against the null hypothesis.

Therefore, we reject the null hypothesis and conclude that the concentration of palmitic acid has a significant effect on the expanded volume of the synthesized sulfur-free expanded graphite. Further analysis, such as post hoc tests, can be conducted to determine specific differences between different PA concentrations.

Null hypothesis (H0): The concentration of palmitic acid does not have a significant effect on the expanded volume of the synthesized sulfur-free expanded graphite.

Alternative hypothesis (H1): The concentration of palmitic acid has a significant effect on the expanded volume of the synthesized sulfur-free expanded graphite.

Table 4.7: Two-way ANOVA of the means of the expanded volume of graphite across the different concentrations of palmitic acid at optimum conditions

	Sum of Squares	df	Mean Square	F	Sig.
Between Groups	90259.333	4	22564.833	1611.774	.000
Within Groups	140.000	10	14.000		
Total	90399.333	14			

The post hoc analysis using the LSD (Least Significant Difference) test was conducted to compare the specific pairs of palmitic acid concentrations and their mean differences in the expanded volume of the synthesized sulfur-free expanded graphite. The results are summarized as follows:

- When comparing the PA concentrations of 4 mL and 5 mL, there is a significant mean difference of -67.333 mL/g ($p < 0.001$), with the 95% confidence interval ranging from -74.14 to -60.53 mL/g. Similarly, for other comparisons involving 4 mL of PA concentration (6 mL, 7 mL, and 8 mL), significant mean differences are observed.

- When comparing the PA concentrations of 5 mL and 6 mL, there is a significant mean difference of -68.333 mL/g ($p < 0.001$), with the 95% confidence interval ranging from -75.14 to -61.53 mL/g. Likewise, for other comparisons involving 5 mL of PA concentration (7 mL and 8 mL), significant mean differences are observed.

- Comparisons involving 6 mL of PA concentration (7 mL and 8 mL) also show significant mean differences in the expanded volume.

- Finally, when comparing the PA concentrations of 8 mL and 7 mL, there is a significant mean difference of -47.333 mL/g ($p < 0.001$), with the 95% confidence interval ranging from -54.14 to -40.53 mL/g.

The significance level for all comparisons is set at $\alpha = 0.05$. The mean differences between the PA concentrations are statistically significant, indicating that different concentrations of palmitic acid have a significant impact on the expanded volume of the synthesized sulfur-free expanded graphite.

Table 4.8: Post-hoc results of mean differences in expanded volume (in mL/g) between different pairs of palmitic acid (I and J), along with the standard error, significance (p-value), and the 95% confidence interval of the difference

(I) PA (mL)	(J) PA (mL)	Mean Difference (I-J)	Std. Error	Sig.	95% Confidence Interval	
					Lower Bound	Upper Bound
4	5	-67.333*	3.055	.000	-74.14	-60.53
	6	-135.667*	3.055	.000	-142.47	-128.86
	7	37.000*	3.055	.000	30.19	43.81
	8	84.333*	3.055	.000	77.53	91.14
5	6	-68.333*	3.055	.000	-75.14	-61.53
	7	104.333*	3.055	.000	97.53	111.14
	8	151.667*	3.055	.000	144.86	158.47
6	7	172.667*	3.055	.000	165.86	179.47
	8	220.000*	3.055	.000	213.19	226.81
8	7	-47.333*	3.055	.000	-54.14	-40.53

*. The mean difference is significant at the 0.05 level.

Figure 4.25 indicate that the different concentrations of palmitic acid have a significant impact on the expanded volume of the synthesized sulfur-free expanded graphite, as evidenced by the significant mean differences observed between the pairwise comparisons. However, EV (mL/g) at 470 is the optimum for 6mL of palmitic acid which is equivalent to 5.1g of palmitic acid

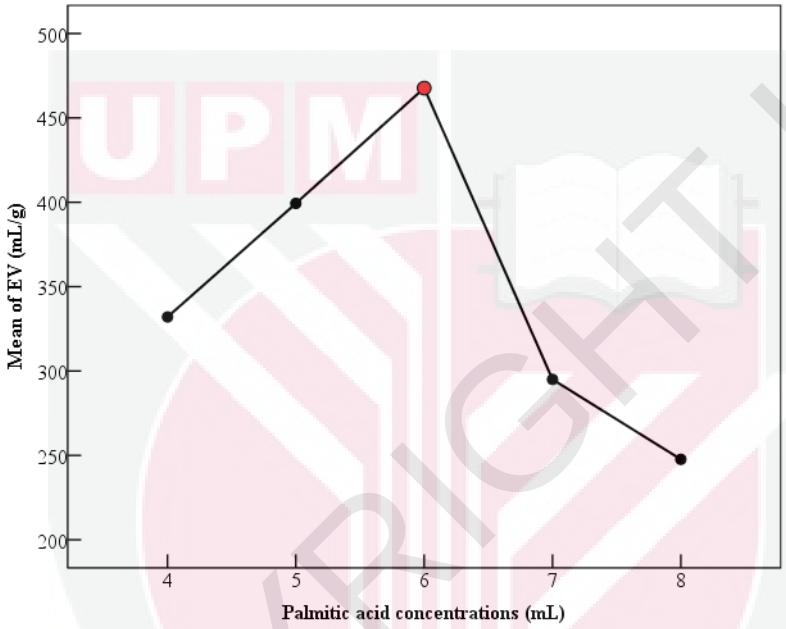

Figure 4.25: Mean of the expanded volume of graphite at different palmitic concentration

4.5.5 Effects of potassium permanganate on graphite expansion volume at optimum condition

First Stage

Null hypothesis (H0): The dosage of potassium permanganate in the first stage does not have a significant effect on the expanded volume of the synthesized sulfur-free expanded graphite.

Alternative hypothesis (H1): The dosage of potassium permanganate in the first stage has a significant effect on the expanded volume of the synthesized sulfur-free expanded graphite.

Table 4.9 shows the results of the analysis conducted to examine the effects of the dosage of potassium permanganate in the first stage on the expanded volume of the synthesized sulfur-free expanded graphite. The table displays the sum of squares, degrees of freedom, mean square, F-value, and significance level.

The between-groups analysis of variance indicates that the sum of squares for the dosage of potassium permanganate is 48871.733, with 4 degrees of freedom. The mean square is calculated as 12217.933. The F-value obtained is 969.677, and the associated significance level is extremely low ($p < 0.001$). These results suggest a significant effect of the dosage of potassium permanganate in the first stage on the expanded volume of the synthesized sulfur-free expanded graphite.

Therefore, we can reject the null hypothesis and conclude that the dosage of potassium permanganate in the first stage has a significant effect on the expanded volume of the synthesized sulfur-free expanded graphite, as evidenced by the high F-value and extremely low p-value.

Table 4.9: Two-way ANOVA of the means of the expanded volume of graphite across the different oxidant agent at optimum conditions

	Sum of Squares	df	Mean Square	F	Sig.
Between Groups	48871.733	4	12217.933	969.677	.000
Within Groups	126.000	10	12.600		
Total	48997.733	14			

Based on the significant results obtained from the ANOVA analysis,

Table 4.10 a post hoc test can be conducted to determine which specific pairs of potassium permanganate in the first stage has a significant effect on the expanded volume of the synthesized sulfur-free expanded graphite, a post hoc test can be performed to identify specific pairs of conditions that differ significantly from each other.

The results of the post hoc test revealed significant mean differences between several pairs of dosage conditions.

Comparing the dosage of 0.1 g with other dosages, significant differences were found for all comparisons. The expanded volume was significantly lower when the dosage increased to 0.15 g, 0.2 g, and 0.3 g. Similarly, when comparing the dosage of 0.15 g with higher dosages (0.2 g and 0.3 g), significant differences were observed, indicating a higher expanded volume for the latter dosages.

Furthermore, significant differences were observed when comparing the dosage of 0.2 g with 0.25 g and 0.3 g, and when comparing the dosage of 0.25 g with 0.25 g. However, no significant difference was observed between the expanded volumes obtained with dosages of 0.25g and 0.3g.

Table 4.10: Post-hoc results of mean differences in expanded volume (in mL/g) between different pairs of potassium permanganate levels (I and J), along with the standard error, significance (p-value), and the 95% confidence interval of the difference

(I) $KMnO_4$ (g)	(J) $KMnO_4$ (g)	Mean Difference (I-J)	Std. Error	Sig.	95% Confidence Interval	
					Lower Bound	Upper Bound
0.1	0.15	-83.000*	2.898	.000	-89.46	-76.54
	0.2	-101.333*	2.898	.000	-107.79	-94.88
	0.25	.667	2.898	.823	-5.79	7.12
	0.3	51.333*	2.898	.000	44.88	57.79
0.15	0.2	-18.333*	2.898	.000	-24.79	-11.88
	0.25	83.667*	2.898	.000	77.21	90.12
	0.3	134.333*	2.898	.000	127.88	140.79
0.2	0.25	102.000*	2.898	.000	95.54	108.46
	0.3	152.667*	2.898	.000	146.21	159.12
0.25	0.3	50.667*	2.898	.000	44.21	57.12

*. The mean difference is significant at the 0.05 level.

Figure 4.26 shows significant differences in expanded volume between various of potassium permanganate dosage conditions in the first stage. These findings suggest that the choice of dosage has a significant impact on the expanded volume of the synthesized sulfur-free expanded graphite, and different dosages lead to varying levels of expansion. Nevertheless, 0.2 dosage of potassium permanganate provides the highest expanded volume of 470 (mL/g).

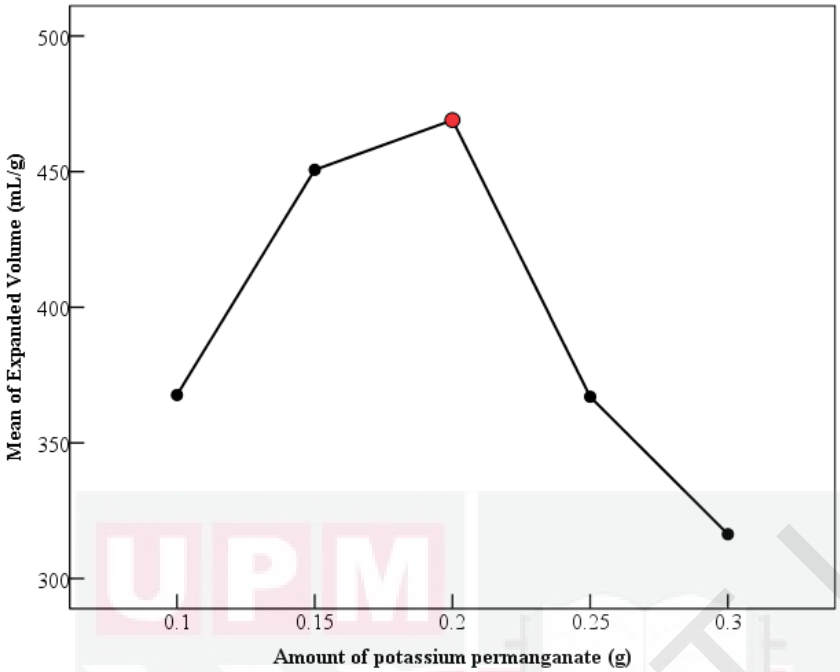

Figure 4.26: Mean of the expanded volume of graphite at different potassium permanganate in first stage

Second Stage

Based on the significant results obtained from the ANOVA analysis Table 4.11, we can determine whether the dosage of potassium permanganate ($KMnO_4$) in the second stage has a significant effect on the expanded volume of the synthesized sulfur-free expanded graphite.

Table 4.11 indicates that there is a significant difference between the groups. The between-groups sum of squares is 119571.733, with 4 degrees of freedom, resulting in a mean square value of 29892.933. The F-value is calculated to be 2166.155, and the p-value is reported as 0.000.

This p-value, which is less than the conventional significance level of 0.05, provides strong evidence to reject the null hypothesis. Therefore, we can conclude that the

dosage of potassium permanganate in the second stage does have a significant effect on the expanded volume of the synthesized sulfur-free expanded graphite.

The analysis suggests that different dosage levels of $KMnO_4$ lead to variations in the expanded volume of the synthesized EG. Further investigation or post hoc tests can be conducted to identify specific pairs of dosage conditions that differ significantly in terms of their impact on expanded volume.

Null hypothesis (H0): The dosage of potassium permanganate in the second stage does not have a significant effect on the expanded volume of the synthesized sulfur-free expanded graphite.

Alternative hypothesis (H1): The dosage of potassium permanganate in the second stage has a significant effect on the expanded volume of the synthesized sulfur-free expanded graphite.

Table 4.11: Two-way ANOVA of the means of the expanded volume of graphite across the different of oxidant agent at optimum conditions

	Sum of Squares	df	Mean Square	F	Sig.
Between Groups	119571.733	4	29892.933	2166.155	.000
Within Groups	138.000	10	13.800		
Total	119709.733	14			

Based on the results of the post hoc analysis Table 4.12 using the LSD (Least Significant Difference) method, significant differences were found between various pairs of potassium permanganate ($KMnO_4$) dosages in the second stage in terms of their effect on the expanded volume of the synthesized sulfur-free expanded graphite.

Comparing the dosages, it was observed that a dosage of 0.01 g of $KMnO_4$ resulted in significantly lower expanded volume compared to dosages of 0.05 g, 0.1 g, 0.15 g, and 0.2 g. Similarly, all other dosages exhibited significant differences when compared to each other.

Specifically, the mean differences (I-J) and their corresponding confidence intervals indicate the magnitude and direction of the differences. For example, when comparing a dosage of 0.01 g to 0.05 g, the mean difference was -144.000 mL/g, with a confidence interval ranging from -150.76 mL/g to -137.24 mL/g. Similar comparisons were made for other dosages, showing significant variations in expanded volume.

In summary, the post hoc analysis revealed significant differences in expanded volume between different dosages of potassium permanganate in the second stage, indicating that the dosage of $KMnO_4$ has a significant effect on the expansion of the synthesized sulfur-free expanded graphite.

Table 4.12: Post-hoc results of mean differences in expanded volume (in mL/g) between different pairs of potassium permanganate levels (I and J), along with the standard error, significance (p-value), and the 95% confidence interval of the difference

(I) $KMnO_4$ (g)	(J) $KMnO_4$ (g)	Mean Difference (I-J)	Std. Error	Sig.	95% Confidence Interval	
					Lower Bound	Upper Bound
0.01	0.05	-144.000*	3.033	.000	-150.76	-137.24
	0.1	-273.333*	3.033	.000	-280.09	-266.58
	0.15	-192.667*	3.033	.000	-199.42	-185.91
	0.2	-132.667*	3.033	.000	-139.42	-125.91
0.05	0.1	-129.333*	3.033	.000	-136.09	-122.58
	0.15	-48.667*	3.033	.000	-55.42	-41.91
	0.2	11.333*	3.033	.004	4.58	18.09
0.1	0.15	80.667*	3.033	.000	73.91	87.42
	0.2	140.667*	3.033	.000	133.91	147.42
0.15	0.2	60.000*	3.033	.000	53.24	66.76

*. The mean difference is significant at the 0.05 level.

Figure 4.27 indicate that the dosage of potassium permanganate in the second stage has a significant effect on the expanded volume of the synthesized sulfur-free expanded graphite. The specific dosage levels of $KMnO_4$ lead to variations in the expanded volume, suggesting that different dosages have different impacts on the synthesis process. Nonetheless, 0.1 dosage of potassium permanganate provides the highest expanded volume of 470 (mL/g).

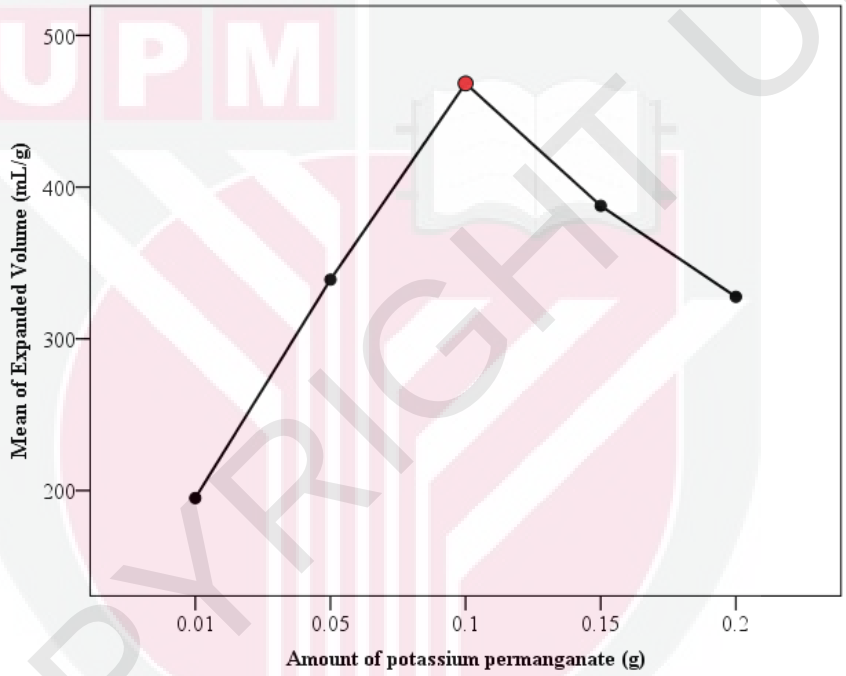

Figure 4.27: Mean of the expanded volume of graphite at different potassium permanganate in second stage

4.5.6 Effects of nitric acid concentration on graphite expansion volume at optimum condition

Based on the ANOVA results Table 4.13, the sum of squares between groups is 121750.400, with 4 degrees of freedom. The mean square is calculated as 30437.600. The F-value is 2623.931, and the significance level (Sig.) is found to be 0.000, which is below the typical threshold of 0.05. This indicates that there is a significant effect of

the concentration of nitric acid on the expanded volume of the synthesized sulfur-free expanded graphite.

Therefore, based on the significant F-value and the low p-value, we can reject the null hypothesis and conclude that the concentration of nitric acid has a significant effect on the expanded volume of the synthesized sulfur-free expanded graphite.

Null hypothesis (H0): The concentration of nitric acid does not have a significant effect on the expanded volume of the synthesized sulfur-free expanded graphite.

Alternative hypothesis (H1): The concentration of nitric acid has a significant effect on the expanded volume of the synthesized sulfur-free expanded graphite.

Table 4.13: Two-way ANOVA of the means of the expanded volume of graphite across the different concentrations of nitric acid at optimum conditions

	Sum of Squares	df	Mean Square	F	Sig.
Between Groups	121750.400	4	30437.600	2623.931	.000
Within Groups	116.000	10	11.600		
Total	121866.400	14			

Table 4.14 post hoc analysis using the LSD test was conducted to compare the mean differences in expanded volume (mL/g) between different concentrations of nitric acid (HNO_3). The results reveal several significant differences.

The mean difference between 0.5 mL and 1 mL of HNO3 is -98.333, indicating a significant decrease in expanded volume. Similarly, significant decreases are observed when comparing 0.5 mL to 1.5 mL (-265.333), 0.5 mL to 2 mL (-197.333), and 0.5 mL to 2.5 mL (-158.000) of HNO_3.

Comparing 1 mL to 1.5 mL of HNO3 shows a significant decrease (-167.000), as well as between 1 mL and 2 mL (-99.000), and 1 mL and 2.5 mL (-59.667).

In contrast, there is a significant increase in expanded volume when comparing 1.5 mL to 2 mL of HNO_3 (68.000), and when comparing 1.5 mL to 2.5 mL (107.333). The comparison between 2 mL and 2.5 mL of HNO_3 also shows a significant increase in expanded volume (39.333).

In summary, the post hoc analysis indicates that the concentration of nitric acid (HNO_3) has a significant effect on the expanded volume of the synthesized sulfur-free expanded graphite, with varying trends and significant mean differences observed between different concentration levels.

Table 4.14: Post-hoc results of mean differences in expanded volume (in mL/g) between different pairs of nitric acid levels (I and J), along with the standard error, significance (p-value), and the 95% confidence interval of the difference

(I) HNO_3 (mL)	(J) HNO_3 (mL)	Mean Difference (I-J)	Std. Error	Sig.	95% Confidence Interval	
					Lower Bound	Upper Bound
0.5	1	-98.333*	2.781	.000	-104.53	-92.14
	1.5	-265.333*	2.781	.000	-271.53	-259.14
	2	-197.333*	2.781	.000	-203.53	-191.14
	2.5	-158.000*	2.781	.000	-164.20	-151.80
1	1.5	-167.000*	2.781	.000	-173.20	-160.80
	2	-99.000*	2.781	.000	-105.20	-92.80
	2.5	-59.667*	2.781	.000	-65.86	-53.47
1.5	2	68.000*	2.781	.000	61.80	74.20
	2.5	107.333*	2.781	.000	101.14	113.53
2	2.5	39.333*	2.781	.000	33.14	45.53

*. The mean difference is significant at the 0.05 level.

Figure 4.28 indicates that the concentration of nitric acid has a significant effect on the expanded volume of the synthesized sulfur-free expanded graphite. Different concentrations of acetic acid led to variations in the expanded volume, with some

concentrations causing a decrease and others causing an increase in the volume. 1.5mL of nitric acid provide the optimum level of the expanded volume at 470 mL/g.

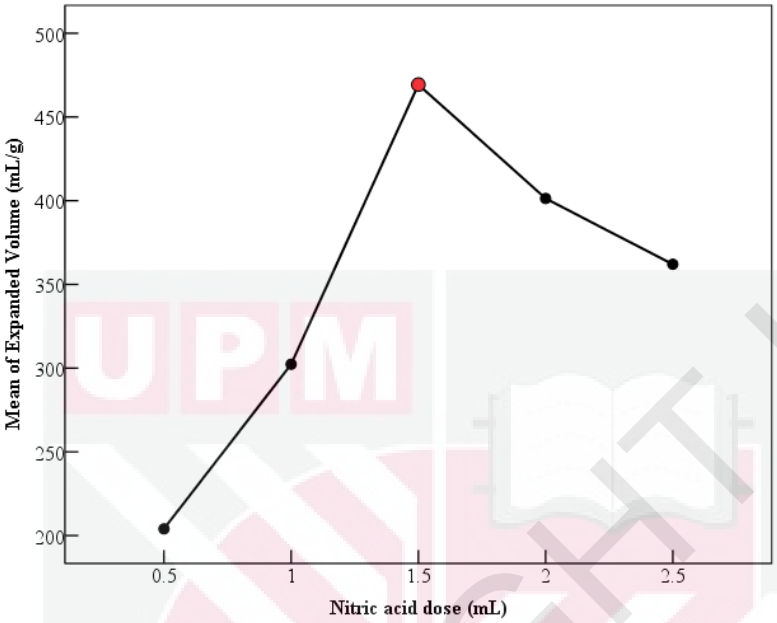

Figure 4.28: Mean of the expanded volume of graphite at different nitric acid concentration

4.5.7 Effects of acetic acid concentration on graphite expansion volume at optimum condition

Based on the ANOVA analysis Table 4.15, the results show a significant effect of the concentration of acetic acid on the expanded volume of the synthesized sulfur-free expanded graphite.

The between-groups analysis reveals a significant F-value of 2871.838, indicating that the variation in the expanded volume between different concentrations of acetic acid is larger than the variation within groups. Additionally, the p-value is reported as 0.000, which is less than the significance level of 0.05, providing strong evidence to reject the null hypothesis.

These results suggest that the concentration of acetic acid has a significant impact on the expanded volume of the synthesized sulfur-free expanded graphite. Therefore, the alternative hypothesis is supported, indicating that the concentration of acetic acid has a significant effect on the expanded volume of the synthesized EG.

Null hypothesis (H0): The concentration of acetic acid does not have a significant effect on the expanded volume of the synthesized sulfur-free expanded graphite.

Alternative hypothesis (H1): The concentration of acetic acid has a significant effect on the expanded volume of the synthesized sulfur-free expanded graphite.

Table 4.15: Two-way ANOVA of the means of the expanded volume of graphite across the different concentrations of acetic acid

	Sum of Squares	df	Mean Square	F	Sig.
Between Groups	78114.000	4	19528.500	2871.838	.000
Within Groups	68.000	10	6.800		
Total	78182.000	14			

The post hoc analysis Table 4.16, using the LSD (Least Significant Difference) method, was conducted to compare the mean differences in the expanded volume of the synthesized sulfur-free expanded graphite for different concentrations of acetic acid (HAc).

The results of the post hoc test indicate significant mean differences between various pairs of HAc concentrations. When comparing the concentration of 2 mL with 4 mL, a significant mean difference of -147.000 mL/g was observed. Similarly, significant mean differences were found when comparing other pairs, such as 2 mL with 6 mL (-

213.667 mL/g), 2 mL with 8 mL (-88.667 mL/g), and 2 mL with 10 mL (-70.667 mL/g), among others.

These significant mean differences suggest that the concentration of acetic acid has a significant effect on the expanded volume of the synthesized EG. The confidence intervals for all the significant mean differences do not include zero, further supporting the significance of the findings. Therefore, it can be concluded that the concentration of acetic acid plays a crucial role in determining the expanded volume of the synthesized sulfur-free expanded graphite.

Table 4.16: Post-hoc results of mean differences in expanded volume (in mL/g) between different pairs of Acetic acid levels (I and J), along with the standard error, significance (p-value), and the 95% confidence interval of the difference

(I) HAc (mL)	(J) HAc (mL)	Mean Difference (I-J)	Std. Error	Sig.	95% Confidence Interval	
					Lower Bound	Upper Bound
2	4	-147.000*	2.129	.000	-151.74	-142.26
	6	-213.667*	2.129	.000	-218.41	-208.92
	8	-88.667*	2.129	.000	-93.41	-83.92
	10	-70.667*	2.129	.000	-75.41	-65.92
4	6	-66.667*	2.129	.000	-71.41	-61.92
	8	58.333*	2.129	.000	53.59	63.08
	10	76.333*	2.129	.000	71.59	81.08
6	8	125.000*	2.129	.000	120.26	129.74
	10	143.000*	2.129	.000	138.26	147.74
8	10	18.000*	2.129	.000	13.26	22.74

*. The mean difference is significant at the 0.05 level.

Figure 4.29 shows the significant differences in the expanded volume of the synthesized sulfur-free expanded graphite for different concentrations of acetic acid. These findings support the alternative hypothesis and suggest that the concentration of acetic acid has a significant effect on the expanded volume of the synthesized EG. However, it appears that 6 mL of acetic acid resulted in the highest expanded volume

of 470 mL/g. This indicates that the expanded volume was significantly higher at 6 mL compared to other concentrations of acetic acid tested in the experiment.

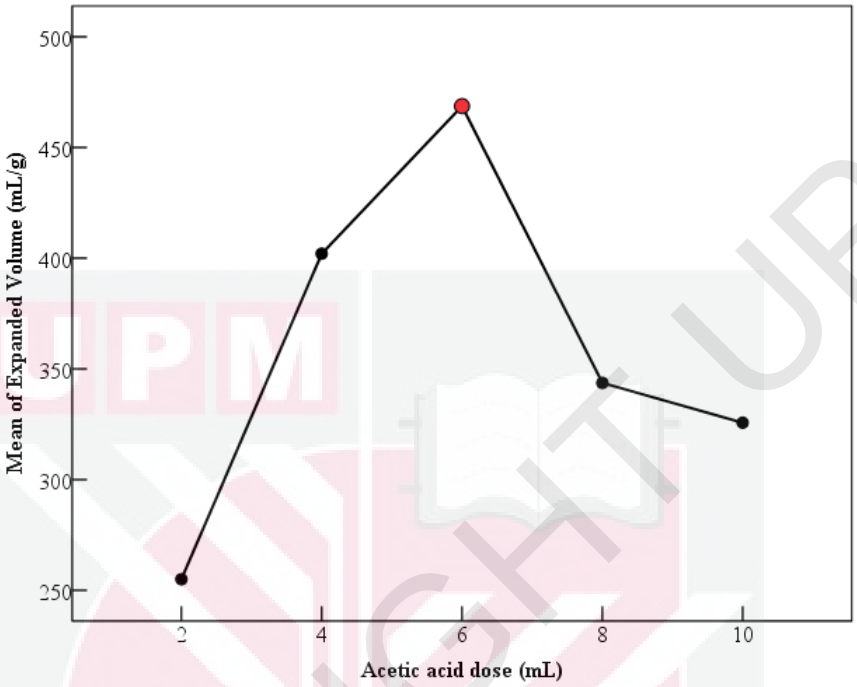

Figure 4.29: Mean of the expanded volume of graphite at different acetic acid concentration

CHAPTER 5

CONCLUSIONS AND RECOMMENDATIONS

5.1 Conclusion

The conclusion is divided into two parts. First, it addresses the rapid preparation of expanded graphite at ambient temperature, emphasizing the efficiency and speed of the expansion process. Second, it highlights the eco-friendly, sulfur-free expanded graphite and its application in oil sorption, demonstrating its potential as a sustainable solution with promising properties for oil sorption applications.

5.1.1 Rapid preparation of mesoporous expanded graphite at ambient temperature

A simple and affordable way of mesoporous expanding graphite at room temperature was devised by mixing natural graphite flakes with an adequate amount of concentrated sulfuric acid and sodium peroxydisulfate without heating. This method is considered effective because all amounts of graphite used were fully converted to expanded graphite with no residue, reaching up to 140 mL/g. Compared to traditional EG, ATEG has a uniform structure and significantly increased volume and surface area. When used in oil absorption, ATEG shows high absorption capacity. Compared to its expanded volume, the oil absorbed by ATEG is higher than that absorbed by HTEG. Therefore, the synthesized ATEG mesoporous materials appear promising for practical applications, particularly oil sorption.

5.1.2 Eco-friendly, mesoporous, sulfur-free, expanded graphite

Expanded graphite with large EV has been prepared by two-step intercalation, in which the mixture of palmitic acid and that of HNO_3 and CH_3COOH were employed as intercalating agent, and $KMnO_4$ was used as oxidant. The amount of water used for material purification is also reduced significantly, and the chemical process is simplified because the intercalant acid is weak. The expansion process was simple and inexpensive, as it utilized microwave heating in a household oven to reduce energy expenses. The microstructure of natural graphite flakes and expanded graphite samples were investigated using X-ray diffraction. The surface functional groups of EG were studied using Fourier transform infrared spectroscopy. The micro-morphologies were examined using field emission scanning electron microscopy. The results show that longitudinal graphite expansion is more obvious than transverse expansion, resulting in a worm-like fluffy rope. When used in oil absorption, EG-PA shows high absorption capacity, achieving an 85 g/g EG-PA/oil ratio and its capability for recycling up to three times. Therefore, the synthesis of EG mesoporous materials appears promising for practical applications, particularly oil sorption.

5.2 Recommendations for Future Research

The results of this study serve to provide a useful baseline from which more detailed studies can be undertaken. The following recommendations are suggested for further works towards a better understanding of graphite expansion:

While this research does not discuss other potential applications of EG, future studies can focus on exploring its applications, particularly in the field of composite materials, with a specific emphasis on its use in food packaging. There is a particular interest in investigating EG as an uncontaminated material for this purpose.

It is important to conduct further research on the utilization of environmentally friendly compounds for EG and explore alternative substances that can be employed on a large scale for the industrial production of EG.

Since the rapid preparation of EG at room temperature is a novel method, it is crucial to further investigate the underlying mechanisms responsible for this expansion. This can be achieved by conducting extensive characterization studies that specifically focus on the analysis of functional groups involved in the expansion process.

a. It is suggested for the next studies of graphite expansion to include more on the weak acid and eco-friendly materials.
b. Future research towards a better understanding of mechanism of expansion of graphite.
c. Future studies should focus on the different application of graphite expansion specifically on composite materials.
d. The harmful effects of strong acid should get more attention.

REFERENCES

Al-Majed, A. A., Adebayo, A. R., & Hossain, M. E. (2012). A sustainable approach to controlling oil spills. *Journal of Environmental Management*, *113*, 213–227. https://doi.org/10.1016/j.jenvman.2012.07.034

Alassod, A., Tina, H., Islam, S. R., Huang, W., & Xu, G. (2022). Using polypropylene needle punch nonwoven sorbents as the interceptor for oil in static and dynamic water experiments. *Environmental Technology (United Kingdom)*, *43*(25), 3919–3934. https://doi.org/10.1080/09593330.2021.1937332

Ardestani, M. M., Mahpishanian, S., Rad, B. F., Janmohammadi, M., & Baghdadi, M. (2022). Preparation and characterization of room-temperature chemically expanded graphite: Application for cationic dye removal. *Korean Journal of Chemical Engineering*, *39*(6), 1496–1506. https://doi.org/10.1007/s11814-022-1084-5

Bannov, A. G., Ukhina, A. V, Maksimovskii, E. A., Prosanov, I. Y., Shestakov, A. A., Lapekin, N. I., Lazarenko, N. S., Kurmashov, P. B., & Popov, M. V. (2021). Highly Porous Expanded Graphite: Thermal Shock vs. Programmable Heating. *Materials*, 1–17.

Bi, H., Xie, X., Yin, K., Zhou, Y., Wan, S., He, L., Xu, F., Banhart, F., Sun, L., & Ruoff, R. S. (2012). Spongy graphene as a highly efficient and recyclable sorbent for oils and organic solvents. *Advanced Functional Materials*, *22*(21), 4421–4425. https://doi.org/10.1002/adfm.201200888

Block, P. A., Brown, R. A., & Robinson, D. (2004). Novel Activation Technologies for Sodium Persulfate in Situ Chemical Oxidation. *In Proceedings of the Fourth International Conference on the Remediation of Chlorinated and Recalcitrant Compounds*, *May*, 24–27. https://doi.org/https://projects.battelle.org/chlorinated-conference/2004Chlor_Proceedings/Papers/2A-05.pdf

Botas, C., Pérez-Mas, A. M., Álvarez, P., Santamaría, R., Granda, M., Blanco, C., & Menéndez, R. (2013). Optimization of the size and yield of graphene oxide sheets in the exfoliation step. *Carbon*, *63*, 576–578. https://doi.org/10.1016/j.carbon.2013.06.096

Bruell, C. J., Liang, C. J., Marley, M. C., & Sperry, K. L. (2003). Thermally activated persulfate oxidation of trichloroethylene (TCE) and 1,1,1-trichloroethane (TCA) in aqueous systems and soil slurries. *Soil and Sediment Contamination*, *12*(2), 207–228. https://doi.org/10.1080/713610970

Cai, M., Thorpe, D., Adamson, H. D., & Schniepp, H. C. (2012). Methods of graphite exfoliation. *Journal of Materials Chemistry*, *22*, 24992–25002. https://doi.org/10.1039/c2jm34517j

Çalın, Ö., Kurt, A., & Çelik, Y. (2020). Influence of expansion conditions and precursor flake size on porous structure of expanded graphite. *Fullerenes Nanotubes and Carbon Nanostructures*, *28*(8), 611–620. https://doi.org/10.1080/1536383X.2020.1726894

Chang, Y., Sun, X., Ma, M., Mu, C., Li, P., Li, L., Li, M., Nie, A., Xiang, J., Zhao, Z., He, J., Wen, F., Liu, Z., & Tian, Y. (2020). Application of hard ceramic materials B4C in energy storage : Design B4C@C core-shell nanoparticles as electrodes for flexible all-solid-state micro-supercapacitors with ultrahigh cyclability. *Nano Energy*, *75*(January), 104947. https://doi.org/10.1016/j.nanoen.2020.104947

Chen, F., Gao, W., Qiu, X., Zhang, H., Liu, L., Liao, P., Fu, W., & Luo, Y. (2018). Graphene quantum dots in biomedical applications: Recent advances and future challenges. *Frontiers in Laboratory Medicine*, *1*(4), 192–199. https://doi.org/10.1016/j.flm.2017.12.006

Chen, J., Yao, B., Li, C., & Shi, G. (2013). An improved Hummers method for eco-friendly synthesis of graphene oxide. *Carbon*, *64*(1), 225–229. https://doi.org/10.1016/j.carbon.2013.07.055

Chen, Y. L., Hsiao, C. H., Ya, J. Y., & Hsieh, P. Y. (2023). Preparation of expanded graphite with (NH4)2S2O8 and H2SO4 by using microwave irradiation. *Journal of the Taiwan Institute of Chemical Engineers*, *1*, 105026. https://doi.org/10.1016/j.jtice.2023.105026

Chin, S. F., Binti Romainor, A. N., & Pang, S. C. (2014). Fabrication of hydrophobic and magnetic cellulose aerogel with high oil absorption capacity. *Materials Letters*, *115*, 241–243. https://doi.org/10.1016/j.matlet.2013.10.061

Chung, D. D. L. (2015). A review of exfoliated graphite. *Journal of Materials Science*. https://doi.org/10.1007/s10853-015-9284-6

Chung, D. D. L. (2016). Graphite Intercalation Compounds. *Reference Module in Materials Science and Materials Engineering*, *April 2015*, 1–6. https://doi.org/10.1016/b978-0-12-803581-8.02311-0

Coha, M., Farinelli, G., Tiraferri, A., Minella, M., & Vione, D. (2021). Advanced oxidation processes in the removal of organic substances from produced water: Potential, configurations, and research needs. *Chemical Engineering Journal*, *414*(September 2020), 128668. https://doi.org/10.1016/j.cej.2021.128668

Cojocaru, C., Dorneanu, P. P., Airinei, A., Olaru, N., Samoila, P., & Rotaru, A. (2017). Design and evaluation of electrospun polysulfone fibers and polysulfone/NiFe2O4 nanostructured composite as sorbents for oil spill cleanup. *Journal of the Taiwan Institute of Chemical Engineers*, *70*, 267–281. https://doi.org/10.1016/j.jtice.2016.11.005

Dai, C., Gu, C., Liu, B., Lyu, Y., Yao, X., He, H., Fang, J., & Zhao, G. (2019). Preparation of low-temperature expandable graphite as a novel steam plugging agent in heavy oil reservoirs. *Journal of Molecular Liquids*, *293*, 111535. https://doi.org/10.1016/j.molliq.2019.111535

Dhakate, S. R., Mathur, R. B., Sharma, S., Borah, M., & Dhami, T. L. (2009). Influence of expanded graphite particle size on the properties of composite bipolar plates for fuel cell application. *Energy and Fuels*, *23*(2), 934–941. https://doi.org/10.1021/ef800744m

Dimiev, A. M., & Tour, J. M. (2014). Mechanism of graphene oxide formation. *ACS Nano*, *8*(3), 3060–3068. https://doi.org/10.1021/nn500606a

Dong, Y., Zhou, G., Ding, H., & Yuan, F. (2021). Preparation technics and application of expanded graphite. *Applied Chemical Engineering*, *4*(2), 37–45. https://doi.org/10.24294/ace.v4i2.1348

Dresselhaus, M. S., & Dresselhaus, G. (1981). Intercalation compounds of graphite. *Advances in Physics*, *51*(1), 1–186. https://doi.org/10.1080/00018738100101367

Dresselhaus, M. S., & Dresselhaus, G. (2002). Intercalation compounds of graphite. *Advances in Physics*, *51*(June 2002), 10–186.

Elbidi, M., Resul, M. F. M. G., Rashid, S. A., & Salleh, M. A. M. (2023). Preparation of eco-friendly mesoporous expanded graphite for oil sorption. *Journal of Porous Materials*, *30*(4), 1359–1368. https://doi.org/10.1007/s10934-023-01428-0

Eltaweil, A. S., Abd El-Monaem, E. M., El-Subruiti, G. M., Ali, B. M., Abd El-Latif, M. M., & Omer, A. M. (2022). Graphene oxide incorporated cellulose acetate beads for efficient removal of methylene blue dye; isotherms, kinetic, mechanism and co-existing ions studies. *Journal of Porous Materials*. https://doi.org/10.1007/s10934-022-01347-6

Gale, M., Nguyen, T., Moreno, M., & Gilliard-Abdulaziz, K. L. (2021). Physiochemical Properties of Biochar and Activated Carbon from Biomass Residue: Influence of Process Conditions to Adsorbent Properties. In *ACS Omega* (Vol. 6, Issue 15, pp. 10224–10233). https://doi.org/10.1021/acsomega.1c00530

Goudarzi, R., & Hashemi Motlagh, G. (2019). The effect of graphite intercalated compound particle size and exfoliation temperature on porosity and macromolecular diffusion in expanded graphite. *Heliyon*, *5*(10), e02595. https://doi.org/10.1016/j.heliyon.2019.e02595

Hadela, A., Lakić, M., Potočnik, M., Košak, A., Gutmaher, A., & Lobnik, A. (2020). Novel reusable functionalized magnetic cobalt ferrite nanoparticles as oil adsorbents. *Adsorption Science and Technology*, *38*(5–6), 168–190. https://doi.org/10.1177/0263617420922014

Han, H. S., You, J., Seol, H., Jeong, H., & Jeon, S. (2014). Electrochemical sensor for hydroquinone and catechol based on electrochemically reduced GO – terthiophene – CNT. *Sensors and Actuators B: Chemical*, *194*, 460–469. https://doi.org/10.1016/j.snb.2014.01.006

He, J., Song, L., Yang, H., Ren, X., & Xing, L. (2017). Preparation of Sulfur-Free Exfoliated Graphite by a Two-Step Intercalation Process and Its Application for Adsorption of Oils. *Journal of Chemistry*, *2017*. https://doi.org/10.1155/2017/5824976

Hoang, N. B., Nguyen, T. T., Nguyen, T. S., Bui, T. P. Q., & Bach, L. G. (2019). The application of expanded graphite fabricated by microwave method to eliminate organic dyes in aqueous solution. *Cogent Engineering*, *6*(1). https://doi.org/10.1080/23311916.2019.1584939

Hou, B., Sun, H. J., Peng, T. J., Zhang, X. Y., & Ren, Y. Z. (2020). Rapid preparation of expanded graphite at low temperature. *Xinxing Tan Cailiao/New Carbon Materials*, *35*(3), 262–268. https://doi.org/10.1016/S1872-5805(20)60488-7

Hou, S., He, S., Zhu, T., Li, J., Ma, L., Du, H., Shen, W., Kang, F., & Huang, Z. (2021). Environment-friendly preparation of exfoliated graphite and functional graphite sheets. *Journal of Materiomics*, *7*(1), 136–145. https://doi.org/10.1016/j.jmat.2020.06.009

Hou, S., Li, J., Huang, X., Wang, X., Ma, L., Shen, W., Kang, F., & Huang, Z. H. (2017). Silver nanoparticles-loaded exfoliated graphite and its anti-bacterial performance. *Applied Sciences (Switzerland)*, *7*(8). https://doi.org/10.3390/app7080852

Hou, S., Zhu, T., Shen, W., Kang, F., Inagaki, M., & Huang, Z. H. (2022). Exfoliated graphite blocks with resilience prepared by room temperature exfoliation and their application for oil-water separation. *Journal of Hazardous Materials*, *424*(PD), 127724. https://doi.org/10.1016/j.jhazmat.2021.127724

Huang, J., Tang, Q., Liao, W., Wang, G., Wei, W., & Li, C. (2017). Green Preparation of Expandable Graphite and Its Application in Flame-Resistance Polymer Elastomer. *Industrial and Engineering Chemistry Research*, *56*(18), 5253–5261. https://doi.org/10.1021/acs.iecr.6b04860

Ifeyinwa Obi, A., Ismael Egbulefu Ajiwe, V., Charity Eboagu, N., Lilian Ekene-Echerebo, I., & Malinda Muobike, C. (2023). Mann's Cucumeropsis Seed Shell as an Oil Sorbent: Kinetic, Isotherm, and Thermodynamic Studies. *World Journal of Applied Chemistry*, *June*. https://doi.org/10.11648/j.wjac.20230801.11

Iqbal, M. Z., & Abdala, A. A. (2013). Oil spill cleanup using graphene. *Environmental Science and Pollution Research*, *20*(5), 3271–3279. https://doi.org/10.1007/s11356-012-1257-6

ITOPF. (2022). *Oil tanker spill statistics 2010*. https://www.itopf.org/knowledge-resources/data-statistics/statistics/

Jacobson, A. J., & Nazar, L. F. (2011). Intercalation Chemistry. *Encyclopedia of Inorganic and Bioinorganic Chemistry*, 1–37. https://doi.org/10.1002/9781119951438.eibc0093

Kartel, M. T., Tolmachova, V. S., Cherniuk, O. A., Hrebelna, Y. V., & Sementsov, Y. I. (2023). Expanded graphite as the best sorbent for hydrocarbons. *IOP Conference Series: Earth and Environmental Science*, *1126*(1), 1–11. https://doi.org/10.1088/1755-1315/1126/1/012025

Keeling, J. (2017). Graphite: properties, uses and South Australian resources. *MESA Journal*, *84*(3), 28–41.

Kim, J., Oh, S., Kim, H., Kim, B., Jeon, K., & Yoon, S. (2014). Expanding characteristics of graphite in microwave- assisted exfoliation. *Scientific Cooperations International Workshops on Engineering Branches*, *1*(August), 273–277.

Kolthoff, I. M., & Miller, I. K. (1951). The Chemistry of Persulfate. I. The Kinetics and Mechanism of the Decomposition of the Persulfate Ion in Aqueous Medium. *Journal of the American Chemical Society*, *73*(7), 3055–3059. https://doi.org/10.1021/ja01151a024

Korhonen, J. T., Kettunen, M., Ras, R. H. A., & Ikkala, O. (2011). Hydrophobic Nanocellulose Aerogels as Floating, Sustainable, Reusable, and Recyclable Oil Absorbents. *Applied Materials and Interfaces*, *3*, 1813–1816. https://doi.org/https://doi.org/10.1021/am200475b

Lan, R., Su, W., & Li, J. (2019). Preparation and catalytic performance of expanded graphite for oxidation of organic pollutant. *Catalysts*, *9*(3). https://doi.org/10.3390/catal9030280

Li, X., Liu, Z., Li, J., Lei, H., Zhuo, W., Qin, W., Cai, X., Hui, K. N., Pan, L., & Mai, W. (2020). Insights on the mechanism of Na-ion storage in expanded graphite anode. *Journal of Energy Chemistry*, *53*, 56–62. https://doi.org/10.1016/j.jechem.2020.05.022

Liu, C., Wang, K., Luo, S., Tang, Y., & Chen, L. (2011). Direct Electrodeposition of Graphene Enabling the One-Step Synthesis of Graphene Metal Nanocomposite Films. *Small*, *7*(9), 1203–1206.

Liu, T., Zhang, R., Zhang, X., Liu, K., Liu, Y., & Yan, P. (2017). One-step room-temperature preparation of expanded graphite. *Carbon*, *119*, 544–547. https://doi.org/10.1016/j.carbon.2017.04.076

Liu, T., Zhang, X., Liu, M., Wu, W., Liu, K., Liu, Y., Gu, Y., & Zhang, R. (2018). One-step room-temperature exfoliation of graphite to 100% few-layer graphene with high quality and large size. *Journal of Materials Chemistry C*, *6*(31), 8343–8348. https://doi.org/10.1039/c8tc02756k

Liu, Z., Hao, Y., Su, Y., Wei, Y., Wang, J., Yan, H., Shen, W., Huang, Z., Wang, X., Zhao, L., & Sun, X. (2018). A novel and facile prepared wound dressing based on large expanded graphite worms. *Journal of Materials Research*, 1–10. https://doi.org/10.1557/jmr.2018.473

Liu, Z. X., Jiang, L. yuan, Wang, X. xin, Ma, M. jie, Lu, Q. qian, & Liang, P. (2022). Novel expanded graphite with a 'Spitball' structure. *Materials Science and Technology (United Kingdom)*, *38*(1), 1–4. https://doi.org/10.1080/02670836.2021.2015857

Liu, Z. X., Zhang, X. W., Zhang, W. J., Wei, X. X., & Liang, P. (2020). Microwave-assisted fabrication of slight-expanded graphite under normal temperature. *Materials Science and Technology*, *36*(2), 251–254. https://doi.org/10.1080/02670836.2019.1693730

Lowe, S. E., Shi, G., Zhang, Y., Qin, J., Wang, S., Uijtendaal, A., Sun, J., Jiang, L., Jiang, S., Qi, D., Al-Mamun, M., Liu, P., Zhong, Y. L., & Zhao, H. (2019). Scalable Production of Graphene Oxide Using a 3D-Printed Packed-Bed Electrochemical Reactor with a Boron-Doped Diamond Electrode. *ACS Applied Nano Materials*, *2*(2), 867–878. https://doi.org/10.1021/acsanm.8b02126

Mahmoud, M. A. (2020). Oil spill cleanup by raw flax fiber: Modification effect, sorption isotherm, kinetics and thermodynamics. *Arabian Journal of Chemistry*, *13*(6), 5553–5563. https://doi.org/10.1016/j.arabjc.2020.02.014

Malard, L. M., Pimenta, M. A., Dresselhaus, G., & Dresselhaus, M. S. (2009). Raman spectroscopy in graphene. *Physics Reports*, *473*(5–6), 51–87. https://doi.org/10.1016/j.physrep.2009.02.003

Marcano, D. C., Kosynkin, D. V, Berlin, J. M., Sinitskii, A., Sun, Z., Slesarev, A., Alemany, L. B., Lu, W., & Tour, J. M. (2010). Improved Synthesis of Graphene Oxide. *ACS Nano*, *4*(8), 4806–4814. https://doi.org/10.1021/nn1006368

Marrani, A. G., Motta, A., Schrebler, R., Zanoni, R., & Dalchiele, E. A. (2019). Insights from experiment and theory into the electrochemical reduction mechanism of graphene oxide. *Electrochimica Acta*, *304*, 231–238. https://doi.org/10.1016/j.electacta.2019.02.108

Mukhopadhyay, P., & Gupta, R. K. (2012). Graphite, Graphene, and Their Polymer Nanocomposites. In *Taylor & Francis Group*. https://doi.org/10.1201/b13051

Mulyadi, A., Zhang, Z., & Deng, Y. (2016). Fluorine-Free Oil Absorbents Made from Cellulose Nanofibril Aerogels. *ACS Applied Materials and Interfaces*, *8*(4), 2732–2740. https://doi.org/10.1021/acsami.5b10985

Murugan, P., Nagarajan, R. D., Shetty, B. H., Govindasamy, M., & Sundramoorthy, A. K. (2021). Recent trends in the applications of thermally expanded graphite for energy storage and sensors - a review. *Nanoscale Advances*, *3*(22), 6294–6309. https://doi.org/10.1039/d1na00109d

Nassar, M. Y., Abdelrahman, E. A., Aly, A. A., & Mohamed, T. Y. (2017). A facile synthesis of mordenite zeolite nanostructures for efficient bleaching of crude soybean oil and removal of methylene blue dye from aqueous media. *Journal of Molecular Liquids*, *248*, 302–313. https://doi.org/10.1016/j.molliq.2017.10.061

Nirwan, A., Matta, R., Kumar, R., Mondal, B., & Bera, A. (2021). Process optimization for mesoporous graphite preparation and its oil spillage remediation application. *Materials Today: Proceedings*, *45*, 5108–5113. https://doi.org/10.1016/j.matpr.2021.01.617

Parvez, K., Wu, Z. S., Li, R., Liu, X., Graf, R., Feng, X., & Müllen, K. (2014). Exfoliation of graphite into graphene in aqueous solutions of inorganic salts. *Journal of the American Chemical Society*, *136*(16), 6083–6091. https://doi.org/10.1021/ja5017156

Peng, T., Liu, B., Gao, X., Luo, L., & Sun, H. (2018). Preparation, quantitative surface analysis, intercalation characteristics and industrial implications of low temperature expandable graphite. *Applied Surface Science*, *444*, 800–810. https://doi.org/10.1016/j.apsusc.2018.03.089

Pham, T. Van, Nguyen, T. T., Nguyen, D. T., Thuan, T. Van, Bui, P. Q. T., Viet, V. N. D., & Bach, L. G. (2019). The Preparation and Characterization of Expanded Graphite via Microwave Irradiation and Conventional Heating for the Purification of Oil Contaminated Water. *Journal of Nanoscience and Nanotechnology*, *19*(2), 1122–1125. https://doi.org/10.1166/jnn.2019.15926

Qiu, T., Yang, J. G., Bai, X. J., & Wang, Y. L. (2019). The preparation of synthetic graphite materials with hierarchical pores from lignite by one-step impregnation and their characterization as dye absorbents. *RSC Advances*, *9*(22), 12737–12746. https://doi.org/10.1039/c9ra00343f

Ren, R. P., Wang, Z., Ren, J., & Lv, Y. K. (2019). Highly compressible polyimide/graphene aerogel for efficient oil/water separation. *Journal of Materials Science*, *54*(7), 5918–5926. https://doi.org/10.1007/s10853-018-03238-1

Rozi, S. K. M., Shahabuddin, S., Manan, N. S. A., Mohamad, S., Kamal, S. A. A., & Rahman, S. A. (2017). Palm Fatty Acid Functionalized Fe3O4 Nanoparticles as Highly Selective Oil Adsorption Material. *Journal of Nanoscience and Nanotechnology*, *18*(5), 3248–3256. https://doi.org/10.1166/jnn.2018.14699

Saikam, L., Arthi, P., Jayram, N. D., & Sykam, N. (2022). Rapid removal of organic dyes from aqueous solutions using mesoporous exfoliated graphite. *Diamond and Related Materials*, *130*(October), 109480. https://doi.org/10.1016/j.diamond.2022.109480

Salvatore, M., Carotenuto, G., De Nicola, S., Camerlingo, C., Ambrogi, V., & Carfagna, C. (2017). Synthesis and Characterization of Highly Intercalated Graphite Bisulfate. *Nanoscale Research Letters*, *12*(1). https://doi.org/10.1186/s11671-017-1930-2

Seredych, M., Mikhalovska, L., Mikhalovsky, S., & Gogotsi, Y. (2018). Adsorption of Bovine Serum Albumin on Carbon-Based Materials. *Journal of Carbon Research*, *4*(1), 3. https://doi.org/10.3390/c4010003

Shokry, H., Elkady, M., & Salama, E. (2020). Eco-friendly magnetic activated carbon nano-hybrid for facile oil spills separation. *Scientific Reports*, *10*(1), 1–17. https://doi.org/10.1038/s41598-020-67231-y

Singh, B., Kumar, S., Kishore, B., & Narayanan, T. N. (2020). Magnetic scaffolds in oil spill applications. *Environmental Science: Water Research and Technology*, *6*(3), 436–463. https://doi.org/10.1039/c9ew00697d

Soliman, E. M., Ahmed, S. A., & Fadl, A. A. (2020). Adsorptive removal of oil spill from sea water surface using magnetic wood sawdust as a novel nano-composite synthesized via microwave approach. *Journal of Environmental Health Science and Engineering*, *18*(1), 79–90. https://doi.org/10.1007/s40201-019-00440-4

Subrahmanyam, K. S., Vivekchand, S. R. C., Govindaraj, A., & Rao, C. N. R. (2008). A study of graphenes prepared by different methods: Characterization, properties and solubilization. *Journal of Materials Chemistry*, *18*(13), 1517–1523. https://doi.org/10.1039/b716536f

Sykam, N., Jayram, N. D., & Rao, G. M. (2018). Highly efficient removal of toxic organic dyes, chemical solvents and oils by mesoporous exfoliated graphite: Synthesis and mechanism. *Journal of Water Process Engineering*, *25*(January), 128–137. https://doi.org/10.1016/j.jwpe.2018.05.013

Sykam, N., & Kar, K. K. (2014). Rapid synthesis of exfoliated graphite by microwave irradiation and oil sorption studies. *Materials Letters*, *117*, 150–152. https://doi.org/10.1016/j.matlet.2013.12.003

Tarango-Rivero, G., Mendoza-Duarte, J. M., Santos-Beltrán, A., Estrada-Guel, I., Garay-Reyes, C. G., Pizá-Ruiz, P., Gómez-Esparza, C. D., Rocha-Rangel, E., & Martínez-Sánchez, R. (2022). Effect of Process Parameters on the Graphite Expansion Produced by a Green Modification of the Hummers Method. *Molecules*, *27*(21), 7399. https://doi.org/10.3390/molecules27217399

Thinh, P. Van, Thuong, N. T., Nguyen, T. D., Thi, N., Linh, N., Hoang, T. M., Thuan, N., Tien, L. X., Thi, B., Quynh, P., & Bach, L. G. (2016). Studying Properties of Expanded Graphite Coated With CoFe2O4 Particles , Application to Remove Oil Spills. *Journal of Materials Science & Surface Engineering*, *4*(4), 400–402.

Thinh, P. Van, Trinh, N. D., Thuong, N. T., Ho, V. T. T., Quynh, B. T. P., & Bach, L. G. (2018). Influence factors of exfoliation synthesis exfoliated graphite from vietnamese natural graphite flakes using microwave irradiation. *Solid State Phenomena*, *279 SSP*, 230–234. https://doi.org/10.4028/www.scientific.net/SSP.279.230

Tian, Y., Zhang, N., Liu, Y., Chen, W., Lv, R., & Ma, H. (2020). Adsorption performance of expanded graphite and its binary composite microbeads toward oil and dyes. *Desalination and Water Treatment*, *178*, 283–295. https://doi.org/10.5004/dwt.2020.24937

Ting, L., & Xuesha, Z. (2017). *One-step room-temperature preparation of expanded graphite_supporting*.

Toh, S. Y., Loh, K. S., Kamarudin, S. K., & Daud, W. R. W. (2014). Graphene production via electrochemical reduction of graphene oxide: Synthesis and characterisation. *Chemical Engineering Journal*, *251*, 422–434. https://doi.org/10.1016/j.cej.2014.04.004

Toyoda, M., & Inagaki, M. (2000). Heavy oil sorption using exfoliated graphite new application of exfoliated graphite to protect heavy oil pollution. *Carbon*, *38*(2), 199–210. https://doi.org/10.1016/S0008-6223(99)00174-8

Trivedi, A., Pisharath, N., & Ramanujam, B. T. S. (2018). Effect of Oxidizing Agents on the Expansion Characteristics of Natural Graphite. *Materials Today: Proceedings*, *5*(8), 16695–16702. https://doi.org/10.1016/j.matpr.2018.06.033

Vocciante, M., D'auris, A. D. F., & Reverberi, A. Pietro. (2022). A Novel Graphite-Based Sorbent for Oil Spill Cleanup. *Materials*, *15*(2). https://doi.org/10.3390/ma15020609

Wahi, R., Chuah, L. A., Choong, T. S. Y., Ngaini, Z., & Nourouzi, M. M. (2013). Oil removal from aqueous state by natural fibrous sorbent: An overview. *Separation and Purification Technology*, *113*, 51–63. https://doi.org/10.1016/j.seppur.2013.04.015

Wang, L., Tieu, A. K., Zhu, H., Deng, G., Hai, G., Wang, J., & Yang, J. (2020). The effect of expanded graphite with sodium metasilicate as lubricant at high temperature. *Carbon*, *159*, 345–356. https://doi.org/10.1016/j.carbon.2019.12.034

Wang, M., & Ji, L. (2012). Expansion mechanism of expandable graphite formed by natural graphite with different particle size. *Advanced Materials Research*, *499*, 16–19. https://doi.org/10.4028/www.scientific.net/AMR.499.16

Wang, P., Sun, H., & Peng, T. (2015). The evolution rule of three-dimensional structures of graphite during oxidation. *Nano*, *10*(1), 1–8. https://doi.org/10.1142/S1793292015500149

Wang, X. L., Li, B., Qu, Z. G., Zhang, J. F., & Jin, Z. G. (2020). Effects of graphite microstructure evolution on the anisotropic thermal conductivity of expanded graphite/paraffin phase change materials and their thermal energy storage performance. *International Journal of Heat and Mass Transfer*, *155*. https://doi.org/10.1016/j.ijheatmasstransfer.2020.119853

Wei, Q., Xu, L., Tang, Z., Xu, Z., Xie, C., Guo, L., & Li, W. (2023). High-performance expanded graphite from flake graphite by microwave-assisted chemical intercalation process. *Journal of Industrial and Engineering Chemistry*, *122*, 562–572. https://doi.org/10.1016/j.jiec.2023.03.020

Wei, T., Fan, Z., Luo, G., Zheng, C., & Xie, D. (2008). A rapid and efficient method to prepare exfoliated graphite by microwave irradiation. *Carbon*, *47*(1), 337–339. https://doi.org/10.1016/j.carbon.2008.10.013

Wu, K. H., Huang, W. C., Hung, W. C., & Tsai, C. W. (2021). Sorption and regeneration of expanded graphite/Fe3O4 composite for removal of oil pollution from the water. *Materials Express*, *11*(4), 579–585. https://doi.org/10.1166/mex.2021.1955

Wu, L. K., Chen, K. Y., Cheng, S. Y., Lee, B. S., & Shu, C. M. (2008). Thermal decomposition of hydrogen peroxide in the presence of sulfuric acid. *Journal of Thermal Analysis and Calorimetry*, *93*(1), 115–120. https://doi.org/10.1007/s10973-007-8829-6

Wu, M. B., Huang, S., Liu, T. Y., Wu, J., Agarwal, S., Greiner, A., & Xu, Z. K. (2021). Compressible Carbon Sponges from Delignified Wood for Fast Cleanup and Enhanced Recovery of Crude Oil Spills by Joule Heat and Photothermal Effect. *Advanced Functional Materials*, *31*(3), 1–8. https://doi.org/10.1002/adfm.202006806

Xu, C., Wang, H., Yang, W., Ma, L., & Lin, A. (2018). Expanded Graphite Modified by CTAB-KBr/H3PO4 for Highly Efficient Adsorption of Dyes. *Journal of Polymers and the Environment*, *26*(3), 1206–1217. https://doi.org/10.1007/s10924-017-1019-0

Yakovlev, A. V., Finaenov, A. I., Zabud'kov, S. L., & Yakovleva, E. V. (2006). Thermally expanded graphite: Synthesis, properties, and prospects for use. *Russian Journal of Applied Chemistry*, *79*(11), 1741–1751. https://doi.org/10.1134/S1070427206110012

Yang, S., Chen, L., Mu, L., Hao, B., & Ma, P. C. (2015). Low cost carbon fiber aerogel derived from bamboo for the adsorption of oils and organic solvents with excellent performances. *RSC Advances*, *5*(48), 38470–38478. https://doi.org/10.1039/c5ra03701h

Yang, S., Chen, L., Mu, L., & Ma, P. C. (2014). Magnetic graphene foam for efficient adsorption of oil and organic solvents. *Journal of Colloid and Interface Science*, *430*, 337–344. https://doi.org/10.1016/j.jcis.2014.05.062

Yao, T., Zhang, Y., Xiao, Y., Zhao, P., Guo, L., Yang, H., & Li, F. (2016). The effect of environmental factors on the adsorption of lubricating oil onto expanded graphite. *Journal of Molecular Liquids*, *218*, 611–614. https://doi.org/10.1016/j.molliq.2016.02.050

Yin, G., Sun, Z., Gao, Y., & Xu, S. (2021). Preparation of expanded graphite for malachite green dye removal from aqueous solution. *Microchemical Journal*, *166*(November 2020), 106190. https://doi.org/10.1016/j.microc.2021.106190

Zhang, Fengshuang, Zhao, Q., Yan, X., Li, H., Zhang, P., Wang, L., Zhou, T., & Li, Y. (2015). Rapid preparation of expanded graphite by microwave irradiation for the extraction of triazine herbicides in milk samples. *Food Chemistry*, *197*, 943–949. https://doi.org/10.1016/j.foodchem.2015.11.056

Zhang, Fengzhen, Wu, K., Zhou, H., Hu, Y., Preis, S. V., Wu, H., & Wei, C. (2018). Ozonation of aqueous phenol catalyzed by biochar produced from sludge obtained in the treatment of coking wastewater. *Journal of Environmental Management*, *224*(December 2017), 376–386. https://doi.org/10.1016/j.jenvman.2018.07.038

Zhang, Y., Huang, Y., Yang, G., Bu, F., Li, K., Shakir, I., & Xu, Y. (2017). Dispersion-Assembly Approach to Synthesize Three-Dimensional Graphene/Polymer Composite Aerogel as a Powerful Organic Cathode for Rechargeable Li and Na Batteries. *ACS Applied Materials and Interfaces*, *9*(18), 15549–15556. https://doi.org/10.1021/acsami.7b03687

Zhao, G., Dai, C., Gu, C., You, Q., & Sun, Y. (2019). Expandable graphite particles as a novel in-depth steam channeling control agent in heavy oil reservoirs. *Chemical Engineering Journal*, *368*(January), 668–677. https://doi.org/10.1016/j.cej.2019.03.028

Zhao, J. J., Li, X. X., Guo, Y. X., & Ma, D. Y. (2014). Preparation and microstructure of exfoliated graphite with large expanding volume by two-step intercalation. *Advanced Materials Research*, *852*, 101–105. https://doi.org/10.4028/www.scientific.net/AMR.852.101

Zhao, M., & Liu, P. (2009). Adsorption of methylene blue from aqueous solutions by modified expanded graphite powder. *Desalination*, *249*(1), 331–336. https://doi.org/10.1016/j.desal.2009.01.037

Zhao, T., Yang, W., Ji, X., Jin, W., Hu, J., & Li, T. (2018). In-situ synthesis of expanded graphite embedded with CuO nanospheres coated with carbon for supercapacitors. *Applied Surface Science*, *460*, 58–64. https://doi.org/10.1016/j.apsusc.2017.09.046

Zhou, T., Zhang, F., Liu, H., Li, H., Xu, Y., Zhao, L., Ding, J., Ding, L., & Li, Y. (2018). Microwave-assisted preparation of boron acid modified expanded graphite for the determination of chloramphenicol in egg samples. *Journal of Chromatography A*, *1565*, 29–35. https://doi.org/10.1016/j.chroma.2018.06.032

Zhuang, Q. Q., Cao, J. P., Zhao, X. Y., Wu, Y., Zhou, Z., Zhao, M., Zhao, Y. P., & Wei, X. Y. (2020). Preparation of layered-porous carbon from coal tar pitch narrow fractions by single-solvent extraction for superior cycling stability electric double layer capacitor application. *Journal of Colloid and Interface Science*, *567*, 347–356. https://doi.org/10.1016/j.jcis.2020.02.022

APPENDICES

Appendix A

Eco-friendly Mesoporous Expanded Graphite

Table A1: Effects of sulfuric acid concentration on graphite expansion volume at optimum condition

Solid-liquid ratio%	Expanded Volume (mL/g)	Expanded Volume (mL/g)	Expanded Volume (mL/g)
1	100	95	98
2	120	116	118
3	130	127	129
5	140	140	139
7	100	99	100
10	70	66	68
13	60	57	60

Table A2: Effects of oxidant dosage on graphite expansion volume at optimum condition

Amount of Oxidant (g)	Expanded Volume (mL/g)	Expanded Volume (mL/g)	Expanded Volume (mL/g)
3	95	94	94
4	97	97	95
5	99	98	95
6	110	108	107
7	140	140	138
8	135	134	134
9	130	130	129
10	133	132	133

Appendix B

Eco-friendly, Mesoporous, Sulfur-free, Expanded Graphite

Table B1: Effects of reaction time on the EV of the synthesized EG for sulfur free EG

Time (min)	Expanded Volume (mL/g)	Expanded Volume (mL/g)	Expanded Volume (mL/g)
10	224	220	219
20	300	300	295
30	470	464	466
40	400	395	397
50	358	357	355
60	300	290	285

Table B2 : Effects of palmitic acid (PA) concentration on the EV of the synthesized EG for sulfur free EG

PA (g)	PA (mL)	EV (mL/g)	EV (mL/g)	EV (mL/g)
0	0	255	250	251
3.41	4	334	333	329
4.265	5	400	398	400
5.1	6	470	463	470
5.971	7	300	297	288
6.824	8	250	245	248

Table B3: Effects of potassium permanganate dosage on the EV of the synthesized EG for sulfur free EG
First stage

KMnO4 (g)	Expanded Volume (mL/g)	Expanded Volume (mL/g)	Expanded Volume (mL/g)
0.1	370	365	368
0.15	455	445	452
0.2	470	468	469
0.25	370	365	366
0.3	320	311	318

Second stage

KMnO4 (g)	Expanded Volume (mL/g)	Expanded Volume (mL/g)	Expanded Volume (mL/g)
0.01	200	197	188
0.05	342	340	335
0.1	470	466	469
0.15	390	388	385
0.2	330	325	328

Table B4: Effects of HNO_3 and CH_3COOH on the EV of the synthesized EG for sulfur free EG

Nitric acid affection

HNO_3 (mL)	Expanded Volume (mL/g)	Expanded Volume (mL/g)	Expanded Volume (mL/g)
0.5	207	205	200
1	304	303	300
1.5	470	470	468
2	403	400	401
2.5	366	365	355

Acetic acid affection

HAc (mL)	Expanded Volume (mL/g)	Expanded Volume (mL/g)	Expanded Volume (mL/g)
2	258	252	255
4	404	402	400
6	470	467	469
8	345	344	342
10	330	325	322

Appendix C

Oil spills data

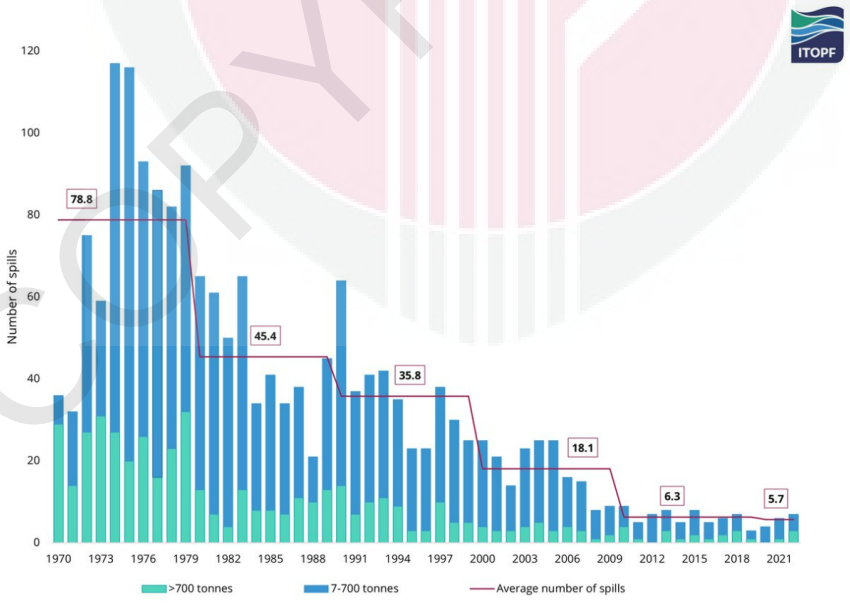

Figure C1: Number of Medium (7-700 tons) and large (>700 tons) tanker spills, 1970-2022

Appendix D

Materials and Chemicals

Figure D1: NGF with a carbon content of (99%) and a 50-mesh particle size

Figure D2: Acetic acid (99.5%)

Figure D3: Potassium permanganates (99.5%)

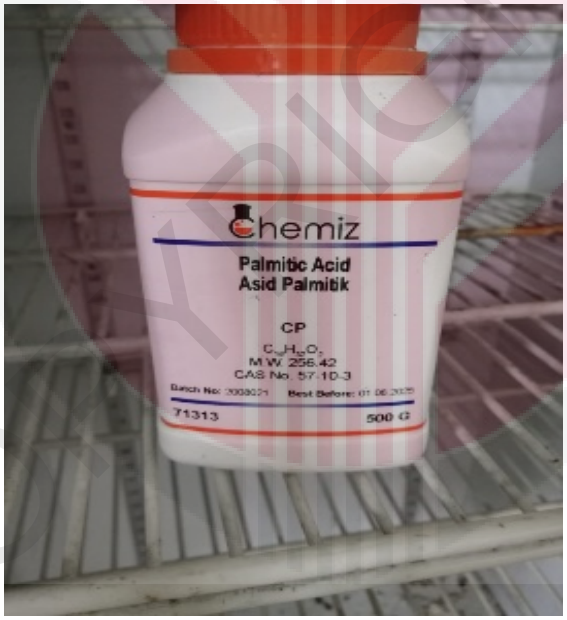

Figure D4: Palmitic acid (hexadecenoic acid)

Figure D5: Phosphoric acid (95-98 %)

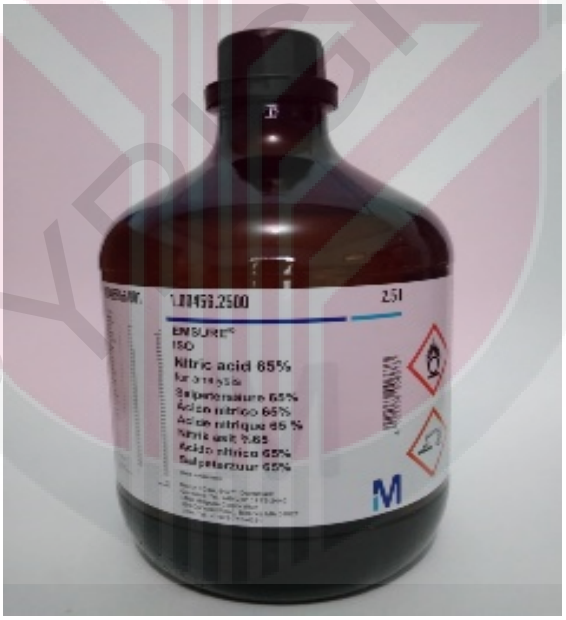

Figure D6: Nitric acid (65 %)

Figure D7: Sulfuric acid (98%)

Figure D8: Sodium peroxydisulfate

Typical Physical Data

Parameters	Method	Unit	Typical Value
Appearance	-	-	Bright & Clear
Density @15°C	ASTM D 4052	g/cm^3	0.8569
Kinematic Viscosity @100°C	ASTM D 445	mm^2/s (cSt)	10.89
Viscosity Index	ASTM D 2270	-	152
Flash Point COC	ASTM D 92	°C	210
Sulphated Ash	ASTM D 874	%	0.8
TBN	ASTM D 2896	mgKOH/g	7.7
CCS at –30°C	ASTM D5293	mPa·s	6040
Pour Point	ASTM D97	°C	-42

All technical data are provided for reference only. These characteristics are typical of current production. Whilst future production will conform to PLI's specification, variations in these characteristics may occur.

Figure D9: Perodua semi-synthetic engine oil

Appendix E

Apparatus and chemical instruments

Figure E1: Precision balance

Figure E2: Burette

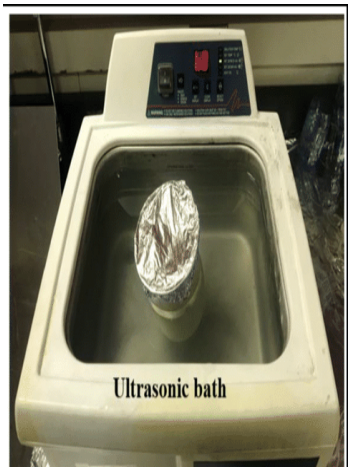

Figure E3: Ultrasonic stirrer

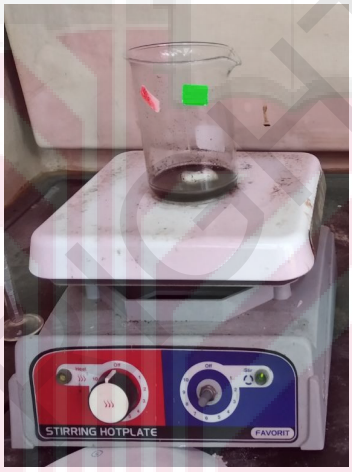

Figure E4: Magnetic stirrer

Figure E5: Water bath

Figure E6: pH meter

Figure E7: Dryer

Figure E8: Measuring cylinder

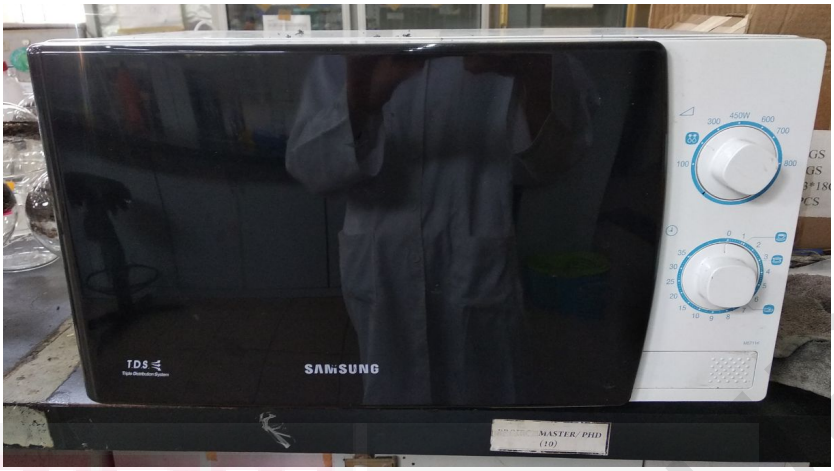

Figure E9: Microwave oven (Samsung ME711K)

Figure E10: Nicolet FT-IR 6700, Thermo Fisher Scientific

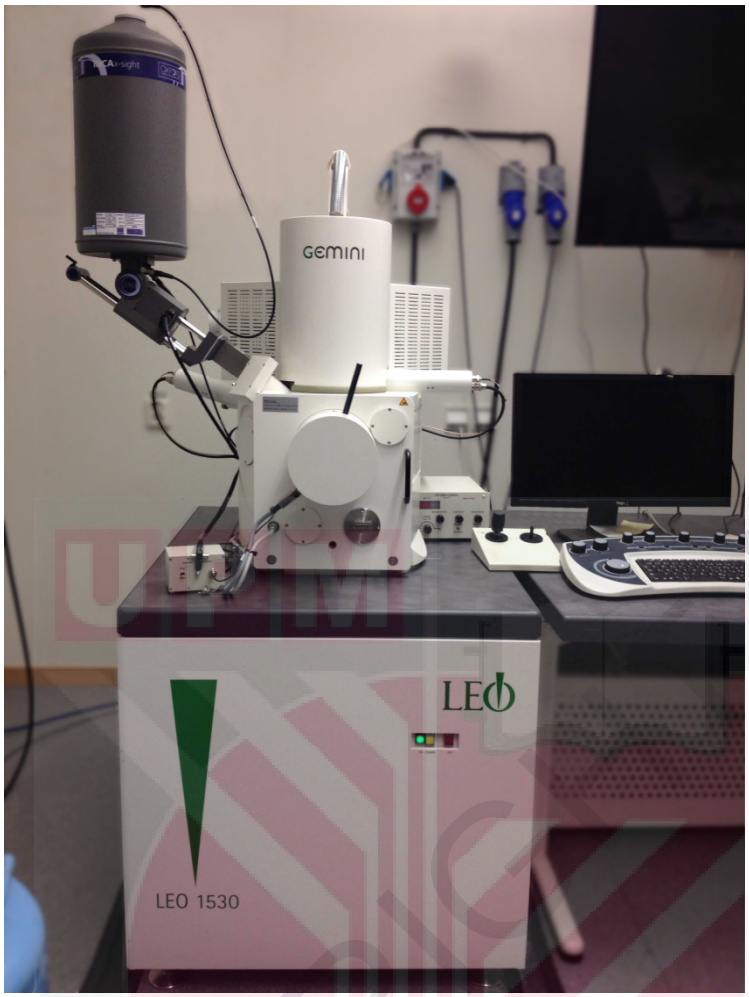

Figure E11: LEO 1445 VP scanning electron microscope

LIST OF PUBLICATIONS

Elbidi, M., Resul, M.F.M.G., Rashid, S.A. et al. Preparation of eco-friendly mesoporous expanded graphite for oil sorption. J Porous Mater 30, 1359–1368 (2023). https://doi.org/10.1007/s10934-023-01428-0

Elbidi, M., Salleh, M.A.M., Resul, M.F.M.G. et al. Synthesis and characterization of mesoporous expanded graphite modified with PA/H_3PO_4 for enhanced oil sorption efficiency. J Porous Mater (2023). https://doi.org/10.1007/s10934-023-01525-0

Elbidi, M., Salleh, M. A. M., Rashid, S. A., & Resul, M. F. M. G. The potential of thermally expanded graphite in oil sorption applications. *RSC advances* (2024), *14*(23), 16466-16485. https://doi.org/10.1039/D4RA00049H

Other Publications

Elbidi, M., Hewas, A., Asar, R., & Mohd Salleh, M. A. (2021). Comparative Study between Activated Carbon and Biochar for Phenol Removal from Aqueous Solution. *BioResources*, 16 (4). 10.15376/biores.16.4.6781-6790

Conference Publications

Workshops

Workshop on Biochar for environmental and agricultural use, 7th June 2023. Organized by Biochar Malaysian Association

Workshop on the International day for the conservation of the mangrove ecosystem focusing on, 'Protection and restoration of mangrove ecosystems in the Tropics' on 26 July 2023. Organized by Mahathir Science Award Foundation, TropSc 2024's.